Neural and Genetic Mechanisms of Sensory Reception in *C. elegans*

By

Elizabeth A. Ronan

A dissertation submitted in partial fulfillment
of the requirements for the degree of
Doctor of Philosophy
(Molecular and Integrative Physiology)
in The University of Michigan
2022

Doctoral Committee:

Professor X.Z. Shawn Xu, Chair
Professor Daniel Michele
Assistant Professor Jun Wu
Professor Bing Ye

Elizabeth A. Ronan

lizronan@umich.edu

ORCID iD: 0000-0001-7400-5718

DEDICATION

To my mother,

Marilyn Yester Ronan,

for being the first scientist to inspire me,

and providing boundless encouragement

to shoot for the moon.

ACKNOWLEDGEMENTS

First and foremost, thank you to my mentor Shawn Xu for believing in me and providing exceptional training in my development as a scientist. Thank you to all past and present members of our lab group for your feedback and support. I especially want to thank my first mentors and colleagues in Shawn Xu Lab, who greatly shaped my scientific and personal growth: Jianke Gong, Bi Zhang, Seth Wescott, Zhaoyu Li, Rui Xiao, and Guang Li. Thank you to Tong Pan, Can Wang, and Yuling Guo: I am appreciative of each of you for your support, friendship, and contributions to this dissertation. Thank you to Erkina Saertbaeva and Elana Elkin for your continual support and friendship since the beginning of my PhD. To Bonnie Zeng and Erica Cech, thank you for keeping me sane during the latter half of this journey, and for joining me for all the coffee breaks and journal club dinners. Also thank you to Feiteng He, Wei Cai, Xinxing Zhang, Adam Iliff, Xia Li, Xiaoqi Wu, Min Guo, Nancy Lan, and Jenn Snedeker. Each of you enriched my training and provided inspiration, guidance, support, and friendship throughout this journey. I will forever consider you all as my lab family.

To my MIP cohort: Ally Cara, Jon Dean, Ian Gonzalez, Natalie Warsinger-Pepe, and Thomas Vigil. I am fortunate to have been able to share this experience with each of you. I'll always remember us bonding as first years while doing our 'Membrane Physiology' homework together at Taubman Library. Thank you for providing support, friendship, and insight during our time together.

Thank you to those who have contributed to my dissertation development, doctoral training, and success. I must especially thank my dissertation committee members for their mentorship and time: Drs. Dan Michele, Jun Wu, and Bing Ye. Thank

you to Drs. Gunho Kim and Kevin Pipe, for creating the innovative technologies used in this dissertation as well as your time and mentorship.

Thank you to the Department of Molecular and Integrative Physiology (MIP) for providing unwavering support and exceptional training to your students. I couldn't ask for a better department to pursue my PhD. Thank you to everyone within the Life Sciences Institute (LSI) for providing an amazing community I can call home. The LSI is truly a special place on campus that continuously inspires me with its core values and scientific excellence. I must give a special thank you to both Nance Hobbs (LSI) and Michele Boggs (MIP) for your administrative support over the years. Additionally, thank you to both PIBS and the Rackham Graduate School for providing funding and outstanding support to your graduate students.

Finally, I want to thank all my family and friends for your continual love and support over the years. To my husband, Vasu Mahalingam, for being my partner and foundation throughout this journey, and for your unwavering support and encouragement in achieving my goals. To my parents, Marilyn and James, and my in-laws Sahuntala and Mahalingam, for your love and encouragement. To my siblings Rebekah and Jonathan, who provided valuable help with multiple aspects of this dissertation including coding and graphic design. Also, thank you to my all my dear friends, especially Veena Janardan, Emily Spannagel, and Ding He for always being there for me.

TABLE OF CONTENTS

CHAPTER:

LIST OF FIGURES

Figure:

LIST OF TABLES

Table:

ABSTRACT

All living organisms interact with diverse external stimuli in order to survive and thrive in their environments. Animals and humans have evolved molecular sensors and sensory neurons/circuits, to detect, respond, and adapt to sensory stimuli. The molecular mechanisms underlying sensation are largely conserved from worms to humans. The nematode *C. elegans* is a powerful genetic model organism that has enabled discovery of molecular sensors and signaling pathways mediating nearly all major sensory modalities. The work presented here consists of two major contributions to the field of sensory biology, each providing unique insight into the evolution of sensory systems. We highlight our use of *C. elegans* to discover a novel molecular cold sensor that is evolutionarily conserved from worms to mammals. Secondly, we show for the first time that *C. elegans* can detect airborne vibrations, revealing the unexpected presence of auditory sensation in lower phyla. Together, this work sheds light on evolutionarily conserved mechanisms of sensation, advancing contemporary views at the molecular, cellular, circuit, and behavioral levels.

CHAPTER I

Introduction

1.1 Background on *C. elegans* as a model organism

When looking back at the history of science, historians will reflect on our present time as the renaissance era of molecular biology. This began in the early 20th century when Frederick Griffith, Alfred Hershey, and Martha Chase (among others), discovered the transfer of genetic information using viruses[1,2]. This pioneering work led to the fundamental realization that DNA, rather than proteins, carries the genetic material of life. Our understanding, however, of molecular biology, continued to remain largely in the dark until 1953, when James Watson and Francis Crick, along with Rosalind Franklin, solved the double helical structure of DNA[2–4]. This discovery would become the missing link unlocking what is now accepted as the *central dogma* of molecular biology: the flow of genetic material occurs from DNA to RNA to protein[4]. During the second half of the 20th century, scientists began to establish model organisms including fruit flies, worms, and fish, to understand eukaryotic genetic principles and how these genes affect other products in the central dogmatic flow[4]. These models have greatly advanced our knowledge across biological disciplines, revealing principles that are strikingly evolutionarily conserved across metazoa.

The tiny, transparent nematode *Caenorhabditis elegans* is a powerful biological model organism that has contributed to six Nobel prize winners thus far, and continues

to shape the landscape of science today[5]. We must largely thank Nobel laureate

Sydney Brenner for the establishment of *C. elegans* as a model organism. Initially,

Brenner worked alongside founding molecular biologists, including Watson and Crick,

who together outlined many fundamental principles of genetics using minuscule viruses

known as bacteriophages (these scientists collectively referred to themselves as "The

Phage Group")[1,2,4]. However, by the mid 1960s, scientific progress began to wane as

the limitations of bacteriophages were becoming apparent[1,4]. This inspired several

scientists to begin developing new model systems. Seymour Benzer, one of the original

"Phage Group" members, began to hypothesize mechanisms of genetics underlying

behavior, and explored this further using the fruit fly *Drosophila melanogaster*[1,4]. George

Streisinger, who also began his career using the T4 bacteriophage, dreamt of using a

vertebrate to ask similar questions related to molecular biology and genetics[1,4]. He

chose to examine the zebra fish *Danio rerio*[1,4]. Brenner faced similar realizations that he

must expand his research to a more complex system. Inspired to look further into the

genetics underlying animal development, he decided to examine the transparent

roundworm *C. elegans*[4]. All three scientists met success, establishing vibrant research

communities surrounding these model organisms that continue to thrive today.

      At the time of conception, Brenner reasoned that *C. elegans* held significant

advantages over the other chosen model organisms[4]. In addition to their small size

(1mm in length and 80μm diameter), transparent bodies, and ease of cultivation, *C.

elegans* possess a much simpler nervous system than *Drosophila*[6]. Furthermore, these

roundworms exist as both self-fertilizing hermaphrodites as well as males, drastically

simplifying the generation and maintenance of stable genetic mutants[6]. In 1973,

Brenner published "*The Genetics of Behavior*", formally establishing *C. elegans* as a model organism[4,7]. This work highlighted the isolation of over 100 mutant strains, giving rise to a variety of developmental and behavioral phenotypes. Notably, Brenner also established the first wiring diagram of a complete nervous system in any organism. Over the following decades, *C. elegans* research flourished into a dynamic community. Brenner, along with John Sulston and Robert Horvitz, earned the Nobel prize in 2002 for their discoveries on the "genetic regulation of organ development and programmed cell death"[11]. *C. elegans* research went on contributing to many paradigm shifting scientific breakthroughs, including Nobel prize winning studies discovering gene silencing through RNA interference, and the development of green fluorescent protein (GFP)[11]. Momentum has not slowed since, and *C. elegans* research continues to make headlines. Exciting recent developments include novel mechanisms underlying sensory physiology, as discussed in this dissertation. Due to its short lifespan (~3 weeks at 20°C), *C. elegans* has also enabled the discovery of environmental and genetic mechanisms underlying aging and longevity, and even mechanisms of transgenerational inheritance, which would be extremely arduous to examine in other model systems[12–14]. As this dissertation centers on the field of sensory biology, we will now focus our attention on how *C. elegans* has shed critical insight into the present understanding of neurobiology and sensation.

1.2 Overview of the *C. elegans* nervous system

Compared to the vast complexity of the 86 billion neurons present in the human brain, the adult hermaphrodite *C. elegans* nervous system is composed of a meager

302 neurons containing approximately 6400 chemical synapses, 900 gap junctions, and 1500 neuromuscular junctions[8,9,15,16]. Despite this simplicity, *C. elegans* exhibit a remarkably complex array of responses. This includes the ability to sense of a variety of external stimuli, learn and remember sensory cues, and perform relevant response behaviors[17,18]. Their nervous system is organized with bilateral symmetry into 118 distinct classes of neurons that are arbitrarily designated as sensory, inter-, or motor neurons based on both neuroanatomical features and physiological function[6]. Most neuronal cell bodies (especially sensory and inter- neurons) are organized into densely packed ganglia located in the head or tail regions. Despite vastly different levels of complexity, the molecular mechanisms of neurotransmission are highly conserved between vertebrates and nematodes, including the presence of both small-molecule neurotransmitters (e.g., acetylcholine, dopamine, glutamate, GABA, serotonin), and dense core vesicle released neuropeptides (e.g., insulin-like peptides)[11,19]. Structurally, *C. elegans* neurons are simple, with the majority classified as having simple monopolar or bipolar structures with limited additional branching[20]. This does not, however, prohibit elaborate neural communication, as many extend processes to a central nerve ring that enables transfer of signals through both *en passant* synapses and gap junctions[11]. Furthermore, neuropeptide secretion into the extracellular space enables possibilities for long-distance communication.

As the only organism with a complete wiring diagram of the nervous system, it is not surprising that *C. elegans* has contributed to major discoveries in the field of neuroscience. Many of Brenner's original studies identified both known and novel genes required for synaptic transmission[6]. Forward genetic screens are performed with relative

simplicity, as genetic mutants can be isolated and maintained quickly due to self-fertilization. Some of the very first mutant strains isolated were found to exhibit defects in sensation, including touch, chemical sensing, and temperature, inspiring the use of *C. elegans* as a model system to study sensory neuroscience. Furthermore, the simplicity of the nervous system makes it very feasible to map the neurons and circuits underlying behavior compared to more complex model systems. Overall, the basic principles of the nervous system are highly conserved between *C. elegans* and higher organisms. The following sections will highlight several major findings that *C. elegans* has contributed to the field of sensory biology, including the research conducted in this dissertation. We will examine how simple roundworms have been utilized to uncover basic principles of sensory neuroscience as well as provide insight on how sensation may have evolved over millions of years.

1.3 The *C. elegans* sensory nervous system

While many *C. elegans* neurons have overlapping functions, at least 70 out of the 302 neurons (in hermaphrodites) are estimated to respond to a variety of environmental stimuli including touch, odors, chemicals, temperature, and light[8,17,21–23]. Sixty of these designated sensory neurons are ciliated, with a single cilium protruding from their dendritic ends[17,21,22,24]. Cilia form a variety of neuron-specific shapes including single or double rods, wings, and even a complex finger-like projection[24]. The "amphid" is considered a sensory organ composed of 12 pairs of ciliated sensory neurons with cilia directly exposed to the external environment via channels created by specialized glia (sheath and socket cells)[24]. Amphid neuronal cell bodies reside near the anterior region

of the pharyngeal bulb with axons synapsing on the central nerve ring and dendrites extending towards the mouth region[24]. In addition to the amphids, 2 posterior neurons (designated as the phasmids) are also exposed to the external environment near the tail[24]. Of note, male worms possess an additional 52 ciliated sensory neurons in the tail that have sex-specific roles in mating behavior and reproduction[6,17,24].

1.4 Mechanosensation in *C. elegans*

Introduction

The ability to sense touch is essential for navigating our environments and avoiding harm. The gentle brush of an eyelash across the worm body is sufficient to elicit avoidance responses in *C. elegans*. Touch of the anterior or posterior regions of the worm stimulates an avoidance behavior that consists of either accelerated forward locomotion, or a backwards "reversal" movement, respectively. Forward genetic screens isolating mutant lines defective in gentle touch avoidance succeeded in cloning the first mechanotransduction complex in any organism[17,25]. These foundational screens, led by Martin Chalfie and John Sulston, culminated in the creation of a strain library comprised of hundreds of *mec* (<u>mec</u>hanosensory abnormal) gene mutant alleles[6,17,25]. Thus, mechanosensation became one of the first well-defined sensory modalities in *C. elegans.* This early work also exemplifies the beautiful simplicity of utilizing forward genetics in nematodes to study sensory physiology. Later work discovered that worms sense both gentle and harsh body touch via distinct mechanisms. The following section will review the current knowledge of the neurons and molecular mechanisms pertaining to mechanosensation in *C. elegans.*

Gentle body touch sensation

Classic forward genetic screens isolating mutants defective in gentle touch avoidance led to the discovery of the six touch receptor neurons (TRNs) in *C. elegans* [25–27]. Gentle touch to the anterior region of the worm is mediated via the left and right **a**nterior **l**ateral **m**icrotubule cells (ALML [Left] and ALMR [Right]), as well as one **a**nterior **v**entral **m**icrotubule cell (AVM)[28]. Similarly, gentle touch of the posterior of the worm is sensed via two **p**osterior **l**ateral **m**icrotubules cells (PLML [Left] and PLMR [Right]), and one **p**osterior **v**entral **m**icrotubule cell (PVM)[28]. TRN mechanosensing depends on proper cellular localization as well as presence of specialized large cytoskeletal microtubules (which were also notably used to designate their cell nomenclature)[6,17,28]. Three major layers comprise the exterior shell of *C. elegans:* the outermost cuticle, hypodermis, and body wall muscles[6,29]. TRN cell bodies are located directly beneath the hypodermis, with processes that extend for 400-500µm along the body wall and in close contact with the hypodermal layer [6,17,28]. This localization enables development of a specialized, electron dense extracellular matrix (ECM) that envelopes the TRN process and contacts the hypodermis, designated the "mantle"[20,26]. Mantle development is essential for TRN touch sensitivity, expressing two unique ECM proteins (MEC-5 and MEC-9) required for proper formation of the molecular mechanotransduction complex (described further in the next section)[30,31]. The TRN cytoskeleton contains distinctively wide-diameter microtubules comprised of an exceptional number of protofilaments (15; for reference, most *C. elegans* cells contain 10 and the highest seen in most other organisms is 13)[17,32–34]. Along its ~500µm

neuronal process, the microtubules are staggered in 10-20µm sections, possessing a unique polarity that is essential for mechanosensing[17,32]. Microtubule proximal ends (relative to the cell body) are sheathed within the protofilament bundle, while distal ends protrude and contact the plasma membrane[6,28,32,33]. Disruption of microtubule structures confers loss of touch avoidance behaviors as well as excitation of TRNs[17,27,32]. Thus, the TRN cytoskeleton is essential for mechanosensation. Similarly, laser ablation of TRNs abrogates gentle touch avoidance responses[35]. Optogenetic activation of anterior or posterior TRNs elicits backwards or forward locomotion, respectively, indicating their excitation directly evokes the avoidance response [17,36,37]. Together, these findings confirm TRNs function as the primary touch receptor neurons that detect gentle touch and elicit avoidance responses.

The mechanical properties that excite TRN neurons are well defined, with *in vivo* imaging and electrophysiology approaches confirming their function as primary mechanosensory neurons[17]. TRN neurons exhibit higher magnitude touch-evoked calcium responses in response to a gentle sinusoidal buzz of the skin surface (peak cuticle displacement of 10 µm) compared to a single inward press of the same mechanical load[17,38–40]. TRN activation is also dependent on stimulus velocity, with slow indentation of the skin failing to elicit calcium responses[17,29,38]. Electrophysiology approaches further reveal that buzzing frequencies of <3 Hz fail to elicit mechanosensitive currents[17,29,38]. Therefore, TRNs appear to sense physical deformation/indentation of the cuticle rather than applied force, and are tuned to respond to mechanical loads of high velocity and frequency[17]. Intriguingly, these

mechanosensing features of TRN excitability show striking resemblance to cellular

pressure sensing in mammalian Pacinian corpuscles[17,41,42].
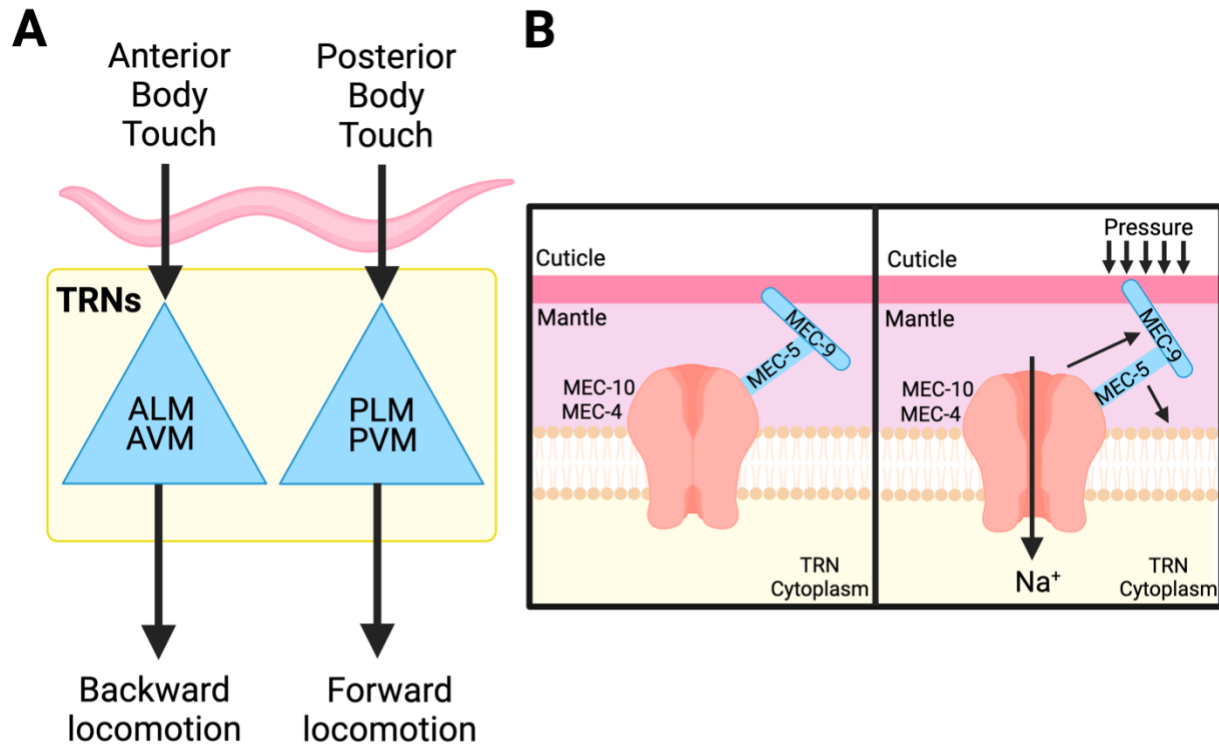
Figure 1.1. Mechanisms mediating gentle body touch sensation
The touch receptor neurons (TRNs) perceive gentle body touch via a defined
mechanotransduction complex to mediate avoidance behaviors.
A) Activation of TRNs by gentle touch to the anterior or posterior body trigger neural
circuits that trigger forward or backwards locomotion, respectively.
B) Model figure of the mechanotransduction complex mediating TRN activation. MEC-4
and MEC-10 make up subunits that form the channel pore. MEC-5 and MEC-9 are
expressed in the nearby extracellular ECM. Gentle touch dislocates MEC-5 and MEC-10
to open the channel pore and allow sodium influx into TRNs.
Model loosely adapted from: Touch. in Biology of Sensory Systems 99–121, John Wiley
& Sons, Ltd, 2009)[28], and made using *Biorender.*

The molecular mechanisms underlying gentle touch sensation in TRNs are well

understood (Figure 1.1). Martin Chalfie's original screen discovered 12 *mec* genes

essential for the mechanosensory function but not development of TRNs[6,26]. These

genes encode a variety of proteins that function together within the TRNs, providing the

first molecularly defined mechanotransduction complex (Figure 1.1). The channel pore

subunits are encoded by *mec-4* and *mec-10*[26]. This channel became the founding

member of the DEG/ENaC/ASIC channel class (<u>deg</u>enerins/<u>e</u>pithelial <u>Na</u>+

<u>c</u>hannels/<u>a</u>cid-<u>s</u>ensitive <u>i</u>on <u>c</u>hannels). As discussed above, two essential proteins are

present in the mantle that directly surrounds the TRN process, MEC-5 (an atypical

collagen protein) and MEC-9 (a protein containing EGF-like and Kunitz-type protease

inhibitor domains whose functions are essential for touch sensation)[6,26,28,30]. These

proteins function together as an extracellular attachment site for the MEC-4

mechanosensory channel subunits, as loss of either MEC-5 or MEC-9 disrupts MEC-4

localization and abrogates touch-evoked currents in TRNs[30]. The overall model is that

mechanical deformation applied to the exterior cuticle displaces specialized ECM

proteins in the underlying mantle (including MEC-5 and MEC-9), which transmits

pressure on MEC-4 channel subunits to open the channel pore leading to sodium ion

influx and cellular depolarization[6,20,43]. Many genes involved in the mechanotransduction

complex have mammalian homologs[35]. Notably, MEC-2 and MEC-4 have roles in gentle

touch sensation and pressure sensing in mice, respectively, indicating that

mechanosensing mechanisms are evolutionarily conserved from worms to

mammals[44,45].

Nose touch sensation

C. elegans elicits robust reversal responses upon touch to its nose tip, which is

not innervated by TRNs. Rather, ciliated sensory neurons extend their dendrites to the

nose tip. Combined laser ablation studies reveal that the ciliated sensory neurons ASH,

FLP, CEP, and OLQ are required for nose touch avoidance (Figure 1.2)[17,46,47]. Calcium

imaging and electrophysiology approaches shed insight into the cellular and molecular

mechanisms mediating nose touch sensation.
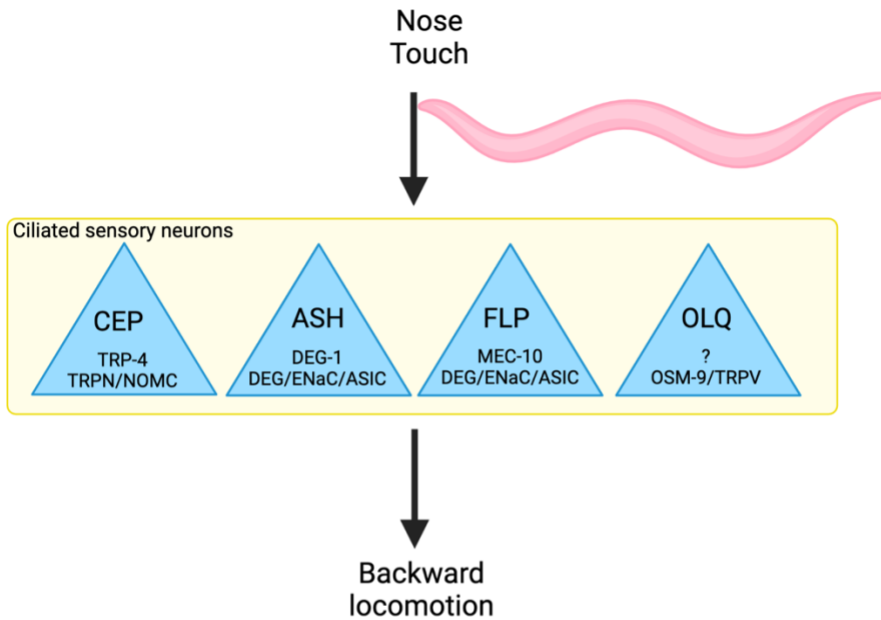
Figure 1.2. TRPN/NOMC and DEG/ENaC/ASIC channels mediate nose touch avoidance.
Nose touch triggers touch-sensing ciliated sensory neurons that innervate the mouth. These neurons activate neural circuits triggering backwards avoidance behaviors. Known mechanosensory signal transduction mechanisms for each neuron are shown. Model made with *Biorender*.

Nose touch evokes a transient calcium increase in ASH that persists in the absence of extracellular synaptic transmission via *unc-13* mutation, indicating that ASH functions as a primary mechanosensory neuron[17,48,49]. Electrophysiology recordings of ASH reveal activation of mechanoreceptor potentials that are dependent on the DEG/ENaC/ASIC channel DEG-1, providing yet another example of this class of channels functioning as mechanosensors in *C. elegans*[17,50,51]. CEP also functions as a primary mechanosensory neuron, as nose touch evokes an inward current that depends on the TRPN (NOMC) channel *trp-4*[52]. Calcium imaging of OLQ reveals transient excitation to nose touch that depends on the TRPV channel *osm-9*[48,53]. However,

further evidence is required to conclude OLQ functions cell-autonomously as a primary

mechanosensory neuron, as single ablation does not result in defective nose touch

avoidance[46]. Additionally, TRPV channels *osm-9* and *ocr-2* are dispensable for touch-

evoked currents in ASH, suggesting TRPV functions downstream in the

mechanotransduction cascade rather than serving as a direct mechanosensor[50]. Of

note, ablation of the amphid sensory neuron IL1 abrogates the head withdrawal reflex

upon nose touch, but further evidence is needed to determine whether it truly plays a

primary role in nose touch avoidance[54]. In conclusion, nose touch avoidance assays

involve several ciliated sensory neurons in the head and provide evidence that both

TRPN and DEG/ENaC/ASIC channels can directly function as mechanosensors (Figure

1.2).

Harsh body touch sensation
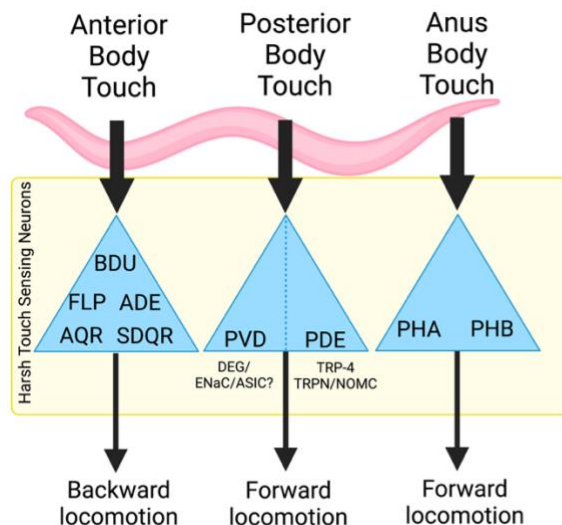
Figure 1.3. Mechanisms mediating harsh body touch sensation
Harsh touch mediates forward or backward avoidance behaviors depending on localization of the stimulus. Many neurons are implicated as being important for harsh anterior body touch (i.e., BDU, FLP, ADE, AQR, SDQR). Posterior harsh body touch is triggered by PVD and PDE via DEG/ENAC/ASIC or TRP-4 channels, respectively. Anus body touch depends on the tail neurons PHA and PHB. Model made using *Biorender*.

Several sensory neurons and channels are known to mediate harsh body touch

sensation in *C. elegans* (Figure 1.3). Compared to gentle, innocuous touch, harsh touch

is defined as noxious, painful touch that organisms must avoid to prevent tissue

damage. As previously described, gentle touch is administered to *C. elegans* by brushing an eyelash hair across the animal. The force applied to the worm body during gentle touch is calculated to be in the range of 1-10µN, and elicits a short-distance avoidance response consisting of ~1-2 headswings[35]. Harsh touch consists of a much larger force (100-200µN), typically applied using a wire pick or glass probe, that provokes a prolonged avoidance response (~5 headswings followed by a direction change)[35]. The TRNs that mediate avoidance of gentle body touch exhibit no defect in harsh body touch avoidance[35]. Laser ablation experiments have identified sensory neurons important for harsh touch avoidance localized at the anterior, posterior, and anus regions of the body[35]. Anterior harsh body touch avoidance implicates both individual and combined roles for BDU, SDQR, ADE, AQR, and FLP neurons[35]. Posterior harsh touch avoidance is mediated by both PVD and PDE [35]. Anus harsh touch avoidance is reliant on both PHA and PHB[35]. Only PVD and PDE have been molecularly characterized further (Figure 1.3). Whole-cell patch clamp recordings indicate that posterior harsh touch evokes inward currents in PVD that are amiloride sensitive, suggesting the role of DEG/ENaC/ASIC channels[35]. Mechanosensitive currents in PDE, however, depend on *trp-4*/TRPN[35]. The interneuron ALA responds cell-autonomously to harsh body touch applied during standard maintenance procedures while moving worms with a platinum wire, but the underlying molecular mechanisms have not been explored[55]. Taken together, harsh body touch assays further corroborate that DEG/ENaC/ASIC and TRPN receptors function in mechanosensory responses in *C. elegans.*

Proprioception in *C. elegans*

C. elegans navigate their environments via locomotion consisting of sinusoidal body bends propagating along its body axis[32,56,57]. Somatosensory feedback relies on perception of body stretch, which is mediated by the mechanosensory receptor TRP-4 in a single posteriorly located neuron, DVA[56]. The multi-dendritic sensory neuron PVD that innervates the body may also be involved in proprioception, as it is transiently activated during locomotion in a MEC-10 dependent manner, and cellular ablation leads to postural defects[58]. Steering behavior during locomotion is shown to depend on proprioceptive feedback via SMD head neurons in a TRP-1/TRPC and TRP-2/TRPC dependent manner[17,59]. Thus, mechanosensory TRP and DEG/ENaC/ASIC channels are also implicated as having roles in the somatosensory feedback of body stretch in C. elegans.

Mechanosensing in male mating behaviors

Male C. elegans have an additional 42 ciliated sensory neurons required for sex-specific mating behaviors and reproduction[17,24] The majority of these neurons are located in specialized male tail structures (rays and hooks) that provide mechanosensory feedback while scanning the hermaphrodite body to detect the vulva and ensure successful copulation[17]. Male Type B ray neurons exhibit touch-evoked calcium transients that are blocked by amiloride, indicating that DEG/ENaC/ASIC channels also function as molecular mechanosensors in male mating behaviors[17,60].

Conclusions

In conclusion, the sense of touch enables worms to navigate their environments both externally to avoid harm and discriminate their environments, and internally via the

sense of proprioception. Studies of mechanosensation in *C. elegans* have contributed

important principles of touch sensation that are evolutionarily conserved. Touch

responses due to indentation and mechanical deformation of the skin have been well

characterized. However, no prior work has shown that airborne vibration can trigger

behavioral responses in organisms lower than arthropods and insects. Later in this

dissertation, we will present our new discovery showing that sound waves traveling

through the air can directly vibrate the *C. elegans* cuticle to activate the nervous system

and elicit behaviors. We designate this response as "auditory sensation", as the

mechanisms of activation are distinct from mechanosensation and show striking

similarity to how sound activates the cochlea in the vertebrate eardrum.

1.5 Thermosensation in *C. elegans*

Introduction

Temperature has profound effects on all life forms ranging from bacteria to

humans. Thermosensation allows animals to avoid potentially harmful conditions in

nature as well as seek out favorable conditions for survival. Animals have evolved

complex sensory systems comprised of molecular thermal sensors, sensory neurons

and circuits to detect and respond to this dynamic thermal environment. *C. elegans*

possess remarkable thermosensing abilities. Worms survive and reproduce in a

temperature range from 12 to 26°C, and discriminate temperature changes as small as

0.01°C[17,61–64]. *C. elegans* detect and avoid localized thermal stimuli in both the

innocuous and noxious temperature range. In addition to thermosensory behaviors, *C.*

elegans also exhibit broader physiological responses to temperature including

regulation of lifespan. This section will review the current knowledge of *C. elegans* thermosensation.

Mechanisms underlying innocuous temperature sensation

     C. elegans preferred temperature is highly plastic within the range of 15 to 25°C depending on their cultivation temperature[61,65]. *C. elegans* learn and remember cultivation temperatures associated with resource abundance (food) and will seek out this temperature when placed on a thermal gradient[17,65,66]. If food supplies diminish, worms will learn to avoid the associated cultivation temperature[17]. This phenomenon, termed thermotaxis, represents another historic discovery in *C. elegans* and has provided valuable insight into mechanisms of thermosensation[65]. The behaviors, neural circuits, and molecular mechanisms underlying thermotaxis behavior have been extensively studied. Thermotaxis behavior requires animals to perform complex, experience-dependent navigation in order to find, maintain, and remember their temperature preference[67].

     Thermotaxis studies have uncovered a wide variety of behaviors that *C. elegans* exhibit in response to innocuous temperature changes. As introduced above, if well-fed *C. elegans* are placed on a spatial thermal gradient, they will migrate to their cultivation temperature (T_C) and perform isothermal tracking to remain at this preferred temperature (Figure 1.4A)[65,68,69]. This requires animals to perform complex, experience-dependent navigation in order to find, maintain, and remember their temperature preference[67]. When placed at temperature $T < T_C$, worms will crawl up the temperature gradient towards the warmer, preferred temperature (positive thermotaxis)[17,67].

Conversely, when worms are placed at temperature $T > T_C$, they will migrate towards cooler temperatures (negative thermotaxis)[17,67]. Once worms reach their preferred temperature T_C they will perform isothermal tracking behaviors with a deviation of no more than 2°C away from T_C[17,65,68]. As little as 4 hours of growth at an innocuous temperature in the range of 15 to 25°C will reset their T_C response when placed on the thermal gradient, revealing worms can both learn and remember sensory stimuli[65,68–70].

As worms crawl along a temperature gradient in search of T_C, they exhibit several stereotyped locomotion behaviors enabling them to find their target. During negative thermotaxis, *C. elegans* perform a biased random walk strategy (klinokinesis) consisting of extended periods of forward locomotion while moving down the thermal gradient, in addition to increased reversals and turns (reorientation behaviors) when they encounter warmer temperatures (Figure 1.4A)[63,69,71,72]. Positive thermotaxis does not involve klinokinesis but is instead directed primarily by reorientation behaviors away from cooler temperatures[17,63]. At T_C, worms exhibit sinusoidal head oscillations to track their preferred temperature via forward locomotion within 2°C[17,63,71]. If they encounter a stimulus outside of this range, reorientation behaviors are triggered to find T_C again. Remarkably, *C. elegans* can retain memory of T_C for several hours[65]. Worms that experience starvation for 2-4 hours also remember the associated T_C and will avoid it[6,67]. The steepness of the temperature gradient also impacts worm behavior. On gradients steeper than >1.5°C/cm, worms will exhibit negative thermotaxis regardless of experience and memory[69,73]. Additionally, at temperatures $T \ll T_C$ worms no longer thermotax (become atactic)[17,68,71].

The amphid ciliated sensory neuron AFD predominantly regulates thermotaxis

behaviors. Also known as the amphid finger neuron, AFD has a unique dendritic process embedded within the glial sheath cells just outside the nose tip[6,24] . Thus, unlike many amphid sensory neurons, AFD sensory cilia are not directly exposed to the external environment[24]. Classic laser ablation studies first identified AFD as being essential for both thermotaxis and isothermal tracking[68,74]. When placed on a thermal gradient, AFD-ablated worms exhibit either atactic behaviors or become intrinsically cryophilic (cold-seeking) regardless of T_C[6]. Calcium imaging experiments show that AFD is a primary warmth sensing neuron that shows increases and decreases in calcium upon warmth and cooling, respectively[17,72,75]. Electrophysiology recordings reveal that nonselective cation currents increase and decrease with warming and cooling, respectively, providing compelling evidence that AFD is intrinsically thermosensitive[17,64]. Analogous to the plasticity of thermotaxis behaviors, the AFD thermal response threshold (T^*_{AFD}) also depends on cultivation temperature[17,70,72,75,76]. When $T_C = 15°C$, calcium transients in AFD are induced upon warming to temperatures $T > T_C$[17,72,75] However, when $T_C = 25°C$, T^*_{AFD} shifts to 23°C[17,72,75]. These paradoxical findings reveal that AFD bidirectionally modulates thermotaxis by mechanisms that are still not well defined. Interestingly, AFD neurons that are isolated and cultured *in vivo* still retain the ability to remember cultivation temperature, providing striking evidence AFD can store temperature memories intracellularly[66,76].

Later work implicates the amphid sensory neurons AWC and ASI as being involved in thermotaxis, although conflicting reports suggest their roles may be condition dependent[6,17,77–79]. Disruption of AWC or ASI activity results in mild thermotaxis defects caused by alterations in reorientation behavior frequency[17,77–79]. Calcium imaging

indicates that both neuron pairs can show T_C-dependent warming responses, but they lack precise threshold dynamics and are more stochastic in nature[17,77–79]. The current consensus is that AWC and ASI likely act as modulators rather than direct sensory neurons in the thermotaxis neural circuit[17].

The first layer interneuron AIY functions downstream of AFD in the neural circuit mediating thermotaxis. While the relationship between AFD and AIY in mediating thermotaxis remains an active area of investigation, we do have some clues as to how they may function together. Classic laser ablation experiments found that killing AIY results in a cryophilic thermotaxis phenotype[6,65]. During locomotion, AIY functions to suppress turns and reversals to enhance forward movement[80–82]. AFD is glutamatergic and shares strong synaptic connection with AIY[8,17,72,78]. Activation of AFD in conditions where $T > T_C$ enables glutamate to bind inhibitory glutamate-gated chloride channels (GLC-3) expressed on AIY[66,83]. This results in downstream inhibition of AIY, which functionally disinhibits the suppression of avoidance behaviors. Therefore, upon AFD excitation where $T > T_C$, animals would increase reorientation responses enabling negative thermotaxis to escape warmth. This model, however, is further complicated by observations that AFD can also excite AIY via unknown peptidergic signaling[66,84–86]. The exact mechanisms triggering excitatory neuropeptide release from AFD, and the underlying neuropeptide(s) and associated receptor(s) on AIY remain to be determined. We do know that increased AIY activation when $T < T_C$ stimulates positive thermotaxis to escape[17,78,87]. It will be exciting to uncover how AFD and AIY bidirectionally modulate thermotaxis in a T_C dependent manner.

In addition to AIY, some evidence implicates the interneurons RIA and AIZ in

mediating thermotaxis responses downstream of AFD[66,68]. For instance, laser ablation

of RIA or AIZ results in cryophilic or thermophilic behaviors, respectively[68]. However,

more recent studies failed to reproduce these findings, which has called into question

whether RIA and/or AIZ truly function in the thermotaxis circuit[66,74].
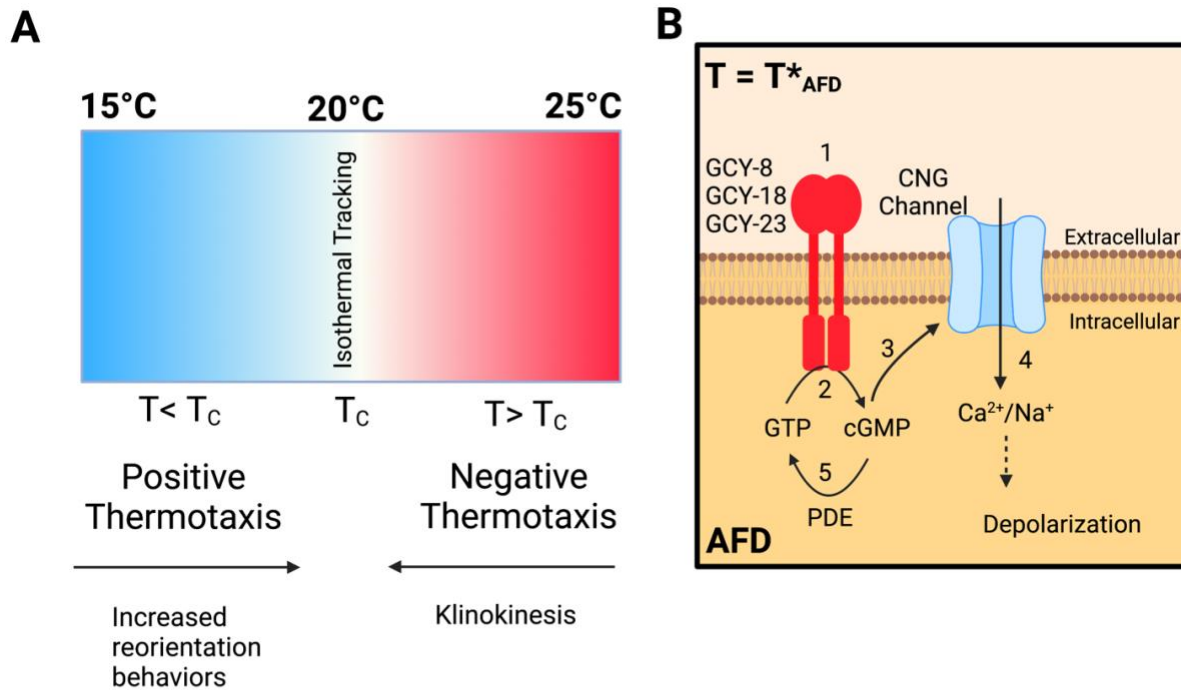
Figure 1.4. Thermotaxis assay and AFD sensory transduction mechanisms
A) Example of thermotaxis assay. C. elegans will seek out their cultivation temperature (Tc) using positive thermotaxis when T<Tc and negative thermotaxis when T>Tc, which utilize distinct behavioral strategies. Once Tc is found, they will isothermally track at this temperature.
B) AFD signal transduction cascade mediating thermotaxis.
1. When T = T*AFD, the guanylyl cyclases GCY-8, GCY-18, and GCY-23 are activated.
2. GCY-8, GCY-18, and GCY-23 function to catalyze the production of cGMP from GTP.
3. cGMP opens the Cyclic Nucleotide Gated (CNG) channel TAX-2/TAX-4
4. Calcium rushes into the cell via TAX-2/TAX-4 channels and leads to depolarization of AFD
5. Phosphodiesterases (PDEs) negatively regulate AFD excitation by catalyzing the conversion of cGMP back to GTP. Models made using *Biorender.*

The molecular mechanisms of thermotransduction in AFD are well defined

(Figure 1.4B). Thermosensing in AFD requires 3 unique guanylyl cyclases (GCYs),

GCY-8, GCY-18, and GCY-23, that are expressed exclusively in AFD and directly sense

temperature to synthesize cGMP from GTP[6,88–90]. This enables cGMP to open cyclic

nucleotide gated (CNG) channels, TAX-2 and TAX-4, located in the plasma membrane, allowing for intracellular calcium influx and subsequent neuronal depolarization[65,75,91,92]. Mutant strains lacking all 3 GCYs or TAX-2/TAX-4 are behaviorally atactic and fail to elicit temperature-induced calcium responses or inward currents in AFD[6,17,68,89,93]. However, it was only recently confirmed that GCYs function as thermosensors in AFD. In an elegant set of experiments, Takeishi and colleagues misexpressed various combinations of GCY-8, GCY-18, and GCY-23 in CNG channel-expressing chemosensory neurons to observe whether they could confer thermosensitivity on thermo-insensitive neurons[94]. They found that misexpression of GCY-18 and GCY-23, but not GCY-8, were sufficient to confer thermosensitivity in chemosensory neurons[94]. Notably, thermosensory thresholds in different chemosensory neurons that misexpressed GCY-23 all varied significantly compared to T*$_{AFD}$, suggesting additional cell-autonomous mechanisms fine-tune thermosensory thresholds independent of GCYs[17,94]. It remains to be determined whether thermosensory responses in AWC or ASI also depend on GCYs. Termination of thermosensory responses in AFD occurs via activation of phosphodiesterases (PDEs), which function to hydrolyze cGMP into GTP to turn off thermoresponses[17,95]. Notably, the mechanisms underlying thermotaxis show striking parallels with phototransduction pathways in other organisms, including reliance on cyclic nucleotide gated (CNG) channels[17].

Mechanisms of noxious temperature avoidance

A handful of studies have examined noxious heat responses in *C.* elegans and identified sensory neurons involved in avoidance behaviors. These experiments

generally use a red diode laser to rapidly heat the worm to high temperatures (35-38°C)[17,96–99]. When noxious heat is applied either globally or locally at the head, worms exhibit a reversal response consisting of transient backward locomotion, which may be followed by a turn to achieve direction change[96–99]. Two sensory neurons, AFD and FLP, have been shown to mediate noxious heat-evoked reversal responses[96]. Noxious heat sensing in AFD relies on same the CNG channels that sense innocuous thermal gradients, *tax-2* and *tax-4*[96]. The GCYs mediating noxious heat sensing in AFD are not yet determined. *gcy-8;gcy-18;gcy-23* exhibits modest defect, suggesting the presence of other GCYs in mediating noxious heat avoidance[96]. The *C. elegans* genome encodes 34 GCYs, requiring an extensive process of elimination to identify other candidates[94,100]. Interestingly, single mutant animals lacking GCY-12, another GCY that is known to be expressed in AFD, reduced but did not completely abrogate noxious heat avoidance[96]. Thus, additional GCYs in AFD are likely involved in noxious heat sensing. FLP noxious heat responses are mediated by OSM-9/TRPV[96]. Importantly, calcium imaging experiments confirm that both AFD and FLP sense noxious heat cell-autonomously, as heat-evoked calcium transients persist in mutants lacking global neurotransmission or neuropeptide release[96]. Laser ablation of FLP or AFD alone partially disrupts noxious heat avoidance, while combined ablation largely abrogates noxious heat avoidance behavior[96]. Thus, AFD and FLP likely function as parallel nociceptive circuits mediating noxious heat avoidance[66,96]. Localized noxious heat aimed at the tail elicits rapid forward locomotion that depends on the thermosensory neuron PHC via OSM-9/TRPV[96]. Of note, neither GCYs nor OSM-9/TRPVs have been confirmed to be activated by noxious heat[66]. Further study must be done to confirm the noxious heat

sensors in *C. elegans.*

Prior to the work performed in this dissertation, very little was known about the mechanisms by which *C. elegans* senses and responds to noxious cold. The multidendritic mechanosensory neuron PVD was shown to mediate cool-evoked turns in a TRPA-1 dependent manner[101]. Indeed, calcium imaging of PVD revealed increased calcium transients upon cooling to 15°C that depend on TRPA-1[101]. However, activation of PVD via either mechanosensory stimuli or optogenetics is known to stimulate forward movement rather than turns[35,102]. Regardless, much remains to be explored as to how *C. elegans* senses noxious cold.

It is well known that animals tend to live longer at colder temperatures, but this was largely assumed to be due to a passive slowing of thermodynamic processes[12,103]. Excitingly, it was recently discovered that *C. elegans* exhibit lifespan extension at cold temperatures in a TRPA-1 dependent manner[104]. Cold temperatures activate TRPA-1 in the intestine, stimulating a pro-longevity transduction cascade that depends on DAF-16/FOXO[104]. Later work also revealed that the ciliated sensory neuron IL1 senses cold via TRPA-1 to extend longevity[105]. Cold-induced activation of IL1 triggers glutamate release onto the serotonergic interneuron NSM, which binds to the serotonin receptor SER-7 on the intestine to activate the DAF-16/FOXO pro-longevity pathway[105]. Importantly, these findings reveal that cold-mediated longevity is not a passive process but rather depends on cold-sensitive activation of genetic program to trigger lifespan extension.

Conclusions

Despite *C. elegans* exhibiting a variety of thermosensitive behaviors and cellular responses, only two classes of molecular thermosensors have been confirmed in worms prior to this dissertation: guanylyl cyclases (the innocuous warmth sensors GCY-18 and GCY-23) and the cold sensor TRPA-1. While OSM-9/TRPV is required in several heat-sensing neurons, many additional sensory neurons that do not sense heat also express OSM-9, suggesting it functions downstream in the thermotransduction cascade[106]. Transient receptor potential (TRP) channels comprise a large subset of evolutionarily conserved thermosensitive membrane proteins, with at least seven known thermosensitive TRP channels. Notably, TRPV and TRPM channels largely mediate noxious heat, pain, and innocuous warmth in a variety of organisms[66]. Surprisingly little is known about the neurons and molecules that mediate the response of animals to cold and cool temperatures. Of the TRP family, only TRPM8 and TRPA1 show *in vivo* physiological defects in cool or cold sensing, respectively[66]. However, it is clear that mice missing both channels are still cold-sensitive, indicating that novel cold-sensitive channels must exist[12]. This encouraged us to identify additional cold sensors using *C. elegans,* with our findings outlined in Chapter 2.

1.6 Chemosensation in *C. elegans*

Introduction

Organisms are constantly exposed to both volatile (olfactory) and water-soluble (gustatory) chemicals as they navigate through their environments. Chemosensation allows evolutionary advantages by enabling detection of resources and reproductive mates, as well as dangers such as predators and poisons. Early classic studies in *C.*

elegans explored their chemosensory abilities, discovering they exhibit both avoidance and attraction behaviors to a wide range of chemicals and odorants[92,107–109]. In 1993, Cori Bargmann cloned the first odorant receptor in *C. elegans*, ODR-10, a member of the G protein couple receptor (GPCR) family, sharing homology with the recently identified mammalian odorant receptors[110]. Importantly, ODR-10 was the first odorant receptor to be paired with its odorant (the volatile compound diacetyl) in any organism[110].

Mechanisms underlying chemosensation

We now know that the *C. elegans* genome contains over 1000 predicted GPCRs, most of which are expressed in chemosensory neurons[106]. Signal transduction downstream of chemosensory GPCRS occurs via TAX-2/TAX-4 CNG channels or OSM-9/TRPV channels[106,111]. Notably, this reveals worms use conserved mechanisms of signal transduction across sensory modalities, as these also function in mechanosensory and/or thermosensory transduction cascades. In this section, we will briefly review the behavioral, neural, and molecular mechanisms underlying chemosensation in *C. elegans.*

C. elegans exhibits both innate attractive and repulsive behaviors to chemicals that can depend on their structure, concentration, or past experiences[106,111]. Worms are innately attracted to or avoid a wide variety of gustatory and volatile compounds (Table 1.1)[111]. It is worth noting that *C. elegans* can also sense physiologically relevant gases such as oxygen and carbon dioxide[5,106].

Table 1.1. Attractive and repulsive compounds (nonexhaustive).[6,111]

Attractants		Repellents	
Water-soluble	Volatile	Water-soluble	Volatile
Cations (e.g., Na^+, K^+)	Alcohols	High osmotic strength	Heptanol, octanol, nonanol
Anions (e.g., Cl^-)	Ketones	Copper ions	Nonanone
Cyclic nucleotides (cAMP, cGMP)	Diketones	Sodium dodecyl sulfate (SDS)	Benzaldehyde (High)
Basic pH (<10.5)	Pyrazines	Acidic pH or Basic pH (>10.5)	Isoamyl alcohol (High)
Amino acids (lysine, histidine, cysteine, methionine)	Thiazoles, aldehydes, aromatics, ethers	Δ-tryptophan	Diacetyl (High)

Several assays can be used to identify *C. elegans* preference (Figure 1.5.). Chemical attraction is measured via the chemotaxis assay (Figure 1.5A). In this assay, a point-source of the compound in question (can be water-soluble or volatile) is placed at a marked location in an agar-filled petri dish. A population of worms is allowed to roam freely around the plate for a set amount of time, and their distribution is monitored to determine whether they are attracted or repelled to the compound. Similar to behaviors observed during thermotaxis, attractive chemicals stimulate a unique worm behavior designated the "pirouette model" of locomotion[112]. This is a biased random walk strategy that worms use to navigate a chemical gradient. Moving up an attractive gradient stimulates longer bouts of forward locomotion with rare direction changes

called pirouettes[111]. When traveling down the attractive gradient, pirouette bouts increase, enabling reorientation towards the attractive compound[112]. Modulation of pirouette frequency enables animals to turn less when moving towards the attractant and reorient more when moving further away[111].
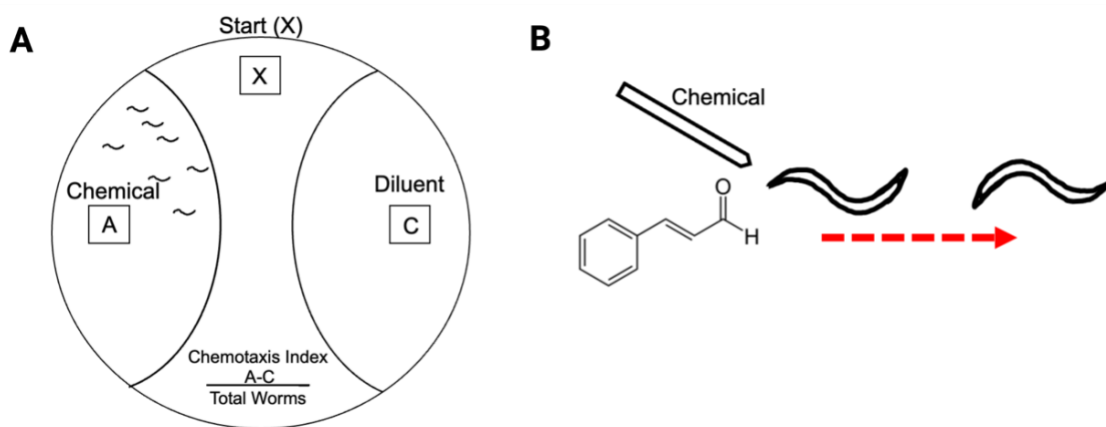
Figure 1.5. *C. elegans* chemosensory assays
A) Diagram of a standard chemotaxis assay. The chemical in question is spotted at a point equidistant from a control diluent and the worms start point. A population of worms are allowed to roam freely around the dish for a set amount of time, and their densities at each point are calculated using the number of animals quadrent using the Chemotaxis Index equation.
B) Example of a chemoavoidance assay. The chemical in question is placed in front of a single forward moving worm and assayed for avoidance response (backwards locomotion). Control experiments are performed using the diluent alone.

Chemical avoidance is easily measured in individual animals by observing whether introduction of the compound induces a reversal response when placed in front of a forward-moving worm (Figure 1.5B). Volatile odorants can be administered through the air by holding the concentrated chemical in front of the animal (contained in a recording pipette or on a cotton tip). Water-soluble compounds are examined using the "drop test", where a drop of liquid containing the chemical is placed in front of the forward moving animal, and avoidance behaviors are scored[113,114]. This assay can also

be used to examine the tail phasmid neurons by localizing the compound near the tail tip and scoring whether this stimulates accelerated forward locomotion[114]. These experiments all require control tests containing the diluent alone to ensure specificity to the compound in question.

Compared to the other sensory modalities, chemosensation is distributed across a much wider range of sensory neurons. There are 32 presumed chemosensory neurons in the hermaphrodite, including most of the head amphid and tail phasmid neurons[111]. The amphid neurons with single rod cilia (i.e. ADL, ADF, ASE, ASG, ASH, ASI, ASJ, ASK) primarily detect gustatory compounds, although ASH and ADL also detect some volatile odorants[6,111]. Of the remaining four amphid neuron pairs with cilia embedded within the glial sheath layer, three (AWA, AWB, AWC) function to detect volatile odors[6,106,111]. AFD is the only amphid sensory neuron that has not been implicated in chemosensation, possibly due to its specialized role in thermosensation as described previously. There are three separate modes of activation that chemosensory neurons may exhibit in response to a compound: ON, OFF, and ON/OFF[49,111,115–119]. ON and OFF responses consist of transient calcium increases when chemical concentration increases or decreases, respectively[114–117,120]. ON/OFF responses occur when a neuron exhibits a transient calcium increase when chemical concentration either increases or decreases (termed a biphasic response)[111,118–120]. Electrophysiology has confirmed a handful of chemosensory responses, including alkaline pH sensing in ASH, AWA responses to the volatile odorant diacetyl, and ASE salt-sensitivity[121–123].

With over 1000 GPCRs encoded in the *C. elegans* genome, we have only begun to scratch the surface of pairing each chemical with their associated receptor(s). A total

of 6 chemical ligands (nonpheromones) have been paired with their chemosensory

receptor in *C. elegans*[111]. Fortunately, the signaling cascades downstream of

chemosensory receptors appear to depend on one of two signal transduction

mechanisms: TAX-2/TAX-4 CNG channels via cGMP, or OSM/OCR-2 TRPV

channels[106]. Of note, while GPCRs can function upstream of guanylyl cyclases (GCYs),

GCYs may also directly bind chemical ligands in some scenarios[111].

Conclusions

In conclusion, the *C. elegans* chemosensory system detects a wide array of

olfactory and gustatory cues. This guides *C. elegans* decision making to determine

behavioral responses to external stimuli. For instance, chemosensory signals can

inform worms as to the presence and quality of a potential food source, or avoid

dangers such as harmful environments, pathogens and predators. Signal transduction

of chemicals is highly conserved with other sensory modalities, implicating CNG and

TRPV channels as important molecules for amplifying sensory signals in the nervous

system.

1.7 Photosensation in *C. elegans*

Introduction

Light sensation is an evolutionarily conserved phenomenon that can be traced

back to the most primitive lifeforms present in ancient fossils. Detection of light cues

allows for organisms to receive critical information about the surrounding environment

that enhances survival. While photosensitive organisms exist across phylogeny, animals

lacking traditional light-sensing organs and living in dark environments were assumed to have lost light-sensitivity over the course of evolution. Surprisingly, despite living in the dark and lacking eyes, the nematode *C. elegans* was discovered to sense short wavelength light through a novel photoreceptor *lite-1* unlike any other known photoreceptor in nature. Here, we review the known behavioral, cellular and molecular mechanisms of photosensation in *C. elegans*.

Mechanisms of photosensation in *C. elegans*

In 2008, rigorous investigation revealed that that despite lacking eyes, *C. elegans* can indeed sense light[124,125]. *C. elegans* light-sensing capabilities were discovered through a series of behavioral tests observing that worms exhibit negative phototaxis, or an escape behavior, in the presence of short wavelength light[124,125]. Discrete illumination of ultraviolet light at various regions along the body revealed that when focused at the head, worms reverse backwards, whereas light aimed at the tail stimulates forward locomotion[124,125]. Entire body illumination results in an immediate initiation of backward locomotion (reversal) immediately followed by accelerated forward locomotion to escape from the stimulus[125]. Phototaxis behavior increases as wavelength decreased, showing the highest sensitivities to UV-A light (long ultraviolet; 350 ± 25 nm) followed by violet (435 ± 10 nm) and blue light (470 ± 20 nm)[124]. A steep drop-off in avoidance was observed at longer wavelengths, with near insensitivity at green (500 ± 10 nm) and yellow (575 ± 25 nm) wavelengths[124]. This indicates that *C. elegans* phototaxis is attuned to detect and respond to short wavelengths of light (UV-A, violet, and blue).

In addition to wavelength specificity, the phototaxis response also shows dose-dependency with the strength of phototaxis response (quantified by latency to respond and severity of the escape response) depending on the strength of the light intensity[124]. Dose-dependency analyses further confirm that *C. elegans* photosensation is selective towards short wavelengths, as little phototaxis response was observed in green and yellow wavelengths even at high intensities[124]. This finding also corroborates that light avoidance response is not due to heat, as green and yellow light produce more heat than lower wavelengths, yet do not stimulate the phototaxis response.

The consequence of phototaxis behaviors is that upon detecting light, *C. elegans* executes behavioral responses to escaping from the light source to return to their preferred dark environment. Blue violet illumination of a small region on a crowded plate of worms containing many animals reveals that animals actively avoid the illuminated area, further supporting that phototaxis behaviors serve to provide an escape mechanism from light[125].

Light-sensing proteins, or photoreceptors, are largely divided into six well-characterized families: rhodopsins; phytochromes; photoactive yellow proteins (PYPs, also known as xanthopsins); cryptochromes; phototropins; and blue-light using flavin (BLUF) proteins[126]. These photoreceptors are comprised of two components: the host protein and a light-absorbing prosthetic chromophore[127,128]. While there is rich diversity in photoreceptor sensitivity, structure, and biophysical properties, there are just four known partner chromophores[128–130]. Of these six classic photoreceptor families, metazoans are known to possess only two: rhodopsins and cryptochromes[127,128]. Paradoxically, despite sensing light, the *C. elegans* genome does not encode any

closely related homologs of known photoreceptor genes[125,131]. This suggests that *C. elegans* senses light through an unknown photoreceptor class, representing a new family of photoreceptor proteins in metazoa.

Forward genetic screens for mutants defective in phototaxis behavior isolated multiple strains with mutant alleles in a single gene subsequently named *lite-1*[125,131]. *lite-1* encodes a seven transmembrane (7-TM) receptor-like protein and is related to the invertebrate gustatory receptor (GR) family[125,131]. *lite-1* was shown to be required for UV-induced light avoidance[125,131]. While attempts to examine the function of LITE-1 in heterologous systems failed, ectopic expression of LITE-1 confers photosensitivity to photo-insensitive cells in the worm[125,131]. For example, ectopic expression of LITE-1 in the body-wall muscle induces contraction in response to UV-light[125,131].

While genetic screens were successful at cloning LITE-1 and identifying it as necessary for *C. elegans* photosensation, there was still insufficient evidence to assert LITE-1 as a *bona fide* photoreceptor. For instance, UV illumination generates ROS such as H_2O_2, which also results in avoidance behaviors similar to the phototaxis response[132]. Also, as a member of the GR family of receptors, it would not be surprising if LITE-1 functioned as a chemoreceptor. This suggests a model where instead of functioning as a photoreceptor, LITE-1 instead senses light-produced chemicals[132].

Opsins are the only known classic photoreceptors which also have 7-TM domains, yet sequence comparison of both LITE-1 and opsins show no significant homology between the two[125,131]. Interestingly, LITE-1 was found to possess a reversed membrane topology compared to conventional 7-TM receptors, with an external C-terminus and internal N-terminus[133]. This inverted topology is also observed in 7-TM insect GR and OR

(olfactory receptor) members[134,135]. Thus, LITE-1 does not appear to be related to any known photoreceptors.

Classification of a protein as a receptor versus sensor requires careful consideration as to whether it functions to merely detect the stimulus (receptor), or also report the activity by exerting an output (sensor). In order to classify LITE-1 as a *bona fide* light sensor, evidence must show that LITE-1 is capable of capturing photons[127,128]. Purification and spectrophotometry analysis of LITE-1 from *C. elegans* lysate revealed it to have an exceptionally high efficiency in photon absorption, with the ability to absorb both UVA (320 nm) and UVB (280nm) light with an extinction coefficient 10-100 times higher than all known photoreceptors[133]. Surprisingly, LITE-1 lacks a prosthetic chromophore and instead relies on its protein confirmation for photon absorption[133]. Rather, two tryptophan residues present in the transmembrane domain regions were found to be required for LITE-1's absorption of both UVA and UVB light[133]. Missense mutations in LITE-1 identified from genetic screens for UVA avoidance eliminated UVA but not UVB absorption, suggesting that UVA and UVB absorption can be separated and demonstrating specificity in the LITE-1 light absorption[133].

Together, these results reveal LITE-1 as a *bona fide* photoreceptor that senses both UVA and UVB light. As such, LITE-1 possesses several unique properties differentiating it from any other known photoreceptor in nature. The photoreceptor classification of LITE-1 does not rule out the possibility that it also senses additional cues such as light-produced chemicals, as some photoreceptors have been shown to be multifunctional, such as *Drosophila* rhodopsin also functioning as a heat sensor[136]. Many questions remain to be addressed regarding LITE-1's curious photoreceptor properties.

For instance, why isn't a prosthetic chromophore necessary? How can LITE-1 achieve such high photon absorption? Detailed structural understanding may be necessary to answer these questions.

Identification of photoreceptor cells was performed via cell ablation experiments where combinations of amphid sensory neurons were killed and phototaxis behavior was examined[124]. Combined ablation of seven pairs of amphid neurons (ASJ, AWB, ASK, ASH, ASI, AWC and ADL) abolished light avoidance in wildtype animals[124]. This list was further narrowed down with differing combinations of neuronal ablation, ultimately revealing four pairs of sensory neurons (ASJ, ASK, AWB and ASH) that when simultaneously were shown to abolish head-avoidance phototaxis, suggesting them as photoreceptor cells[124]. Differing combinations or ablation either together or individually did not result in defective phototaxis, suggesting functional redundancy in the nervous system to mediate phototactic responses[124].

In determining the downstream phototransduction pathway, CNG channels represent strong candidates as they are required for vertebrate phototransduction and are conserved in the *C. elegans* genome[137]. Indeed, loss of the CNG channel *tax-2* resulted in loss of head-avoidance phototaxis[124]. Importantly, functional rescue of *tax-2* genomic DNA under its own promoter as well as individually in ASJ, ASK, or AWB neurons restored the phototaxis response, indicating that CNG channel mediated phototransduction mechanisms are conserved in these neurons[124]. As rescue of *tax-2* in ASJ resulted in the highest restoration of phototaxis among the three candidate photoreceptor cells, phototransduction mechanisms were further characterized in detail in this neuron[124,131].

Recording cellular activity in response to light provides the most direct evidence that a neuron functions as a photoreceptor. The sensory neuron ASJ was the first confirmed photosensory neuron in the worm as verified using whole-cell electrophysiology recordings showing that light evokes an inward current in ASJ[124]. Initial work confirmed that the ASJ photocurrent is dependent on the CNG channel *tax-2* and cGMP signaling, similar to vertebrate phototransduction mechanisms[124].

The molecular mechanisms of ASJ phototransduction were later confirmed to require the photoreceptor LITE-1, and functional rescue specifically in ASJ is sufficient to rescue the photocurrent[131]. G protein signaling downstream of LITE-1 is required for phototransduction (through redundant functions of $G_{i/o}$ proteins GOA-1 and GPA-3)[131]. Unlike vertebrate phototransduction, however, PDEs are not required for *C. elegans* phototransduction, as loss of known PDEs did not lead to any reduction in the ASJ photocurrent but rather potentiated the response with a current density up to five-fold greater than wildtype[131,137]. This suggests a distinct mechanism from PDE-dependent phototransduction in vertebrates where light induce PDE-dependent inhibition (rods and cones) or activation (parietal eyes) of CNG channels[137].

If regulation of PDE activity is not required for ASJ phototransduction, how is light inducing CNG channel activation in ASJ? Guanylate cyclases present likely candidates as they function to generate cGMP from GTP. There are two membrane-bound guanylate cyclases expressed in ASJ, ASK, and AWB (*daf-11* and *odr-1)*[131]. Indeed, loss of function of either *daf-11* or *odr-1* significantly reduced the photocurrent in ASJ, indicating that guanylate cyclases are required for ASJ phototransduction[131]. Several lines of evidence suggest that guanylate cyclases function downstream of G proteins to

mediate CNG channel activation: 1. Direct application of cGMP induces inward currents in ASJ even in the presence of $G_{i/o}$ inhibitor pertussis toxin (PTX), 2. Activation of G proteins via GTPγS failed to stimulate CNG channels in ASJ in *daf-11* mutants, 3. Application of cGMP could still effectively stimulate CNG channels in ASJ in *daf-11* mutants[131]. Together, these findings suggest the following model of phototranduction in ASJ: light activates the photoreceptor LITE-1, leading to activation of $G_{i/o}$ proteins, in turn stimulating guanylate cyclases which act to increase cGMP, leading to CNG channel activation (Figure 1.6.)[131].
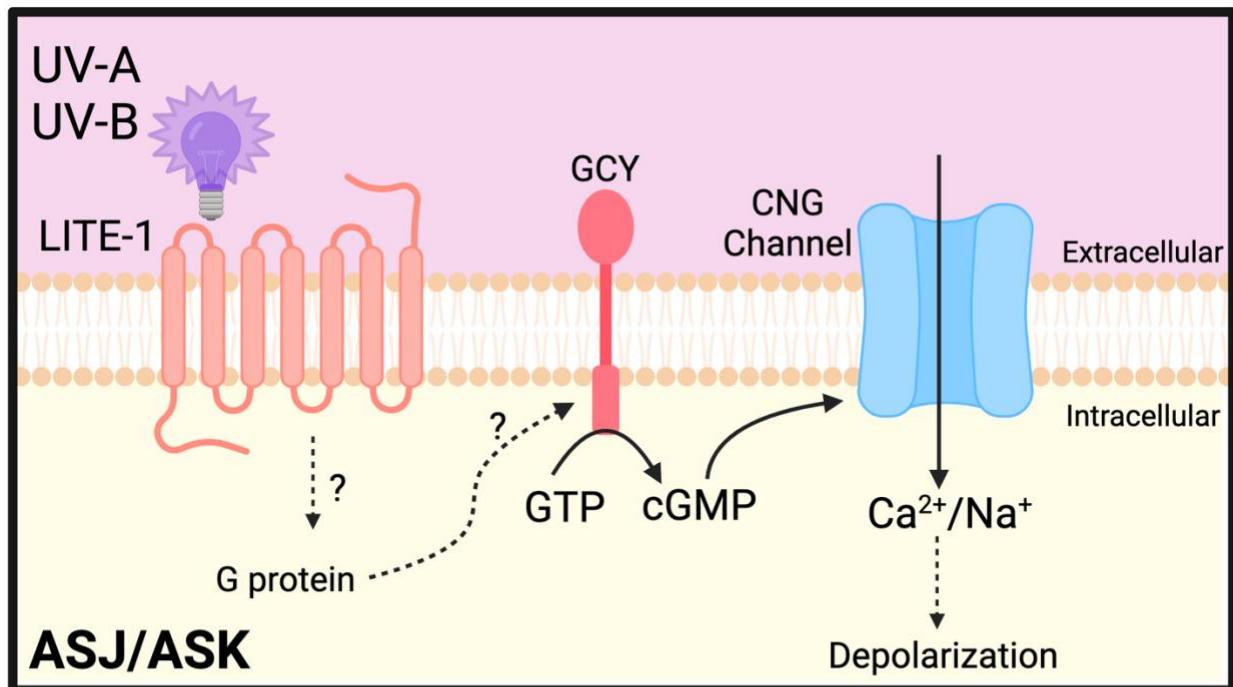
Figure 1.6. Phototransduction Cascade in ASJ/ASK sensory neurons
UV-A/UV-B light activates the photoreceptor LITE-1, leading to activation of G proteins via unknown mechanisms. G proteins lead to activation of GCYs that catalyze conversion of GTP to cGMP. Next, cGMP binds CNG channels in the plasma membrane to allow influx of calcium and sodium ions. This leads to neuronal excitation and the phototaxis response. Model made with *Biorender.*

Initial ablation experiments revealed ASH to be required for phototaxis in addition to ASJ, ASK, and AWB[124]. ASH is not known to express guanylate cyclases or utilize cGMP signal transduction, suggesting that photosensation in ASH must be transduced through a different, unknown mechanism.

Having shown that LITE-1 functions as a photoreceptor to mediate phototaxis behavior in *C. elegans,* the question remains as to how LITE-1 functions[133]. With no similar homology to known photoreceptors and lacking a chromophore, LITE-1 must exhibit a unique mechanism of activation. Despite some evidence shedding glimpses into the receptor properties of LITE-1, its exact classification is still unclear. LITE-1 has an inverted membrane topology indicating it does not function as a classic GPCR, although this does not rule out that it may still possess GPCR activity[133]. Thus it is unclear whether G proteins directly or indirectly binds with LITE-1 to modulate guanylate cyclases in ASJ.

Electrophysiology recordings in photosensory neurons reveal that LITE-1 mediated light responses show a long delay (100-400 ms latency), suggesting that the major current in the cell is mediated by a downstream signaling pathway mediated by CNG channels[124,131]. Nevertheless, it is possible that a small current escaping immediate detection is present, and this response could be amplified by downstream signaling, which could include G proteins and cGMP. A similar phenomenon is observed in *Drosophila* olfactory neurons where ionotropic signal amplification occurs downstream of olfactory receptors via epithelial sodium channels (ENaC)[138]. While it cannot be ruled out that LITE-1 may have ion channel activity, evidence suggests that

the major cellular responses are mediated by downstream transduction mechanisms at least in ASJ and ectopically in the body-wall muscle[124,125,131].

While laser ablation experiments reveal that LITE-1 functions in many sensory neurons, the complete expression pattern for LITE-1 is still not fully known. Antibody staining has failed to produce reliable results, likely due at least in part to variations in protein expression level[125,131,133].

lite-1 lies within a large and complex operon and transgenic approaches have been largely unsuccessful at revealing its true expression pattern due to highly variable results ranging from 2 to 29 cells[131,125]. These expression patterns are highly inconsistent with reported LITE-1 function. For instance, the touch receptor neurons (TRNs) ALM and PLM are reported to exhibit blue light activation that depends on *lite-1* despite the lack of transgenic reports showing that they functionally express *lite-1*[139]. Conversely, the sensory neuron ASI has been reported to express *lite-1* yet does not exhibit any photoactivation[124,132]. Complicating this further, overexpressing *lite-1* in ASI induces light sensitivity[131]. Transgenic expression reports as well as recent single-cell RNA-sequencing profiling suggest *lite-1* expression in many non-neuronal cells (e.g., hypoderm and socket cells) as well as interneurons (i.e., AVA, AVB, RIM) with no known light-dependent functions[132]. This may suggest that *lite-1* has additional, unknown physiological functions in addition to sensing light.

Conclusions

In conclusion, the eyeless nematode *C. elegans* is able to sense and respond to light in order to survive. Light avoidance is mediated by the gustatory receptor LITE-1,

representing a new type of short-wavelength photoreceptor unlike any other observed in nature. LITE-1 adopts an inversed membrane topology, suggesting it functions unlike traditional GPCRs. The receptor properties of LITE-1 remain to be elucidated. For example, does LITE-1 possess intrinsic GPCR activity, and if so, how? If not, how does it couple to G proteins downstream to mediate its responses in photoreceptor cells? Does LITE-1 possess ion channel functions? Answers to these questions may lie in a detailed structural analysis of LITE-1. The absence of CNG channels in some LITE-1 expressing neurons such as ASH indicates that additional unknown phototransduction mechanisms must exist.

1.8 Closing remarks

This dissertation is centered on uncovering novel mechanisms of sensation using *C. elegans*. Most of the major sensory modalities present in vertebrates (touch, temperature, taste/smell, and light) show remarkable conservation in *C. elegans,* as discussed above. Here, we outline discoveries in two major sensory modalities. In Chapter 2, we identify a novel evolutionarily conserved cold receptor and uncover the downstream signaling mechanisms leading to cold-induced neuronal activation[140]. In Chapter 3, we show for the first time that *C. elegans* detect airborne vibrations (sound), revealing the unexpected presence of this sensory modality in lower phyla[141]. The findings of this dissertation work shed insight into novel evolutionarily conserved mechanisms of sensation at the molecular, cellular, circuit, and behavioral levels.

References

1. Bretscher, M. S. & Mitchison, G. Francis Harry Compton Crick OM. 8 June 1916 — 28 July 2004. *Biogr. Mem. Fellows R. Soc.* **63**, 159–196 (2017).

2. Dahm, R. Discovering DNA: Friedrich Miescher and the early years of nucleic acid research. *Hum. Genet.* **122**, 565–581 (2008).

3. Watson, J. D. & Crick, F. H. Molecular structure of nucleic acids: a structure for deoxyribose nucleic acid. J.D. Watson and F.H.C. Crick. Published in Nature, number 4356 April 25, 1953. *Nature* **248**, 765 (1974).

4. Goldstein, B. Sydney Brenner on the Genetics of *Caenorhabditis elegans*. *Genetics* **204**, 1–2 (2016).

5. Iliff, A. J. & Xu, X. Z. S. *C. elegans:* a sensible model for sensory biology. *J. Neurogenet.* **34**, 347–350 (2020).

6. Riddle, D. L., Blumenthal, T., Meyer, B. J. & Priess, J. R. *C. elegans II. 2nd edition.* (Cold Spring Harbor (NY): Cold Spring Harbor Laboratory Press, 1997).

7. Brenner, S. THE GENETICS OF *CAENORHABDITIS ELEGANS*. *Genetics* **77**, 71–94 (1974).

8. White, J. G., Southgate, E., Thomson, J. N. & Brenner, S. The structure of the nervous system of the nematode Caenorhabditis elegans. *Philos. Trans. R. Soc. Lond. B. Biol. Sci.* **314**, 1–340 (1986).

9. Allen, E. N., Ren, J., Zhang, Y. & Alcedo, J. Sensory systems: their impact on C. elegans survival. *Neuroscience* **296**, 15–25 (2015).

10. Brenner, S. The genetics of behaviour. *Br. Med. Bull.* **29**, 269–271 (1973).

11. Corsi, A. K., Wightman, B. & Chalfie, M. A Transparent Window into Biology: A Primer on *Caenorhabditis elegans*. *Genetics* **200**, 387–407 (2015).

12. Xiao, R., Liu, J. & Xu, X. Z. S. Thermosensation and longevity. *J. Comp. Physiol. A Neuroethol. Sens. Neural. Behav. Physiol.* **201**, 857–867 (2015).

13. Miska, E. A. & Rechavi, O. Can brain activity transmit transgenerationally? in *Current Topics in Developmental Biology* vol. 144 1–18 (Elsevier, 2021).

14. Rechavi, O. Transgenerational Inheritance: That Pathogen Gut Feeling. *Curr. Biol. CB* **30**, R1486–R1488 (2020).

15. Azevedo, F. A. C. *et al.* Equal numbers of neuronal and nonneuronal cells make the human brain an isometrically scaled-up primate brain. *J. Comp. Neurol.* **513**, 532–541 (2009).

16. Herculano-Houzel, S. The human brain in numbers: a linearly scaled-up primate brain. *Front. Hum. Neurosci.* **3**, 31 (2009).

17. Goodman, M. B. & Sengupta, P. How *Caenorhabditis elegans* Senses Mechanical Stress, Temperature, and Other Physical Stimuli. *Genetics* **212**, 25–51 (2019).

18. Colbert, H. A. & Bargmann, C. I. Environmental signals modulate olfactory acuity, discrimination, and memory in Caenorhabditis elegans. *Learn. Mem.* **4**, 179–191 (1997).

19. Hobert, O. The neuronal genome of Caenorhabditis elegans. *WormBook* 1–106 (2013) doi:10.1895/wormbook.1.161.1.

20. Z.F. Altun & Hall, D. H. Nervous system, general description. *In WormAtlas* doi:10.3908/wormatlas.1.18.

21. Ward, S., Thomson, N., White, J. G. & Brenner, S. Electron microscopical reconstruction of the anterior sensory anatomy of the nematode Caenorhabditis elegans.?2UU. *J. Comp. Neurol.* **160**, 313–337 (1975).

22. Perkins, L. A., Hedgecock, E. M., Thomson, J. N. & Culotti, J. G. Mutant sensory cilia in the nematode Caenorhabditis elegans. *Dev. Biol.* **117**, 456–487 (1986).

23. Hall, D. H., Lints, R. & Altun, Z. Nematode neurons: anatomy and anatomical methods in Caenorhabditis elegans. *Int. Rev. Neurobiol.* **69**, 1–35 (2006).

24. Inglis, P. N., Ou, G., Leroux, M. R. & Scholey, J. M. *The sensory cilia of Caenorhabditis elegans. WormBook: The Online Review of C. elegans Biology [Internet]* (WormBook, 2018).

25. Chalfie, M. *et al.* The neural circuit for touch sensitivity in Caenorhabditis elegans. *J. Neurosci. Off. J. Soc. Neurosci.* **5**, 956–964 (1985).

26. Chalfie, M. & Sulston, J. Developmental genetics of the mechanosensory neurons of Caenorhabditis elegans. *Dev. Biol.* **82**, 358–370 (1981).

27. Chalfie, M. & Au, M. Genetic control of differentiation of the Caenorhabditis elegans touch receptor neurons. *Science* **243**, 1027–1033 (1989).

28. Touch. in *Biology of Sensory Systems* 99–121 (John Wiley & Sons, Ltd, 2009). doi:10.1002/9780470694374.ch8.

29. Petzold, B. C. *et al.* Caenorhabditis elegans Body Mechanics Are Regulated by Body Wall Muscle Tone. *Biophys. J.* **100**, 1977–1985 (2011).

30. Du, H., Gu, G., William, C. M. & Chalfie, M. Extracellular proteins needed for C. elegans mechanosensation. *Neuron* **16**, 183–194 (1996).

31. Emtage, L., Gu, G., Hartwieg, E. & Chalfie, M. Extracellular proteins organize the mechanosensory channel complex in C. elegans touch receptor neurons. *Neuron* **44**, 795–807 (2004).

32. Chalfie, M. & Thomson, J. N. Organization of neuronal microtubules in the nematode Caenorhabditis elegans. *J. Cell Biol.* **82**, 278–289 (1979).

33. Chalfie, M. & Thomson, J. N. Structural and functional diversity in the neuronal microtubules of Caenorhabditis elegans. *J. Cell Biol.* **93**, 15–23 (1982).

34. Fukushige, T. *et al.* MEC-12, an alpha-tubulin required for touch sensitivity in C. elegans. *J. Cell Sci.* **112 (Pt 3)**, 395–403 (1999).

35. Li, W., Kang, L., Piggott, B. J., Feng, Z. & Xu, X. Z. S. The neural circuits and sensory channels mediating harsh touch sensation in Caenorhabditis elegans. *Nat. Commun.* **2**, 315 (2011).

36. Leifer, A. M., Fang-Yen, C., Gershow, M., Alkema, M. J. & Samuel, A. D. T. Optogenetic manipulation of neural activity in freely moving Caenorhabditis elegans. *Nat. Methods* **8**, 147–152 (2011).

37. Stirman, J. N. *et al.* Real-time multimodal optical control of neurons and muscles in freely behaving Caenorhabditis elegans. *Nat. Methods* **8**, 153–158 (2011).

38. Eastwood, A. L. *et al.* Tissue mechanics govern the rapidly adapting and symmetrical response to touch. *Proc. Natl. Acad. Sci. U. S. A.* **112**, E6955-6963 (2015).

39. Suzuki, H. *et al.* In vivo imaging of C. elegans mechanosensory neurons demonstrates a specific role for the MEC-4 channel in the process of gentle touch sensation. *Neuron* **39**, 1005–1017 (2003).

40. Nekimken, A. L. *et al.* Pneumatic stimulation of C. elegans mechanoreceptor neurons in a microfluidic trap. *Lab. Chip* **17**, 1116–1127 (2017).

41. Sato, M. Response of Pacinian corpuscles to sinusoidal vibration. *J. Physiol.* **159**, 391–409 (1961).

42. Loewenstein, W. R. & Mendelson, M. COMPONENTS OF RECEPTOR ADAPTATION IN A PACINIAN CORPUSCLE. *J. Physiol.* **177**, 377–397 (1965).

43. Transducing Touch in Caenorhabditis elegans | Annual Review of Physiology. https://www-annualreviews-org.proxy.lib.umich.edu/doi/10.1146/annurev.physiol.65.092101.142659.

44. Lu, Y. *et al.* The ion channel ASIC2 is required for baroreceptor and autonomic control of the circulation. *Neuron* **64**, 885–897 (2009).

45. Wetzel, C. *et al.* A stomatin-domain protein essential for touch sensation in the mouse. *Nature* **445**, 206–209 (2007).

46. Kaplan, J. M. & Horvitz, H. R. A dual mechanosensory and chemosensory neuron in Caenorhabditis elegans. *Proc. Natl. Acad. Sci. U. S. A.* **90**, 2227–2231 (1993).

47. Bounoutas, A. & Chalfie, M. Touch sensitivity in Caenorhabditis elegans. *Pflugers Arch.* **454**, 691–702 (2007).

48. Kindt, K. S., Tam, T., Whiteman, S. & Schafer, W. R. Serotonin promotes G(o)-dependent neuronal migration in Caenorhabditis elegans. *Curr. Biol. CB* **12**, 1738–1747 (2002).

49. Hilliard, M. A. *et al.* In vivo imaging of C. elegans ASH neurons: cellular response and adaptation to chemical repellents. *EMBO J.* **24**, 63–72 (2005).

50. Geffeney, S. L. *et al.* DEG/ENaC but Not TRP Channels Are the Major Mechanoelectrical Transduction Channels in a C. elegans Nociceptor. *Neuron* **71**, 845–857 (2011).

51. Ding, G. *et al.* In vivo tactile stimulation-evoked responses in Caenorhabditis elegans amphid sheath glia. *PloS One* **10**, e0117114 (2015).

52. Kang, L., Gao, J., Schafer, W. R., Xie, Z. & Xu, X. Z. S. C. elegans TRP Family Protein TRP-4 Is a Pore-Forming Subunit of a Native Mechanotransduction Channel. *Neuron* **67**, 381–391 (2010).

53. Chatzigeorgiou, M. & Schafer, W. R. Lateral Facilitation between Primary Mechanosensory Neurons Controls Nose Touch Perception in C. elegans. *Neuron* **70**, 299–309 (2011).

54. Hart, A. C., Sims, S. & Kaplan, J. M. Synaptic code for sensory modalities revealed by C. elegans GLR-1 glutamate receptor. *Nature* **378**, 82–85 (1995).

55. Sanders, J. *et al.* The Caenorhabditis elegans interneuron ALA is (also) a high-threshold mechanosensor. *BMC Neurosci.* **14**, 156 (2013).

56. Li, W., Feng, Z., Sternberg, P. W. & Shawn Xu, X. Z. A C. elegans stretch receptor neuron revealed by a mechanosensitive TRP channel homologue. *Nature* **440**, 684–687 (2006).

57. Samuel, A. D. T. & Sengupta, P. Sensorimotor integration: locating locomotion in neural circuits. *Curr. Biol. CB* **15**, R341-343 (2005).

58. Albeg, A. *et al.* C. elegans multi-dendritic sensory neurons: morphology and function. *Mol. Cell. Neurosci.* **46**, 308–317 (2011).

59. Yeon, J. *et al.* A sensory-motor neuron type mediates proprioceptive coordination of steering in C. elegans via two TRPC channels. *PLoS Biol.* **16**, e2004929 (2018).

60. Zhang, H. *et al.* OSM-9 and an amiloride-sensitive channel, but not PKD-2, are involved in mechanosensation in C. elegans male ray neurons. *Sci. Rep.* **8**, 7192 (2018).

61. Anderson, J. L., Albergotti, L., Ellebracht, B., Huey, R. B. & Phillips, P. C. Does thermoregulatory behavior maximize reproductive fitness of natural isolates of Caenorhabditis elegans? *BMC Evol. Biol.* **11**, 157 (2011).

62. Schulenburg, H. & Félix, M.-A. The Natural Biotic Environment of Caenorhabditis elegans. *Genetics* **206**, 55–86 (2017).

63. Luo, L., Clark, D. A., Biron, D., Mahadevan, L. & Samuel, A. D. T. Sensorimotor control during isothermal tracking in Caenorhabditis elegans. *J. Exp. Biol.* **209**, 4652–4662 (2006).

64. Ramot, D., MacInnis, B. L. & Goodman, M. B. Bidirectional temperature-sensing by a single thermosensory neuron in C. elegans. *Nat. Neurosci.* **11**, 908–915 (2008).

65. Hedgecock, E. M. & Russell, R. L. Normal and mutant thermotaxis in the nematode Caenorhabditis elegans. *Proc. Natl. Acad. Sci. U. S. A.* **72**, 4061–4065 (1975).

66. Xiao, R. & Xu, X. Z. S. Temperature Sensation: From Molecular Thermosensors to Neural Circuits and Coding Principles. *Annu. Rev. Physiol.* **83**, 205–230 (2021).

67. Goodman, M. B. Thermotaxis navigation behavior. *WormBook* 1–10 (2014) doi:10.1895/wormbook.1.168.1.

68. Mori, I. & Ohshima, Y. Neural regulation of thermotaxis in Caenorhabditis elegans. *Nature* **376**, 344–348 (1995).

69. Ramot, D., MacInnis, B. L., Lee, H.-C. & Goodman, M. B. Thermotaxis is a Robust Mechanism for Thermoregulation in Caenorhabditis elegans Nematodes. *J. Neurosci.* **28**, 12546–12557 (2008).

70. Biron, D. *et al.* A diacylglycerol kinase modulates long-term thermotactic behavioral plasticity in C. elegans. *Nat. Neurosci.* **9**, 1499–1505 (2006).

71. Ryu, W. S. & Samuel, A. D. T. Thermotaxis in Caenorhabditis elegans Analyzed by Measuring Responses to Defined Thermal Stimuli. *J. Neurosci.* **22**, 5727–5733 (2002).

72. Clark, D. A., Gabel, C. V., Gabel, H. & Samuel, A. D. T. Temporal Activity Patterns in Thermosensory Neurons of Freely Moving Caenorhabditis elegans Encode Spatial Thermal Gradients. *J. Neurosci.* **27**, 6083–6090 (2007).

73. Yamada, Y. & Ohshima, Y. Distribution and movement of Caenorhabditis elegans on a thermal gradient. *J. Exp. Biol.* **206**, 2581–2593 (2003).

74. Luo, L. *et al.* Bidirectional thermotaxis in Caenorhabditis elegans is mediated by distinct sensorimotor strategies driven by the AFD thermosensory neurons. *Proc. Natl. Acad. Sci. U. S. A.* **111**, 2776–2781 (2014).

75. Kimura, K. D., Miyawaki, A., Matsumoto, K. & Mori, I. The C. elegans Thermosensory Neuron AFD Responds to Warming. *Curr. Biol.* **14**, 1291–1295 (2004).

76. Kobayashi, K. *et al.* Single-Cell Memory Regulates a Neural Circuit for Sensory Behavior. *Cell Rep.* **14**, 11–21 (2016).

77. Biron, D., Wasserman, S., Thomas, J. H., Samuel, A. D. T. & Sengupta, P. An olfactory neuron responds stochastically to temperature and modulates Caenorhabditis elegans thermotactic behavior. *Proc. Natl. Acad. Sci.* **105**, 11002–11007 (2008).

78. Kuhara, A., Ohnishi, N., Shimowada, T. & Mori, I. Neural coding in a single sensory neuron controlling opposite seeking behaviours in Caenorhabditis elegans. *Nat. Commun.* **2**, 355 (2011).

79. Beverly, M., Anbil, S. & Sengupta, P. Degeneracy and Neuromodulation among Thermosensory Neurons Contribute to Robust Thermosensory Behaviors in Caenorhabditis elegans. *J. Neurosci.* **31**, 11718–11727 (2011).

80. Gray, J. M., Hill, J. J. & Bargmann, C. I. A circuit for navigation in Caenorhabditis elegans. *Proc. Natl. Acad. Sci.* **102**, 3184–3191 (2005).

81. Wakabayashi, T., Kitagawa, I. & Shingai, R. Neurons regulating the duration of forward locomotion in Caenorhabditis elegans. *Neurosci. Res.* **50**, 103–111 (2004).

82. Tsalik, E. L. & Hobert, O. Functional mapping of neurons that control locomotory behavior in Caenorhabditis elegans. *J. Neurobiol.* **56**, 178–197 (2003).

83. Ohnishi, K. *et al.* OSM-9 and OCR-2 TRPV channels are accessorial warm receptors in Caenorhabditis elegans temperature acclimatisation. *Sci. Rep.* **10**, 18566 (2020).

84. *WormBook.* (WormBook, 2018).

85. Narayan, A., Laurent, G. & Sternberg, P. W. Transfer characteristics of a thermosensory synapse in Caenorhabditis elegans. *Proc. Natl. Acad. Sci. U. S. A.* **108**, 9667–9672 (2011).

86. Ikeda, M. *et al.* Context-dependent operation of neural circuits underlies a navigation behavior in *Caenorhabditis elegans*. *Proc. Natl. Acad. Sci.* **117**, 6178–6188 (2020).

87. Hawk, J. D. *et al.* Integration of Plasticity Mechanisms within a Single Sensory Neuron of C. elegans Actuates a Memory. *Neuron* **97**, 356-367.e4 (2018).

88. Yu, S., Avery, L., Baude, E. & Garbers, D. L. Guanylyl cyclase expression in specific sensory neurons: a new family of chemosensory receptors. *Proc. Natl. Acad. Sci. U. S. A.* **94**, 3384–3387 (1997).

89. Inada, H. *et al.* Identification of Guanylyl Cyclases That Function in Thermosensory Neurons of *Caenorhabditis elegans*. *Genetics* **172**, 2239–2252 (2006).

90. Ortiz, C. O. *et al.* Searching for neuronal left/right asymmetry: genomewide analysis of nematode receptor-type guanylyl cyclases. *Genetics* **173**, 131–149 (2006).

91. Coburn, C. M., Mori, I., Ohshima, Y. & Bargmann, C. I. A cyclic nucleotide-gated channel inhibits sensory axon outgrowth in larval and adult Caenorhabditis elegans: a distinct pathway for maintenance of sensory axon structure. *Dev. Camb. Engl.* **125**, 249–258 (1998).

92. Dusenbery, D. B., Sheridan, R. E. & Russell, R. L. Chemotaxis-defective mutants of the nematode Caenorhabditis elegans. *Genetics* **80**, 297–309 (1975).

93. Wasserman, S. M., Beverly, M., Bell, H. W. & Sengupta, P. Regulation of Response Properties and Operating Range of the AFD Thermosensory Neurons by cGMP Signaling. *Curr. Biol.* **21**, 353–362 (2011).

94. Takeishi, A. *et al.* Receptor-type Guanylyl Cyclases Confer Thermosensory Responses in C. elegans. *Neuron* **90**, 235–244 (2016).

95. Wang, D., O'Halloran, D. & Goodman, M. B. GCY-8, PDE-2, and NCS-1 are critical elements of the cGMP-dependent thermotransduction cascade in the AFD neurons responsible for C. elegans thermotaxis. *J. Gen. Physiol.* **142**, 437–449 (2013).

96. Liu, S., Schulze, E. & Baumeister, R. Temperature- and Touch-Sensitive Neurons Couple CNG and TRPV Channel Activities to Control Heat Avoidance in Caenorhabditis elegans. *PLoS ONE* **7**, e32360 (2012).

97. Wittenburg, N. & Baumeister, R. Thermal avoidance in Caenorhabditis elegans: an approach to the study of nociception. *Proc. Natl. Acad. Sci. U. S. A.* **96**, 10477–10482 (1999).

98. Glauser, D. A. *et al.* Heat Avoidance Is Regulated by Transient Receptor Potential (TRP) Channels and a Neuropeptide Signaling Pathway in *Caenorhabditis elegans*. *Genetics* **188**, 91–103 (2011).

99. Mohammadi, A., Byrne Rodgers, J., Kotera, I. & Ryu, W. S. Behavioral response of Caenorhabditis elegans to localized thermal stimuli. *BMC Neurosci.* **14**, 66 (2013).

100. Kuhn, M. Molecular Physiology of Membrane Guanylyl Cyclase Receptors. *Physiol. Rev.* **96**, 751–804 (2016).

101. Chatzigeorgiou, M. *et al.* Specific roles for DEG/ENaC and TRP channels in touch and thermosensation in C. elegans nociceptors. *Nat. Neurosci.* **13**, 861–868 (2010).

102. Husson, S. J. *et al.* Optogenetic Analysis of a Nociceptor Neuron and Network Reveals Ion Channels Acting Downstream of Primary Sensors. *Curr. Biol.* **22**, 743–752 (2012).

103. Conti, B. Considerations on Temperature, Longevity and Aging. *Cell. Mol. Life Sci.* **65**, 1626–1630 (2008).

104. Xiao, R. *et al.* A Genetic Program Promotes C. elegans Longevity at Cold Temperatures via a Thermosensitive TRP Channel. *Cell* **152**, 806–817 (2013).

105. Zhang, B. *et al.* Brain–gut communications via distinct neuroendocrine signals bidirectionally regulate longevity in *C. elegans*. *Genes Dev.* **32**, 258–270 (2018).

106. Bargmann, C. Chemosensation in C. elegans. *WormBook* (2006) doi:10.1895/wormbook.1.123.1.

107. Dusenbery, D. B. Countercurrent Separation: A New Method for Studying Behavior of Small Aquatic Organisms. *Proc. Natl. Acad. Sci. U. S. A.* **70**, 1349–1352 (1973).

108. Dusenbery, D. B. Analysis of chemotaxis in the nematode Caenorhabditis elegans by countercurrent separation. *J. Exp. Zool.* **188**, 41–47 (1974).

109. Ward, S. Chemotaxis by the nematode Caenorhabditis elegans: identification of attractants and analysis of the response by use of mutants. *Proc. Natl. Acad. Sci. U. S. A.* **70**, 817–821 (1973).

110. Sengupta, P., Chou, J. H. & Bargmann, C. I. odr-10 Encodes a Seven Transmembrane Domain Olfactory Receptor Required for Responses to the Odorant Diacetyl. *Cell* **84**, 899–909 (1996).

111. Ferkey, D. M., Sengupta, P. & L'Etoile, N. D. Chemosensory signal transduction in *Caenorhabditis elegans*. *Genetics* **217**, iyab004 (2021).

112. Pierce-Shimomura, J. T., Morse, T. M. & Lockery, S. R. The fundamental role of pirouettes in Caenorhabditis elegans chemotaxis. *J. Neurosci. Off. J. Soc. Neurosci.* **19**, 9557–9569 (1999).

113. Hart, A. Behavior. *WormBook* (2006) doi:10.1895/wormbook.1.87.1.

114.   Hilliard, M. A., Bargmann, C. I. & Bazzicalupo, P. C. elegans responds to chemical repellents by integrating sensory inputs from the head and the tail. *Curr. Biol. CB* **12**, 730–734 (2002).

115.   Tanimoto, Y. *et al.* Calcium dynamics regulating the timing of decision-making in C. elegans. *eLife* **6**, e21629 (2017).

116.   Liu, H. *et al.* Cholinergic Sensorimotor Integration Regulates Olfactory Steering. *Neuron* **97**, 390-405.e3 (2018).

117.   Thiele, T. R., Faumont, S. & Lockery, S. R. The neural network for chemotaxis to tastants in Caenorhabditis elegans is specialized for temporal differentiation. *J. Neurosci. Off. J. Soc. Neurosci.* **29**, 11904–11911 (2009).

118.   Chronis, N., Zimmer, M. & Bargmann, C. I. Microfluidics for in vivo imaging of neuronal and behavioral activity in Caenorhabditis elegans. *Nat. Methods* **4**, 727–731 (2007).

119.   Kato, S., Xu, Y., Cho, C. E., Abbott, L. F. & Bargmann, C. I. Temporal responses of C. elegans chemosensory neurons are preserved in behavioral dynamics. *Neuron* **81**, 616–628 (2014).

120.   Wang, W. *et al.* Off-response in ASH neurons evoked by CuSO4 requires the TRP channel OSM-9 in Caenorhabditis elegans. *Biochem. Biophys. Res. Commun.* **461**, 463–468 (2015).

121.   Wang, X., Li, G., Liu, J., Liu, J. & Xu, X. Z. S. TMC-1 Mediates Alkaline Sensation in C. elegans through Nociceptive Neurons. *Neuron* **91**, 146–154 (2016).

122.   Liu, Q., Kidd, P. B., Dobosiewicz, M. & Bargmann, C. I. C. elegans AWA Olfactory Neurons Fire Calcium-Mediated All-or-None Action Potentials. *Cell* **175**, 57-70.e17 (2018).

123.   Shindou, T. *et al.* Active propagation of dendritic electrical signals in C. elegans. *Sci. Rep.* **9**, 3430 (2019).

124.   Ward, A., Liu, J., Feng, Z. & Xu, X. Z. S. Light-sensitive neurons and channels mediate phototaxis in C. elegans. *Nat. Neurosci.* **11**, 916–922 (2008).

125.   Edwards, S. L. *et al.* A Novel Molecular Solution for Ultraviolet Light Detection in Caenorhabditis elegans. *PLoS Biol.* **6**, e198 (2008).

126.   van der Horst, M. A. & Hellingwerf, K. J. Photoreceptor Proteins, "Star Actors of Modern Times": A Review of the Functional Dynamics in the Structure of Representative Members of Six Different Photoreceptor Families. *Acc. Chem. Res.* **37**, 13–20 (2004).

127.   Wang, T. & Montell, C. Phototransduction and retinal degeneration in Drosophila. *Pflugers Arch.* **454**, 821–847 (2007).

128.   Yau, K.-W. & Hardie, R. C. Phototransduction motifs and variations. *Cell* **139**, 246–264 (2009).

129.   Falciatore, A. & Bowler, C. The Evolution and Function of Blue and Red Light Photoreceptors. in *Current Topics in Developmental Biology* vol. 68 317–350 (Elsevier, 2005).

130.   Radding, C. M. & Wald, G. Acid-base properties of rhodopsin and opsin. *J. Gen. Physiol.* **39**, 909–922 (1956).

131.   Liu, J. *et al.* C. elegans phototransduction requires a G protein–dependent cGMP pathway and a taste receptor homolog. *Nat. Neurosci.* **13**, 715–722 (2010).

132.   Bhatla, N. & Horvitz, H. R. Light and Hydrogen Peroxide Inhibit C. elegans Feeding through Gustatory Receptor Orthologs and Pharyngeal Neurons. *Neuron* **85**, 804–818 (2015).

133.   Gong, J. *et al.* The C. elegans Taste Receptor Homolog LITE-1 Is a Photoreceptor. *Cell* **167**, 1252-1263.e10 (2016).

134.   Benton, R., Sachse, S., Michnick, S. W. & Vosshall, L. B. Atypical membrane topology and heteromeric function of Drosophila odorant receptors in vivo. *PLoS Biol.* **4**, e20 (2006).

135.   Zhang, H.-J. *et al.* Topological and functional characterization of an insect gustatory receptor. *PloS One* **6**, e24111 (2011).

136.   Shen, W. L. *et al.* Function of rhodopsin in temperature discrimination in Drosophila. *Science* **331**, 1333–1336 (2011).

137.   Fu, Y. & Yau, K.-W. Phototransduction in mouse rods and cones. *Pflüg. Arch. - Eur. J. Physiol.* **454**, 805–819 (2007).

138.   Ng, R. *et al.* Amplification of Drosophila Olfactory Responses by a DEG/ENaC Channel. *Neuron* **104**, 947-959.e5 (2019).

139.   Nechipurenko, I. V. & Sengupta, P. The rise and fall of basal bodies in the nematode Caenorhabditis elegans. *Cilia* **6**, 9 (2017).

140.   Gong, J. *et al.* A Cold-Sensing Receptor Encoded by a Glutamate Receptor Gene. *Cell* **178**, 1375-1386.e11 (2019).

141.   Iliff, A. J. *et al.* The nematode C. elegans senses airborne sound. *Neuron* **109**, 3633-3646.e7 (2021).

CHAPTER II

A Cold-Sensing Receptor Encoded By A Glutamate Receptor Gene

2.1 Acknowledgements

Contributions:

Jianke Gong (J.G.), Jinzhi Liu (J.L.), **Elizabeth A. Ronan (E.A.R.)**, Feiteng He (F.H.), Wei Cai (W.C.), Mahar Fatima (M.F.), Wenyuan Zhang (W.Z.), Hankyu Lee (H.L.), Zhaoyu Li (Z.L.), Gun-Ho Kim (G.K.), Kevin P. Pipe (K.P.P.), Bo Duan (B.D.), Jianfeng Liu (J.L.), and X.Z. Shawn Xu (X.Z.S.X.) were the authors for Chapter 2. J.G. and **E.A.R.** performed in vivo experiments and analyzed the data. J.G. and F.H. performed in vitro experiments and analyzed the data. Jinzhi Liu generated nearly all the worm strains and plasmids. W.C., M.F., H.L., and B.D. performed mouse DRG experiments and analyzed the data. W.Z. assisted J.G. in performing some experiments. Z.L. helped identify GLR-3 expression pattern. G.-H.K and K.P.P. contributed to the design and fabrication of cooling devices. J.G., **E.A.R.**, Jianfeng Liu, and X.Z.S.X. wrote the paper with input from other authors.

2.2 Abstract

In search of the molecular identities of cold-sensing receptors, we carried out an unbiased genetic screen for cold-sensing mutants in *C. elegans*, and isolated a mutant allele of *glr-3* gene that encodes a kainate-type glutamate receptor. While glutamate receptors are best known to transmit chemical synaptic signals in the central nervous system, we show that GLR-3 senses cold in the peripheral sensory neuron ASER to trigger cold-avoidance behavior. GLR-3 transmits cold signals via G protein signaling independently of its glutamate-gated channel function, suggesting GLR-3 as a metabotropic cold receptor. The vertebrate GLR-3 homolog GluK2 from zebrafish, mouse and human can all function as a cold receptor in heterologous systems. Mouse DRG sensory neurons express GluK2, and GluK2 knockdown in these neurons suppresses their sensitivity to cold but not cool temperatures. Our study identifies an evolutionarily-conserved cold receptor, revealing that a central chemical receptor unexpectedly functions as a thermal receptor in the periphery.

2.3 Introduction

The ability to sense cold is essential for life. Cold temperatures trigger profound physiological and behavioral responses in nearly every organism (Bandell et al., 2007; Schepers and Ringkamp, 2010). For example, cold stimuli, particularly noxious cold, are not only life-threatening, but also cause severe tissue damage and evokes pain in animals and humans (Foulkes and Wood, 2007). To survive, organisms have evolved

exquisite thermosensory systems to detect and react to cold temperatures (Bandell et al., 2007; Schepers and Ringkamp, 2010). Molecular cold sensors are a central player in cold sensation (Bandell et al., 2007; Schepers and Ringkamp, 2010). These cold receptors, which are expressed in cold-sensitive neurons/cells in the periphery, sense cold temperatures and relay the signals to the central nervous system to trigger nocifensive behaviors and elicit pain (Schepers and Ringkamp, 2010).

Despite decades of intensive research, little is known about the molecular mechanisms underlying cold sensation. Thus far, only one cold receptor, TRPM8, which is a TRP family channel, has been verified both *in vivo* and *in vitro* in mammals. TRPM8 senses cool temperatures with an activation threshold at ~26°C and mediates cool sensation in mice (Bautista et al., 2007; Dhaka et al., 2007; McKemy et al., 2002; Peier et al., 2002). Some other mammalian TRP channels (e.g. TRPA1) have also been suggested as a cold receptor, but their function in thermosensation appears complex and remains to be defined (Moparthi et al., 2016; Story et al., 2003; Vandewauw et al., 2018; Winter et al., 2017). As such, the molecular identities of cold receptors remain largely elusive. As animals and humans are clearly capable of sensing temperatures below 26°C, and TRPM8 knockout mice show robust responses to noxious cold (Bautista et al., 2007; Dhaka et al., 2007), unknown cold receptors, particularly those sensing noxious cold, must exist but remain to be identified.

Glutamate receptors, such as kainate, AMPA, and NMDA receptors, are glutamate-gated ion channels that are primarily expressed in the brain. These chemical-sensing receptors transmit chemical signals between neurons and mediate the majority of excitatory chemical synaptic transmission in the central nervous system (Traynelis et

al., 2010). These receptors also mediate synaptic plasticity in the central nervous system, which underlies learning and memory (Traynelis et al., 2010). Dysfunction of glutamate receptors leads to a wide variety of central nervous system disorders, ranging from epilepsy, ischemic stroke, and neurodegeneration (e.g Alzheimer's disease and Parkinson's disease), to mental retardation (Bowie, 2008). These together highlight a fundamental role of glutamate receptors in the function and organization of the central nervous system.

Here, we designed an unbiased, activity-based genetic screen for cold receptors in *C. elegans*, a model organism widely used for the study of sensory biology (Bargmann, 2006; Garrity et al., 2010; Goodman, 2006; Ward et al., 2008). To do so, we employed a real-time PCR thermocycler, which allowed us to conduct a high throughput genetic screen for mutants defective in cold sensation using live animals. We identify GLR-3, a kainate-type glutamate receptor homolog, as a cold receptor. GLR-3 senses cold temperatures in the sensory neuron ASER to trigger cold-avoidance behavior, indicating that GLR-3 functions in the peripheral nervous system to mediate cold sensation. Heterologous expression of GLR-3 in mammalian cell lines confers cold sensitivity, suggesting that it is sufficient to function as a cold receptor. The activation threshold of GLR-3 is below 20°C, suggesting that it mainly senses noxious cold rather than cool temperatures. Surprisingly, GLR-3 functions as a metabotropic cold receptor rather than a typical temperature-gated ion channel, and its role in cold sensation is independent of its glutamate receptor function. The GLR-3 homolog GluK2 from fish, mouse and human can all function as a cold receptor *in vitro*, and mouse GluK2 can functionally substitute for GLR-3 *in vivo*. Mouse GluK2 is expressed in dorsal root

ganglion (DRG) sensory neurons, and knockdown of GluK2 in DRG neurons suppresses the sensitivity of these sensory neurons to cold but not cool temperatures. Our studies identify an evolutionarily-conserved cold receptor. As glutamate receptors are best known to transmit chemical signals across synapses in the central nervous system, our studies also present a striking case where a central chemical receptor functions as a thermal receptor in the periphery.

2.4 Materials and Methods

EXPERIMENTAL MODEL AND SUBJECT DETAILS

C. elegans strains were maintained at 20 ^{o}C on nematode growth medium (NGM) plates seeded with OP50 bacteria unless otherwise specified. Transgenic lines were generated by injecting plasmid DNA directly into hermaphrodite gonad. Mutant strains and integrated transgenic strains were outcrossed at least six times before use.

CHO cells were cultured in DMEM/F12 media with 10% FBS (heat-inactivated) at 37°C under 5% CO2. DMEM media with 10% FBS (heat-inactivated) were used to culture COS-7 and Hela cells. These cell lines were obtained from the ATCC. See Table 2.1 for details.

METHODS DETAILS

Table 2.1 Chapter 2 Key Resource Table

REAGENT or RESOURCE	SOURCE	IDENTIFIER
Bacterial and Virus Strains		
E. coli:OP50	Caenorhabditis Genetics Center	OP50
Chemicals, Peptides, and Recombinant Proteins		
TRIzol LS Reagent	Thermo Fisher Scientific	10-296-010
Power SYBR Green	Thermo Fisher Scientific	4367659
M-MLV Reverse Transcriptase	Thermo Fisher Scientific	28025013
RNAscope 3-plex Negative Control Probe	Advanced Cell Diagnostics	320871
RNAscope 3-plex Positive Control Probe	Advanced Cell Diagnostics	320881
RNAscope Probe Mm-Gluk2	Advanced Cell Diagnostics	438781
L-Glutamic acid	Sigma	49449
Lipofectamine 2000	Thermo Fisher Scientific	11668-019
Fura-2 AM	Thermo Fisher Scientific	F1221
Pluronic F-127	Sigma	P2443
mSIRK	Millipore	371818
YM-254890	WAKO-Chemicals	257-00631
Pertussis Toxin	Thermo Fisher Scientific	PHZ1174

Papain	Sigma	10108014001
Collagenase/Dispase	Sigma	11097113001
4D-Nucleofector™ X Kit	Lonza	V4XP-3024
Critical Commercial Assays		
TruSeq Nano DNA LT Sample Preparation Kit – Set A	Illumina	FC-121-4001
TruSeq Nano DNA LT Sample Preparation Kit – Set B	Illumina	FC-121-4002
Experimental Models: Cell Lines		
CHO	ATCC	CCL-61
COS-7	ATCC	CRL-1651
HeLa	ATCC	CCL-2
Experimental Models: Organisms/Strains		
C. elegans: Strain N2 var. Bristol: wild-type	Caenorhabditis Genetics Center	WB Strain: N2
C. elegans: glr-3(tm6403)	Shohei Mitani	WB Strain: tm6403
C. elegans: xuIs189[Plfe-2::GCaMP3.0+Plfe-2::DsRed]	This paper	TQ3700
C. elegans: xuIs189[Plfe-2::GCaMP3.0+Plfe-2::DsRed]; glr-3(tm6403)	This paper	TQ5945

C. elegans: xuIs189[Plfe-2::GCaMP3.0+Plfe-2::DsRed]; glr-3(xu261)	This paper	TQ4308
C. elegans: xuIs189[Plfe-2::GCaMP3.0+Plfe-2::DsRed]; xuEx2021[Pges-1::glr-3(gDNA)::SL2::CFP]; glr-3(tm6403)	This paper	TQ5946
C. elegans: xuEx2250[Pges-1::glr-3::SL2::CFP]	This paper	TQ6409
C. elegans: xuEx2021[Pges-1::glr-3(gDNA)::SL2::CFP]; glr-3(tm6403)	This paper	TQ5947
C. elegans: xuEx3000[Pgcy-5::GCaMP6(f)]	This paper	TQ8078
C. elegans: xuEx2902[glr-3(7kb)::sl2::YFP]	This paper	TQ7749
C. elegans: xuEx2994[Pgcy-5::glr-3(cDNA)::sl2::CFP]; glr-3(tm6403)	This paper	TQ8072
C. elegans: xuEX3000[Pgcy-5::GCaMP6(f)]; xuEx2994[Pgcy-5::glr-3(cDNA)::sl2::CFP]; glr-3(tm6403)	This paper	TQ8138
C. elegans: xuEx3144[Pgcy-5::mGluK2::sl2::CFP]; glr-3(tm6403)	This paper	TQ8700
C. elegans: xuEx2383[Pmyo-3::GCaMP6(f)]; xuEx3143[Pmyo-3::mGluk2::sl2::CFP]	This paper	TQ8832

C. elegans: xuEx3000[Pgcy-5::GCaMP6(f)]; xuEx3144[Pgcy-5::mGluk2::sl2::CFP]; glr-3(tm6403)	This paper	TQ8869
C. elegans: xuEx3000[Pgcy-5::GCaMP6(f)]; unc-31(e169)	This paper	TQ9038
C. elegans: xuEx3000[Pgcy-5::GCaMP6(f)]; unc-13(e51)	This paper	TQ9040
C. elegans: xuEx3000[Pgcy-5::GCaMP6(f)]; eat-4(ky5)	This paper	TQ9045
C. elegans: xuEx2383[Pmyo-3::GCaMP6(f)]; xuEX3175[Pmyo-3::glr-3(cDNA)::sl2::CFP]	This paper	TQ9174
C. elegans: xuEx2383[Pmyo-3::GCaMP6(f)]; xuEx3182[Pmyo-3::glr-3(M582R)::sl2::CFP]	This paper	TQ9175
C. elegans: xuEx2383[Pmyo-3::GCaMP6(f)]; xuEx3184[Pmyo-3::glr-3(Q584R)::sl2::CFP]	This paper	TQ9177
C. elegans: xuEX3000[Pgcy-5::GCaMP6(f)]; xuEx3186[Pgcy-5::glr-3(M582R)::sl2::CFP]; glr-3(tm6403)	This paper	TQ9179

C. elegans: xuEx3000[Pgcy-5::GCaMP6(f)]; xuEx3188[Pgcy-5::glr-3(Q584R)::sl2::CFP]; glr-3(tm6403)	This paper	TQ9180
C. elegans: xuEx2383[Pmyo-3::GCaMP6(f)]; xuEx3191[Pmyo-3::mGluk2(Q622R)::sl2::CFP]	This paper	TQ9228
C. elegans: xuEx2383[Pmyo-3::GCaMP6(f)]; xuEx3197[Pmyo-3::mGluk2(M620R)::sl2::CFP]	This paper	TQ9269
C. elegans: xuEx3000[Pgcy-5::GCaMP6(f)]; xuEx3193[Pgcy-5::mGluk2(Q622R)::sl2::CFP]; glr-3(tm6403)	This paper	TQ9227
C. elegans: xuEx3000[Pgcy-5::GCaMP6(f)]; xuEx3200[Pgcy-5::mGluk2(M620R)::sl2::CFP]; glr-3(tm6403)	This paper	TQ9271
C. elegans: xuEx3000[Pgcy-5::GCaMP6(f)]; gpa-3(pk35)	This paper	TQ9289
C. elegans: xuEx3000[Pgcy-5::GCaMP6(f)]; goa-1(n1134)	This paper	TQ9290

C. elegans: xuEx3000[Pgcy-5::GCaMP6(f)]; gpa-3(pk35); goa-1(n1134)	This paper	TQ9291
C. elegans: xuEx3000[Pgcy-5::GCaMP6(f)]; che-2(e1033)	This paper	TQ9667
C. elegans: xuEx3251[Pgcy-5::goa-1(cDNA)::sl2::mcherry2]; xuEx3000[Pgcy-5::GCaMP6(f)]; goa-1(n1134)	This paper	TQ9625
C. elegans: xuIs259 [Plfe-2::GCamp3.0+Plfe-2::DsRed]; goa-1(n1134)	This paper	TQ9671
C. elegans: xuIs259 [Plfe-2::GCamp3.0+Plfe-2::DsRed]; glr-3(xu261)	This paper	TQ9741
C. elegans: xuIs259 [Plfe-2::GCamp3.0+Plfe-2::DsRed]; trpa-1(ok999); glr-3(tm6403)	This paper	TQ9740
Oligonucleotides		
siRNA targeting sequence: GluK2 #1:ACGCAGATTGGTGGCCTTATA	This paper	N/A
siRNA targeting sequence: GluK2 #2:AAGGTACAATCTTCGACTTAA	This paper	N/A
siRNA targeting sequence: GluK2 #3:TCGCTTCATGAGCCTAATTAA	This paper	N/A

siRNA targeting sequence: GluK2 #4:TACAGGCAGAATTACATTTAA	This paper	N/A
Primer: For qPCR mGluK2: fwd: GCGCAACCATGACGTTTTTCAAG	This paper	N/A
Primer: For qPCR mGluK2: rev: CCATGGGAGTGCCAACACCATAG	This paper	N/A
Primer: For glr-3 promoter: fwd: TTAATTCACATTCCATCGGAAAAATC	This paper	N/A
Primer: For glr-3 promoter: rev: GCCTAGTGACTCGGTCTCTACTCGTA	This paper	N/A
Recombinant DNA		
Plasmid: Pglr-3::sl2::YFP	This paper	pSX2074
Plasmid: Pgcy-5::glr-3(cDNA):sl2::CFP	This paper	pSX2101
Plasmid: Pmyo-3::glr-3(cDNA)::sl2::mcherry	This paper	pSX2120
Plasmid: PcDNA3.1-Flag-glr-3(cDNA)	This paper	pSX2177
Plasmid: PcDNA3.1+N-DYK-hGluK2	GenScript	OHu23233
Plasmid: PcDNA3.1+N-DYK -mGluK2	GenScript	OMu13059
Plasmid: PcDNA3.1+N-DYK -fGluK2	GenScript	ODa42289
Plasmid: Pmyo-3::mGluK2::sl2::CFP	This paper	pSX2191
Plasmid: Pgcy-5::mGluK2::sl2::CFP	This paper	pSX2192

Plasmid: PcDNA3.1-Flag-glr-3(cDNA,M582R)	This paper	pSX2791
Plasmid: PcDNA3.1-Flag-glr-3(cDNA,Q584R)	This paper	pSX2792
Plasmid: PcDNA3.1-Flag-glr-3(cDNA,P121L)	This paper	pSX2869
Plasmid: PcDNA3.1-Flag-glr-3(cDNA,P130L)	This paper	pSX2870
Plasmid: Pmyo-3::glr-3(cDNA,M582R)::sl2::mcherry	This paper	pSX2795
Plasmid: Pmyo-3::glr-3(cDNA,Q584R)::sl2::mcherry	This paper	pSX2796
Plasmid: Pgcy-5::glr-3(cDNA,M582R):sl2::CFP	This paper	pSX2793
Plasmid: Pgcy-5::glr-3(cDNA,Q584R):sl2::CFP	This paper	pSX2794
Plasmid: PcDNA3.1-Flag-mGluK2(M620R)	This paper	pSX2797
Plasmid: PcDNA3.1-Flag-mGluK2(Q622R)	This paper	pSX2798
Plasmid: PcDNA3.1-Flag-mGluK2(P151L)	This paper	pSX2868
Plasmid: Pmyo-3::mGluK2(M620R)::sl2::CFP	This paper	pSX2802

Plasmid: Pmyo-3::mGluK2(Q622R)::sl2::CFP	This paper	pSX2803
Plasmid: Pgcy-5::mGluK2(M620R)::sl2::CFP	This paper	pSX2800
Plasmid: Pgcy-5::mGluK2(Q622R)::sl2::CFP	This paper	pSX2801
Plasmid: Pgcy-5::goa-1(cDNA)::sl2::CFP	This paper	pSX2822
Software and Algorithms		
MetaFluor	Molecular Devices Inc.	N/A
GraphPad	GraphPad Software, Inc	N/A

Molecular biology and genetics

For the experiments involving transgenes, two to three independent transgenic lines were tested to confirm the results. *glr-3* cDNA was cloned by RT-PCR from total RNA isolated from WT (N2) worms. The expression of the transgene was verified by CFP, YFP or mCherry expression, which was driven by SL2 from the same transcript. Mouse, human and zebrafish GluK2 cDNA plasmids were obtained from GenScript (all in the pcDNA3.1+N-DYK vector). See Table 2.1 for plasmid information.

Genetic screen

EMS was used to mutagenize worms carrying a transgene co-expressing GCaMP and DsRed, which enables ratiometric detection of changes in GCaMP fluorescence by a real-time qPCR thermocycler (ABI 7500). Worms from each F2 plate

were washed with M9 buffer and transferred to an unseeded NGM plate to clean off bacteria. Five individual worms from each strain were picked to a well of a 96-well plate with 20 µl recording buffer (10 mM HEPES at pH 7.4, 5 mM KCl, 145 mM NaCl, 1.2 mM MgCl2, 2.5 mM CaCl2, 10 mM glucose). PCR plates were loaded onto a real-time qPCR thermocycler and cooled from 23°C to 10°C. Those candidates that failed to respond to cooling were recovered, outcrossed to the parental strain for six times. Both the parental and mutant strains were then subjected to whole-genome sequencing (WGS). Analysis of the sequencing data was done as described (Minevich et al., 2012). By comparing the WGS data between parental and mutant strain, we obtained a density map of single nucleotide variants and mapped the mutation in *xu261* to the gene *glr-3*, which mutated P121 residue to L. By testing the deletion null mutant *glr-3(tm6403)*, we found that it exhibited the same cold-sensing phenotype as *glr-3(xu261)* in the intestine, which was rescued by transgenic expression of wild-type *glr-3* gene in the intestine.

C. elegans calcium imaging and behavioral assays

Calcium imaging was performed on an Olympus IX73 inverted microscope under a 40X objective. Images were acquired using an ORCA-Flash 4.0 sCMOS camera (Hammatsu Inc.) with MetaFluor software (Molecular Devices Inc.). To imaging the intestine, ASER neuron and body-wall muscle cells in response to temperature stimuli, we glued worms on a cover glass covered with a thin layer of agarose pad. A Bipolar In-line Cooler/Heater (SC-20 from Warner Instruments) was used to control the temperature of the recording solution, which was perfused towards the worm. Recording buffer: 10 mM HEPES at pH 7.4, 5 mM KCl, 145 mM NaCl, 1.2 mM MgCl2,

2.5 mM CaCl2, 10 mM glucose. The temperature was initially set at 23°C; after

achieving a basal line, the temperature was cooled to 10°C over 120 sec, and heated

back to 23°C. Faster cooling can be achieved by perfusing pre-cooled (4°C) solution

towards the subject, and similar results were obtained (Figure 2.9A-F); but since this

protocol does not permit precise control of the end temperature, we focused on the use

of the former. To image ASER neuron in response to salt gradient, we used a

microfluidic system as described previously (Wang et al., 2016). Briefly, worms were

loaded into the chip mounted on the microscope, and 50 to 0 mM salt concentration

steps were performed by switching solutions administered to the nose tip (25 mM

potassium phosphate [pH 6.0], 1 mM $CaCl_2$, 1 mM $MgSO_4$, 0.02% gelatin, and either 50

or 0 mM NaCl with glycerol to adjust osmolarity to 350 mOsm). For intestine calcium

imaging, we scored the peak percentage change in the ratio of GCaMP/DsRed

fluorescence. For ASER and muscle imaging, we scored the peak percentage change

in in the intensity of GCaMP fluorescence.

Cooling-evoked swimming assay was performed in a recording chamber (RC-26

from Warner Instruments) filled with M9 buffer using day 1 adult hermaphrodites. The

temperature was initially set at 21°C, gradually cooled to 18 °C over 40 sec, and then

heated back to 21°C by slowly perfusing the chamber with M9 buffer of varying

temperatures with a Bipolar In-line Cooler/Heater (Warner Instruments). The number of

turns that worms displayed every 10 sec was scored.

Cooling-evoked probe assay was performed in an environmentally controlled

room set at 21°C and 30% humidity. Day 1 adult hermaphrodites were tested. Animals

were tested on standard NGM plates dried for one hour without lids to remove any

65

excess surface moisture. Prior to testing, plates were seeded with a thin lawn of fresh OP50 in the center of the plate to prevent animals from leaving, which was allowed to dry for 10 minutes prior to placing animals on the plate. To deliver localized cooling stimuli to a region of the worm, we used a custom-built thermoelectric cooling probe with a tip size of 50 μm. The design and fabrication of the cooling device will be described elsewhere. The probe tip was pre-cooled to 17°C and placed ~100 μm above the head of the animal (without touching the animal) for 5 seconds using a micromanipulator. An avoidance response was scored if the worm stopped forward movement and initiated a reversal with at least half a head swing within the 5 seconds period. Five animals were tested on a single plate. Each animal was tested only once as we observed *C. elegans* could quickly adapt to acute cooling stimuli, resulting in a blunted response upon multiple trials. The response rate for five animals on one plate was averaged and counted as a single trial, and repeated for a total of 10 trials per genotype.

Salt chemotaxis assay was carried out as previously described (Tomioka et al., 2006). Briefly, young adult animals were collected, washed, and transferred with chemotaxis buffer (25 mM potassium phosphate (pH 6.0), 1 mM $CaCl_2$, 1 mM $MgSO_4$) followed by a final wash in ddH_2O. Test plates were made using 10 cm diameter assay plates (5 mM KPO_4, pH 6.0, 1 mM $CaCl_2$, 1mM $MgSO_4$, 2% agar), on which a salt gradient was formed by placing a 2% agar plug (10 mm diameter) made in chemotaxis buffer containing 100 mM of NaCl. Fifty to two hundred animals were tested for each plate. The chemotaxis index (C.I.) was calculated as described previously (Tomioka et al., 2006).

Cell culture and calcium imaging

CHO cells were cultured in DMEM/F12 media with 10% FBS (heat-inactivated) at 37°C under 5% CO2. DMEM media with 10% FBS (heat-inactivated) were used to culture COS-7 and Hela cells. Cells grown on cover glasses coated with poly-lysine were transfected in 35 mm dishes using Lipofectamine 2000 (ThermoFisher) for 4 hours. The lipid/DNA ratio was 3:1, and the total DNA was 1.5 µg except for fish GluK2. For fish GluK2, to maximize its expression level, we used 12 µl lipid and 3 µg DNA for transfection.

18 hours after the transfection, cells were loaded with 4 µM Fura-2 AM and 0.2% Pluronic F127 in HBSS buffer at 37°C for 30 min, washed for 3 times with HBSS, and incubated in the recording buffer for 30 min before calcium imaging. It is important to use a ratiometric dye such as Fura-2 to image cold responses, as single wavelength dyes may show intrinsic responses to cold. Recording buffer: 10 mM HEPES at pH 7.4, 5 mM KCl, 145 mM NaCl, 1.2 mM MgCl2, 2.5 mM CaCl2, 10 mM glucose. Calcium imaging was performed as described above for *C. elegans* imaging with the following modification: to obtain better Fura-2 images under 340/380 nm, we used a 40x water-immersion objective with high transmission efficiency of UV light. The same temperature control protocol was used as described above for *C. elegans* imaging. For those experiments involving inhibitors, cells were pretreated with inhibitors (mSIRK: 50 µM; YM-254890: 10 µM) right after Fura-2 AM loading. For PTX, we pretreated cells with 100 ng/ml of PTX for 10 hours before the imaging experiment.

Mouse DRG neuron culture, transfection, qPCR, and calcium imaging

DRG culture and siRNA transfection were carried out as described previously (Lou et al., 2013). Briefly, mice were euthanized at the age of P14-15 by CO2 inhalation. DRGs were isolated from T10-L6 and collected in Ca^{2+}- and Mg^{2+}-free Hank's buffered salt solution (HBSS). Following isolation, DRGs were digested with papain (1.5 mg/ml, MilliporeSigma) for 10 minutes and then collagenase/dispase for 12 minutes (1 mg/ml, MilliporeSigma) at 37°C. After digestion, the culture was then triturated and dissociated using fire-polished Pasteur pipettes for further siRNA transfection. To knockdown GluK2 mRNA transcripts, a pool of 4 different siRNA (250 nM, Qiagen. Target sequences: ACGCAGATTGGTGGCCTTATA, AAGGTACAATCTTCGACTTAA, TCGCTTCATGAGCCTAATTAA, TACAGGCAGAATTACATTTAA) was electroporated into the freshly dissociated DRG neurons using P3 Primary Cell 4D-Nucleofector™ X Kit (V4XP-3024, Lonza). A scrambled siRNA (250 nM, Qiagen) was transfected as a control. A MaxGFP construct (1 μl, Lonza) was co-transfected as a marker.

Two days post-transfection, DRG neurons were harvested, and the total RNA was extracted with TRIzol (Life Technologies) for quantitative real-time PCR (qPCR) analysis. qPCR reactions were performed in a 384-well format using Power SYBR Green (Thermo Fisher Scientific). Relative mRNA levels were calculated using the $\Delta\Delta C_T$ method and normalized to *Tbp, 36B4*. Primer sequences: mGluK2 fwd: GCGCAACCATGACGTTTTTCAAG, mGluK2 rev: CCATGGGAGTGCCAACACCATAG.

Calcium imaging of cultured DRG neurons was carried out two days post-transfection. The imaging protocol was similar to that described above for CHO cell

imaging, except that a 20x rather than 40x water-immersion objective with high

transmission efficiency of UV light was used for imaging. DRG neurons showing ≥25%

increase in fura-2 F_{340}/F_{380} fluorescence ratio (ΔR/R) in response to temperature

stimulation were scored positive.

Mouse DRG in situ hybridization (RNAscope)

PFA-fixed DRG samples from P30 mice was frozen in optimal cutting

temperature (OCT) freezing medium and then the DRGs were used to prepare six

adjacent sections at 12 μm thickness. GluK2 mRNA transcript in the DRG sections was

detected using RNAscope assay (Wang et al., 2012a). The probes were designed and

provided by Advanced Cell Diagnostics, Inc (Advanced Cell Diagnostics, Newark, CA).

Staining was performed using the RNAscope multiplexed fluorescent in situ

hybridization kit, according to manufacturer's instructions. For quantification of GluK2-

positive population, neurons that had at least four positive signals (observed as puncta)

within the periphery of the neurons, as defined by the phase contrast image, were

considered as GluK2-positive. Around 300-450 neurons from each animal were

analyzed for GluK2 mRNA transcripts. For categorization of GluK2-positive neuronal

population, the type of the neurons was assigned by measuring their size. Only the

neurons containing nuclei were counted. As described previously (Fang et al., 2005),

neurons with a surface area <400 μm^2, 400-800 μm^2, and >800 μm^2 were categorized

as small-diameter, medium-diameter and large-diameter cells, respectively.

Electrophysiology

Whole-cell patch-clamp recording was performed on an Olympus IX73 inverted microscope under a 40x objective with a Multiclamp 700B amplifier. Transfected cells were identified with a co-transfection RFP marker. Bath solution (in mM): 145 NaCl, 2.5 KCl, 1 $CaCl_2$, 1 $MgCl_2$, 10 glucose, and 5 HEPES (pH adjusted to 7.2). Pipette solution: 115 K-gluconate, 15 KCl, 1 $MgCl_2$, 10 HEPES, 0.25 $CaCl_2$, 20 sucrose, 5 BAPTA, and 5 Na_2ATP. Glutamate (10 mM) was diluted in bath solution and perfused towards the cell using a rapid perfusion system (Bio-Logic) to evoke glutamate-gated currents. Pipette resistance: 2-4 MΩ. Series resistance and capacitance were compensated during recording. Voltage was clamped at -70 mV.

QUANTIFICATION AND STATISTICAL ANALYSIS

Quantification and statistical parameters were indicated in the legends of each figure, including the statistical method, error bars (SEM), n numbers, and p values. We applied ANOVA, t test, and χ^2 test to determine statistical significance. Specifically, for those analyses involving multiple group comparisons, we applied one-way ANOVA followed by a post hoc test (Bonferroni test). For those only involving two groups, we applied t test (Figure 2.7C) and ^{2} test (Figure 2.7F). We considered p values of <0.05 significant. All analyses were performed using SPSS Statistics software (IBM, Inc).

DATA AND CODE AVAILABILITY

This study did not generate/analyze datasets or code.

2.5 Results

Designing an unbiased, activity-based genetic screen for cold receptors

Previous efforts to identify cold receptors mostly focused on the use of candidate gene approaches but not unbiased genetic screens (Bandell et al., 2007; Castillo et al., 2018). Those cold receptors that do not fall into the category of known thermosensors (e.g. TRP family channels) would thus have escaped detection. To overcome this difficulty, one approach is to design and conduct an unbiased screen, which has the potential to uncover new types of cold receptors.

Thus, we sought to design a forward genetic screen for mutants defective in cold sensation in *C. elegans*, an organism widely used as a genetic model for sensory biology. Traditionally, behavioral assays are employed to conduct such a genetic screen in *C. elegans*. Despite its convenience, this type of screen lacks specificity, as the phenotype in isolated mutants might simply result from defects in sensory processing by downstream neural circuits rather than in cold sensing by sensory neurons/cells. We thus decided to design an activity-based genetic screen by directly targeting sensory neurons/cells.

We previously reported that worm intestinal cells directly sense cold (Xiao et al., 2013). Cooling induces robust calcium response in the intestine dissected out of the worm, shown by calcium imaging using the genetically-encoded calcium sensor GCaMP (Xiao et al., 2013). The intestine is the largest worm tissue composed of 20 epithelial cells (McGhee, 2007). The large size of the intestine makes it possible to conduct a high throughput activity-based screen by monitoring cooling-triggered calcium response in the intestine. To design such a screen, we considered using a real-time PCR thermal cycler that is designed for amplifying and quantifying cDNA (Figure 2.1A). This type of

71

equipment can rapidly and precisely cool/heat the sample while monitoring changes in

the fluorescence (e.g. GCaMP) level of the sample in real time. This feature and the

convenience that worms can readily fit into PCR tubes motivated us to employ such a

thermal cycler to conduct a high throughput activity-based screen using live worms

(Figure 2.1A). Though TRPA-1 contributes to cold-evoked calcium response in the

intestine, robust cold response persists in *trpa-1* mutant worms (Xiao et al., 2013),

indicating the presence of unknown cold receptor(s). We thus performed a large scale

chemical mutagenesis screen for such unknown cold receptor(s) using this strategy

(Figure 2.1A).

glr-3 mutants show a strong defect in cooling-evoked calcium response

After screening >30,000 F2 strains, we recovered 11 mutants. We focused on

xu261, a mutant allele that showed a strong phenotype in cooling-evoked calcium

response (Figure 2.1A). By whole-genome sequencing, we mapped the mutation to *glr-3* gene that encodes a kainate-type glutamate receptor (Brockie et al., 2001) (Figure

2.1A).

To further characterize GLR-3, we performed standard calcium imaging

experiments by fluorescence microscopy. We found that *glr-3* null mutant worms [i.e.

glr-3(tm6403)] displayed a severe defect in cooling-evoked calcium increase in the

intestine, a phenotype that was rescued by transgenic expression of wild-type *glr-3*

gene in the intestine using an intestine-specific promoter (Figure 2.1B-C). *glr-3(xu261)*

mutant worms also displayed a similar phenotype (Figure 2.8). These results identify a

key role for GLR-3 in mediating cooling-evoked cold response in the intestine.

The sensory neuron ASER is cold-sensitive and requires GLR-3 to sense cold

We next set out to characterize the *in vivo* functions of GLR-3 in cold sensation. GLR-3 has been reported to be expressed in central neurons (i.e., RIA interneurons in the head) (Brockie et al., 2001). Using a longer promoter, we found that GLR-3 was also expressed in the intestine (Figure 2.1D), as well as the sensory neuron ASER (Figure 2.1E). The intestinal expression of GLR-3 is consistent with our finding that GLR-3 mediates cooling-evoked calcium response in the intestine. As we are more curious about the potential role of GLR-3 in regulating sensory behavior, we decided to focus on its function in the nervous system.

The expression of GLR-3 in the sensory neuron ASER suggests that GLR-3 may regulate sensory behavior in response to cold. While ASER was originally identified as a chemosensory neuron (Ortiz et al., 2009; Pierce-Shimomura et al., 2001), the fact that GLR-3 is expressed in ASER suggests that this chemosensory neuron may also be cold-sensitive. Indeed, cooling evoked robust calcium response in ASER (Figure 2.2A-B and Figure 2.9A-B). *glr-3* mutant worms exhibited a severe defect in this cooling response, a phenotype that was rescued by transgenic expression of wild-type *glr-3* gene in ASER using an ASER-specific promoter (Figure 2.2A-B). By contrast, loss of GLR-3 did not affect salt-evoked (NaCl) calcium response in ASER neuron (Figure 2.2C-D), indicating that the chemosensory function of ASER neuron was not compromised in *glr-3* mutant worms. As a control, *che-2* mutant worms, which are known to be defective in chemosensation (Perkins et al., 1986), showed a severe defect in salt-evoked calcium transients in ASER (Figure 2.2C-D). Thus, GLR-3 acts in ASER

neuron to mediate cold sensation. These results suggest that ASER is a cold-sensitive neuron.

Nevertheless, it remains possible that the observed cooling-evoked response in ASER neuron might arise from another sensory neuron(s) via neurotransmission cell-non-autonomously. To exclude this possibility, we repeated the calcium imaging experiment in *unc-13* and *unc-31* mutant backgrounds, in which secretion of neurotransmitters and neuropeptides from synaptic vesicles (SV) and dense-core vesicles (DCV) is abolished, respectively (Richmond et al., 1999; Speese et al., 2007). Cooling-evoked calcium response in ASER neuron persisted in *unc-13* and *unc-31* mutant worms (Figure 2.2E-F). Thus, ASER neuron can sense cold without inputs from other neurons, providing further evidence supporting that ASER is a cold-sensitive neuron.

As GLR-3 is a member of the glutamate receptor family, we also examined mutant worms lacking *eat-4*, a gene that encodes the sole vesicular glutamate transporter in the worm genome (Lee et al., 1999). *eat-4* mutant worms, which are devoid of glutamate signaling, displayed normal cooling-evoked response in ASER neuron (Figure 2.2E-F), providing additional evidence that ASER is a cold-sensitive neuron. This experiment also demonstrates that the role of GLR-3 in ASER cold sensation is independent of its function as a glutamate receptor.

GLR-3 acts in the ASER neuron to mediate cold-avoidance behavior

What would be the behavioral consequences following GLR-3-mediated activation of ASER neuron by cold? Activation of ASER neuron is known to trigger

backward movement (reversals) followed by turns, a type of avoidance response (Suzuki et al., 2008). We first used a swimming assay to quantify turns. We found that cooling triggered turns in wild-type worms (Figure 2.2G). *glr-3* mutant worms exhibited a severe defect in this cold-avoidance behavior (Figure 2.2G), while no such defect was detected in *trpa-1* mutant worms (Figure 2.9G). Transgenic expression of wild-type *glr-3* gene specifically in ASER neuron rescued this behavioral phenotype (Figure 2.2G). By contrast, *glr-3* mutant worms exhibited normal salt chemotaxis behavior compared to wild-type worms, though *che-2* mutant worms were severely defective (Figure 2.2H). To provide additional evidence, we sought to develop another cold-avoidance behavioral assay. We examined whether cold stimuli can trigger avoidance response in worms crawling on the surface of an agar plate by cooling the air near the worm head with a cold probe. Indeed, cooling triggered backward movement (reversals) in wide-type worms (Figure 2.9H), and this avoidance behavioral response was defective in *glr-3* mutant worms, a phenotype that was rescued by transgenic expression of wild-type *glr-3* gene specifically in ASER neuron (Figure 2.9H). As the swimming assay allows us to deliver cold stimuli to the worm with greater ease, we decided to focus on this assay for further characterizations. These behavioral data, together with calcium imaging results, demonstrate that GLR-3 acts in ASER sensory neuron to mediate cold sensation *in vivo*, suggesting GLR-3 as a cold receptor.

GLR-3 can function as a cold receptor

While our *in vivo* data show that GLR-3 is required for cold sensation *in vivo*, they do not constitute sufficient evidence supporting that GLR-3 is a cold receptor, as the

observed effect might be indirect, which could potentially be contributed by a different

protein. To demonstrate that a candidate protein can function as a cold receptor, a

commonly employed approach is to express it in cold-insensitive heterologous cells to

test whether it can confer cold sensitivity to these otherwise cold-insensitive cells

(Bandell et al., 2007; Castillo et al., 2018). To this end, we first ectopically expressed

GLR-3 in worm body-wall muscle cells that are commonly used as a vehicle to express

exogenous proteins, particularly membrane receptors (Gong et al., 2016; Wang et al.,

2012b). While body-wall muscle cells were insensitive to cold, ectopic expression of

GLR-3 in muscle cells conferred cold sensitivity to these otherwise cold-insensitive cells

(Figure 2.3A-B and Figure 2.9C-D), providing strong evidence that GLR-3 is sufficient to

function as a cold receptor.

To gather further evidence, we expressed GLR-3 in mammalian cell lines.

Transfection of GLR-3 in CHO cells conferred cold sensitivity to these cells (Figure

2.3C-D and Figure 2.9E-F). Transfection of GLR-3 in COS-7 and Hela cells also

yielded a similar result (Figure 2.10A-D). These heterologous expression data provide

further evidence that GLR-3 can function as a cold receptor.

The mouse GLR-3 homolog GluK2 can functionally substitute for worm GLR-3 *in vivo* and function as a cold receptor *in vitro*

Having characterized GLR-3 both *in vivo* and *in vitro*, we then wondered if the

role of GLR-3 in cold sensation is evolutionarily conserved. One of the closest mouse

homologs of GLR-3 is GluK2, which is also a kainate-type glutamate receptor. We

expressed mouse GluK2 as a transgene in ASER neuron and found that mouse GluK2

can restore cooling-evoked calcium response in ASER neuron of *glr-3* mutant worms

(Figure 2.3E-F). In addition, mouse GluK2 expression in ASER also rescued the cold-

avoidance behavioral phenotype in *glr-3* mutant worms (Figure 2.3G). Thus, mouse

GluK2 can functionally substitute for GLR-3 in cold sensation *in vivo*, suggesting that

mouse GluK2 has the potential to function as a cold receptor.

We also expressed mouse GluK2 as a transgene in worm muscle cells, and

found that it conferred cold sensitivity to these cells (Figure 2.3A-B and Figure 2.9C-D).

Heterologous expression of mouse GluK2 in CHO cells also conferred cold sensitivity

(Figure 2.3C-D and Figure 2.9E-F). Cooling-evoked calcium response mediated by

GluK2 and GLR-3 appears to primarily result from calcium influx (Figure 2.10E-F). As

was the case with GLR-3, transfection of mouse GluK2 in COS-7 cells and Hela cells

also conferred cold sensitivity to these cells (Figure 2.10A-D). For simplicity, we

focused on using CHO cells as our main heterologous expression system for further

characterization of GLR-3/GluK2 *in vitro*. In summary, heterologous expression data

demonstrate that mouse GluK2 can function as a cold receptor *in vitro*, suggesting that

the role of GLR-3/GluK2 as a cold receptor might be evolutionarily conserved.

GLR-3/GluK2 mainly senses cold but not cool temperatures

To further characterize GLR-3/GluK2, we determined its activation threshold.

TRPM8 is a cool sensor with an activation threshold at ~26°C (Bandell et al., 2007;

McKemy et al., 2002). Indeed, cooling from 32°C to 20°C evoked robust calcium

response in CHO cells transfected with TRPM8 (Figure 2.4A-B). As TRPM8 is also a

menthol receptor, we tested menthol on these cells. As predicted, methanol activated

TRPM8 but not GLR-3 or mouse GluK2 in CHO cells (Figure 2.4A-B). By contrast,

cooling from 32°C to 20°C triggered little, if any, calcium response in CHO cells

expressing GLR-3 or mouse GluK2 (Figure 2.4A-B). This indicates that GLR-3/GluK2

was activated at a temperature much lower than TRPM8, and that the activation

threshold of GLR-3/GluK2 is below 20°C. Indeed, we estimated that the activation

threshold for GLR-3/GluK2 in CHO cells was ~18°C (18.2 ± 0.14 for GLR-3; 18.3 ± 0.16

for mGluK2; n=20). Similar results were obtained in ASER neuron *in vivo* (18.9 ± 0.14;

n=15; Figure 2.11), as well as in muscle cells ectopically expressing GLR-3 and mouse

GluK2 (18.4 ± 0.16 for GLR-3; 18.5 ± 0.18 for mGluK2; n=15). These observations

together suggest GLR-3/GluK2 as a noxious cold receptor.

The cold sensitivity of GLR-3/GluK2 is independent of its channel activity *in vitro*

and *in vivo*

We made the surprising observation that while glutamate can activate mouse

GluK2 in CHO cells as predicted, it cannot activate GLR-3 using the calcium imaging

assay (Figure 2.4A-B). We thus recorded these CHO cells by whole-cell patch-

clamping. Glutamate evoked a typical glutamate-gated current in CHO cells expressing

mouse GluK2 (Figure 2.12D and I), but not GLR-3 (Figure 2.12H-I), indicating that GLR-

3 lacked glutamate-gated channel activity, even though it can function as a cold

receptor in these cells (Figure 2.3C-D). This surprising finding suggests that the

observed cold response mediated by GLR-3/GluK2 may be independent of its channel

function. To test this model, we generated two channel-dead mutants of mouse GluK2:

M620R and Q622R (Figure 2.12A), which mutated residues adjacent to the Q/R RNA

editing site in the channel pore region (Dingledine et al., 1992; Robert et al., 2002). As reported previously (Dingledine et al., 1992; Robert et al., 2002), these two point mutations abolished glutamate-gated current of mouse GluK2 in CHO cells (Figure 2.12E, 2.12F, and 2.12I). Strikingly, these two channel-dead GluK2 variants were still cold-sensitive in these cells (Figure 2.5A and 2.5C). Though GLR-3 lacked glutamate-gated channel activity in our assay, we introduced similar point mutations (M582R and Q584R) to disrupt any potential channel activity (Figure 2.12A), and found that these two channel-dead GLR-3 variants also retained normal cold sensitivity when expressed in CHO cells (Figure 2.5B-C). These results demonstrate that the cold sensitivity of GLR-3/GluK2 is independent of its channel function *in vitro*.

To obtain further evidence, we tested the two channel-dead GLR-3/GluK2 variants *in vivo*. We found that both GLR-3 and mouse GluK2 channel-dead variants can still function as a cold receptor in ASER neuron, as transgenic expression of these variants restored cooling-evoked calcium response in ASER neuron of *glr-3* mutant worms (Figure 2.5D-F). Furthermore, ectopic expression of these channel-dead variants in worm muscle cells can still confer cold-sensitivity to these cells (Figure 2.5G-I). We thus conclude that the cold sensitivity of GLR-3/GluK2 is independent of its channel function both *in vitro* and *in vivo*.

We also explored the converse scenario: can we identify mutations that disrupt the cold sensitivity of GLR-3/GluK2 but not its glutamate-gated channel function? The *glr-3(xu261)* mutant isolated from our genetic screen carried a P121L missense mutation (Figure 2.12B). This point mutation abolished the cold sensitivity of GLR-3 (Figure 2.5J and 5L). As GLR-3 did not exhibit channel activity on its own, we tested

our model in mouse GluK2. Since this P residue is not found in mouse GluK2, we

mutated an adjacent P residue P151 to L in the mouse protein (Figure 2.12B). These P

residues are located in the N-terminal ATD domain of GLR-3/GluK2 (Traynelis et al.,

2010). P151L mutation disrupted the cold sensitivity of mouse GluK2 in CHO cells

(Figure 2.5K-L), and a corresponding P130L mutation in GLR-3 exerted a similar effect

(Figure 2.5J and 2.5L). This demonstrates that the N-terminal ATD domain is required

for the cold-sensitivity of GLR-3/GluK2. Strikingly, despite its lack of cold sensitivity,

GluK2(P151L) retained glutamate-evoked channel activity in calcium imaging assay

(Figure 2.5K-L). Whole-cell recording also showed that GluK2(P151L) retained

glutamate-gated current, though its kinetics was altered (Figure 2.12G and 2.12I). This

is consistent with the notion that the ATD domain of glutamate receptors is not required

for their channel function and only plays a modulatory role (Traynelis et al., 2010).

Thus, it appears that the cold-sensing and glutamate-gated channel functions of GLR-

3/GluK2 can be dissociated and may require distinct domains. Together, our results

suggest that GLR-3/GluK2 may function as a receptor-type cold sensor rather than a

cold-activated channel.

GLR-3/GluK2 functions as a metabotropic cold receptor and requires G protein

signaling to transmit cold signals *in vitro* and *in vivo*

Interestingly, mammalian kainate receptors have been reported to possess both

metabotropic and ionotropic functions (Rodriguez-Moreno and Lerma, 1998; Rozas et

al., 2003; Valbuena and Lerma, 2016). When acting as metabotropic receptors, they

transmit glutamate signals via G proteins (Rodriguez-Moreno and Lerma, 1998; Rozas

et al., 2003; Valbuena and Lerma, 2016). In this case, these kainate receptors act as "GPCR-like" glutamate receptors rather than glutamate-gated channels (Rodriguez-Moreno and Lerma, 1998; Rozas et al., 2003; Valbuena and Lerma, 2016). This led us to hypothesize that GLR-3/GluK2 may also function as a "GPCR-like" cold receptor. If so, GLR-3/GluK2 should depend on G proteins to transmit cold signals. To test this, we examined mSIRK, a membrane-permeable peptide that dissociates Gα from Gβγ without stimulating its GTP-binding activity, thereby inhibiting receptor-mediated activation of G proteins (Goubaeva et al., 2003). mSIRK abolished cooling-evoked calcium response in CHO cells expressing GLR-3 or mouse GluK2 (Figure 2.6A-D). Pertussis toxin (PTX), a Gi/o inhibitor (Gierschik, 1992), also blocked the cold sensitivity of GLR-3 and mouse GluK2 in CHO cells (Figure 2.6A-D). By contrast, the Gq/11 inhibitor, YM-254890 (Takasaki et al., 2004), had no effect on the cold sensitivity of GLR-3/GluK2 (Figure 2.6A-D). As a control, this Gq/11 inhibitor can block bradykinin-evoked calcium response (Figure 2.13A-B), which was mediated by endogenous Gq/11-coupled bradykinin receptors in CHO cells (Pauwels and Colpaert, 2003), whereas the Gi/o inhibitor PTX had no effect on bradykinin-evoked response (Figure 2.13A-B). These results demonstrate that GLR-3/GluK2 transmits cold signals via Gi/o signaling *in vitro*.

Encouraged by our *in vitro* results, we next tested whether GLR-3 transmits cold signals via Gi/o signaling *in vivo*. ASER neuron expresses at least two Gi/o genes: *goa-1* and *gpa-3* (Jansen et al., 1999). Mutations in *goa-1,* but not *gpa-3,* led to a severe defect in cooling-evoked calcium response in ASER neuron (Figure 2.6E-F), a phenotype that was rescued by transgenic expression of wild-type *goa-1* gene

81

specifically in ASER neuron (Figure 2.6E-F), suggesting that GLR-3 transmits cold signals via Gi/o signaling *in vivo*. A similar result was obtained with cooling-evoked calcium response in the intestine (Figure 2.13C-D). Taken together, both of our *in vitro* and *in vivo* results support the model that GLR-3/GluK2 functions as a metabotropic, rather than an ionotropic, cold receptor, and does so by transmitting cold signals via Gi/o proteins. This identifies GLR-3/GluK2 as a previously unknown type of cold receptor.

Mouse DRG neurons express GluK2 and knockdown of GluK2 in DRG neurons suppresses their sensitivity to cold but not cool temperatures

Mammalian glutamate receptors are best known to function in the brain to regulate synaptic transmission and plasticity. Interestingly, some of these receptors are also expressed in the peripheral nervous system such as DRG sensory neurons but with an unknown function (Coggeshall and Carlton, 1998; Huettner, 1990). We thus wondered if GluK2 is expressed in DRG neurons. These primary sensory neurons detect somatosensory and painful stimuli in the periphery, including temperature cues. Using RNAscope assay, we detected GluK2 mRNA transcripts in mouse DRGs (Figure 2.7A-B). About 13.6% (140/1031) DRG neurons expressed GluK2. Among them, most were small-diameter neurons (75.0%, 105/140), while a small percentage (24.2%, 34/140) were medium-diameter neurons. This data suggests that GluK2 is expressed in DRG neurons.

We next knocked down GluK2 expression in cultured DRG neurons with siRNA (Figure 2.7C). While knockdown of GluK2 did not affect the sensitivity of DRG neurons

to cool temperatures (cooling to 22°C)(Figure 2.7D and 7F; 30/699 control cells *vs.* 26/598 siRNA cells responded), it greatly reduced the sensitivity of these sensory neurons to cold temperatures (cooling to 10°C)(Figure 2.7E-F; 131/699 control cells *vs.* 45/598 siRNA cells responded; χ^2 test, p<0.0001). This is consistent with our data that GluK2 primarily senses cold but not cool temperatures. These observations suggest that GluK2 may sense cold temperatures in mouse DRG neurons.

The fish and human GLR-3/GluK2 homologs can also function as a cold receptor *in vitro*

Our observation that both GLR-3 and mouse GluK2 can function as a cold receptor prompted us to ask how deeply the role of GLR-3/GluK2 as a cold receptor is conserved across the phylogeny. We thus tested the zebrafish and human homologs of GluK2. Transfection of both zebrafish and human GluK2 in CHO cells conferred cold sensitivity to these cells (Figure 2.7G-H), suggesting that they both can function as a cold receptor in heterologous systems. Thus, GLR-3/GluK2 from worms, zebrafish, mice, and humans all have the capacity to function as a cold receptor, suggesting that the function of GLR-3/GluK2 in cold sensation might be evolutionarily conserved from worms to humans.

2.6 Discussion

Despite decades of intensive research, little is known about the molecular mechanisms underlying cold sensation. Previous efforts to identify cold sensors using candidate gene approaches have not been very fruitful, though this approach is highly

successful in identifying heat sensors such as thermo-TRP channels (Bandell et al., 2007; Castillo et al., 2018). To overcome this technical difficulty, in the current study, we designed an unbiased, activity-based genetic screen for cold-sensing receptors in *C. elegans* using a real-time PCR thermocycler. We showed that GLR-3, a member of the kainate-type of glutamate receptors, surprisingly functions as a cold receptor.

GLR-3 possesses several interesting features. First, its activation threshold is lower than that of TRPM8 (i.e. ~18°C vs. ~26°C), which is close to the range of noxious cold, suggesting that GLR-3 may primarily sense noxious cold rather than cool temperatures. Second, unlike other thermal receptors that are temperature-gated ion channels (Bandell et al., 2007; Castillo et al., 2018), GLR-3 functions as a metabotropic thermal receptor. This is supported by the observation that channel-dead GLR-3 and mouse GluK2 variants show normal cold sensitivity. In addition, though worm GLR-3 is cold-sensitive, it does not display any detectable channel activity. Furthermore, both GLR-3 and mouse GluK2 rely on G proteins to transmit cold signals. Another interesting feature of GLR-3 is that glutamate is not required for this receptor to sense cold *in vivo*, as *eat-4* mutant worms, which are devoid of glutamate signaling, show normal cold sensitivity in ASER neuron. GLR-3 and mouse GluK2 can also sense cold in the absence of glutamate in heterologous systems. This suggests that the cold-sensing activity of GLR-3/GluK2 is independent of its glutamate receptor function. Furthermore, mutations in the N-terminal ATD domain of GluK2, which disrupt the cold sensitivity of mouse GluK2, spare its glutamate-gated channel activity, suggesting that the functions of cold-sensing and glutamate-sensing of GluK2 could be dissociated and may require distinct domains. We thus propose that some glutamate receptors, such as GLR-

3/GluK2, are multifunctional, acting as a chemical receptor in the central nervous system but functioning as a thermal receptor in the periphery.

As a metabotropic cold receptor, GLR-3 requires G proteins to transmit cold signals, which would presumably lead to the activation of downstream transduction channel(s) and hence cooling-evoked calcium response. Indeed, cooling-activated calcium response mediated by GLR-3/GluK2 primarily results from calcium influx (Figure 2.10E-F), suggesting the presence of downstream transduction channel(s). The identity of the transduction channel(s) acting downstream of GLR-3 and G proteins is currently unknown. Future studies are needed to address this question, as well as to identify the detailed transduction mechanisms. We found that a Gi/o protein is required for GLR-3 to transduce cold signals. Though Gi/o is known to trigger inhibitory signaling, interestingly, it can also be coupled to excitatory signaling mediated mostly by its Gβγ subunits (Neves et al., 2002). Notably, in addition to channels, G proteins can also regulate many other types of effectors, such as enzymes, transporters, transcriptional machinery, mobility/contractibility machinery, secretory machinery, etc (Neves et al., 2002). In this regard, a metabotropic thermal receptor would be more functionally versatile and may potentially regulate a wider range of cellular processes. GLR-3 thus represents a previously unknown class of thermal receptor.

Glutamate receptors are chemical-sensing receptors that are well known to mediate chemical synaptic transmission/plasticity in the central nervous system. Our results reveal an unexpected case where a central chemical receptor functions as a thermal receptor in the periphery. As glutamate receptors are evolutionarily conserved, this raises the intriguing possibility that in addition to sensing chemicals (i.e. glutamate),

one ancestral function of glutamate receptors might be to sense non-chemical cues such as temperature. Interestingly, some insect chemical-sensing ionotropic receptors (IRs) regulate thermosensation (Budelli et al., 2019). It would be interesting to test whether they can directly sense temperature.

Another interesting observation is that the vertebrate GLR-3 homolog GluK2 from mouse, human and zebrafish can all function as a cold receptor in heterologous systems. Mouse GluK2 can also functionally substitute for worm GLR-3 in cold sensation *in vivo*. In addition to the brain, we found that mouse GluK2 is expressed in DRG neurons in the periphery, and knockdown of GluK2 in DRG neurons greatly reduced the sensitivity of these primary sensory neurons to cold but not cool temperatures, raising the possibility that GluK2 may function as a cold receptor in DRG neurons in mammals. We thus propose that the role of GLR-3/GluK2 as a cold receptor may be evolutionarily conserved from worms to humans.

References

1. Bandell, M., Macpherson, L.J., and Patapoutian, A. (2007). From chills to chilis: mechanisms for thermosensation and chemesthesis via thermoTRPs. Curr Opin Neurobiol *17*, 490-497.

2. Bargmann, C.I. (2006). Chemosensation in C. elegans. WormBook, 1-29.

3. Bautista, D.M., Siemens, J., Glazer, J.M., Tsuruda, P.R., Basbaum, A.I., Stucky, C.L., Jordt, S.E., and Julius, D. (2007). The menthol receptor TRPM8 is the principal detector of environmental cold. Nature *448*, 204-208.

4. Bowie, D. (2008). Ionotropic glutamate receptors & CNS disorders. CNS & neurological disorders drug targets *7*, 129-143.

5. Brockie, P.J., Madsen, D.M., Zheng, Y., Mellem, J., and Maricq, A.V. (2001). Differential expression of glutamate receptor subunits in the nervous system of Caenorhabditis elegans and their regulation by the homeodomain protein UNC-42. The Journal of neuroscience : the official journal of the Society for Neuroscience *21*, 1510-1522.

6. Budelli, G., Ni, L., Berciu, C., van Giesen, L., Knecht, Z.A., Chang, E.C., Kaminski, B., Silbering, A.F., Samuel, A., Klein, M.*, et al.* (2019). Ionotropic Receptors Specify the Morphogenesis of Phasic Sensors Controlling Rapid Thermal Preference in Drosophila. Neuron *101*, 738-747 e733.

7. Castillo, K., Diaz-Franulic, I., Canan, J., Gonzalez-Nilo, F., and Latorre, R. (2018). Thermally activated TRP channels: molecular sensors for temperature detection. Phys Biol *15*, 021001.

8. Coggeshall, R.E., and Carlton, S.M. (1998). Ultrastructural analysis of NMDA, AMPA, and kainate receptors on unmyelinated and myelinated axons in the periphery. J Comp Neurol *391*, 78-86.

9. Dhaka, A., Murray, A.N., Mathur, J., Earley, T.J., Petrus, M.J., and Patapoutian, A. (2007). TRPM8 is required for cold sensation in mice. Neuron *54*, 371-378.

10. Dingledine, R., Hume, R.I., and Heinemann, S.F. (1992). Structural determinants of barium permeation and rectification in non-NMDA glutamate receptor channels. The Journal of neuroscience : the official journal of the Society for Neuroscience *12*, 4080-4087.

11. Fang, X., Djouhri, L., McMullan, S., Berry, C., Okuse, K., Waxman, S.G., and Lawson, S.N. (2005). trkA is expressed in nociceptive neurons and influences electrophysiological properties via Nav1.8 expression in rapidly conducting nociceptors. The Journal of neuroscience : the official journal of the Society for Neuroscience *25*, 4868-4878.

12. Foulkes, T., and Wood, J.N. (2007). Mechanisms of cold pain. Channels *1*, 154-160.

13. Garrity, P.A., Goodman, M.B., Samuel, A.D., and Sengupta, P. (2010). Running hot and cold: behavioral strategies, neural circuits, and the molecular machinery for thermotaxis in C. elegans and Drosophila. Genes Dev *24*, 2365-2382.

14. Gierschik, P. (1992). ADP-ribosylation of signal-transducing guanine nucleotide-binding proteins by pertussis toxin. Curr Top Microbiol Immunol *175*, 69-96.

15. Gong, J., Yuan, Y., Ward, A., Kang, L., Zhang, B., Wu, Z., Peng, J., Feng, Z., Liu, J., and Xu, X.Z. (2016). The C. elegans Taste Receptor Homolog LITE-1 Is a Photoreceptor. Cell *167*, 1252-1263 e1210.

16. Goodman, M.B. (2006). Mechanosensation. WormBook, 1-14.

17. Goubaeva, F., Ghosh, M., Malik, S., Yang, J., Hinkle, P.M., Griendling, K.K., Neubig, R.R., and Smrcka, A.V. (2003). Stimulation of cellular signaling and G protein subunit dissociation by G protein betagamma subunit-binding peptides. J Biol Chem *278*, 19634-19641.

18. Huettner, J.E. (1990). Glutamate receptor channels in rat DRG neurons: activation by kainate and quisqualate and blockade of desensitization by Con A. Neuron *5*, 255-266.

19. Jansen, G., Thijssen, K.L., Werner, P., van der Horst, M., Hazendonk, E., and Plasterk, R.H. (1999). The complete family of genes encoding G proteins of Caenorhabditis elegans. Nat Genet *21*, 414-419.

20. Lee, R.Y., Sawin, E.R., Chalfie, M., Horvitz, H.R., and Avery, L. (1999). EAT-4, a homolog of a mammalian sodium-dependent inorganic phosphate cotransporter, is necessary for glutamatergic neurotransmission in caenorhabditis elegans. The Journal of neuroscience : the official journal of the Society for Neuroscience *19*, 159-167.

21. Lou, S., Duan, B., Vong, L., Lowell, B.B., and Ma, Q. (2013). Runx1 controls terminal morphology and mechanosensitivity of VGLUT3-expressing C-mechanoreceptors. The Journal of neuroscience : the official journal of the Society for Neuroscience *33*, 870-882.

22. McGhee, J.D. (2007). The C. elegans intestine. WormBook, 1-36.

23. McKemy, D.D., Neuhausser, W.M., and Julius, D. (2002). Identification of a cold receptor reveals a general role for TRP channels in thermosensation. Nature *416*, 52-58.

24. Minevich, G., Park, D.S., Blankenberg, D., Poole, R.J., and Hobert, O. (2012). CloudMap: a cloud-based pipeline for analysis of mutant genome sequences. Genetics *192*, 1249-1269.

25. Moparthi, L., Kichko, T.I., Eberhardt, M., Hogestatt, E.D., Kjellbom, P., Johanson, U., Reeh, P.W., Leffler, A., Filipovic, M.R., and Zygmunt, P.M. (2016). Human TRPA1 is a heat sensor displaying intrinsic U-shaped thermosensitivity. Sci Rep *6*, 28763.

26. Neves, S.R., Ram, P.T., and Iyengar, R. (2002). G protein pathways. Science *296*, 1636-1639.

27. Ortiz, C.O., Faumont, S., Takayama, J., Ahmed, H.K., Goldsmith, A.D., Pocock, R., McCormick, K.E., Kunimoto, H., Iino, Y., Lockery, S.*, et al.* (2009). Lateralized gustatory behavior of C. elegans is controlled by specific receptor-type guanylyl cyclases. Current biology : CB *19*, 996-1004.

28. Pauwels, P.J., and Colpaert, F.C. (2003). Ca2+ responses in Chinese hamster ovary-K1 cells demonstrate an atypical pattern of ligand-induced 5-HT1A receptor activation. The Journal of pharmacology and experimental therapeutics *307*, 608-614.

29. Peier, A.M., Moqrich, A., Hergarden, A.C., Reeve, A.J., Andersson, D.A., Story, G.M., Earley, T.J., Dragoni, I., McIntyre, P., Bevan, S.*, et al.* (2002). A TRP channel that senses cold stimuli and menthol. Cell *108*, 705-715.

30. Perkins, L.A., Hedgecock, E.M., Thomson, J.N., and Culotti, J.G. (1986). Mutant sensory cilia in the nematode Caenorhabditis elegans. Dev Biol *117*, 456-487.

31. Pierce-Shimomura, J.T., Faumont, S., Gaston, M.R., Pearson, B.J., and Lockery, S.R. (2001). The homeobox gene lim-6 is required for distinct chemosensory representations in C. elegans. Nature *410*, 694-698.

32. Richmond, J.E., Davis, W.S., and Jorgensen, E.M. (1999). UNC-13 is required for synaptic vesicle fusion in C. elegans. Nat Neurosci *2*, 959-964.

33. Robert, A., Hyde, R., Hughes, T.E., and Howe, J.R. (2002). The expression of dominant-negative subunits selectively suppresses neuronal AMPA and kainate receptors. Neuroscience *115*, 1199-1210.

34. Rodriguez-Moreno, A., and Lerma, J. (1998). Kainate receptor modulation of GABA release involves a metabotropic function. Neuron *20*, 1211-1218.

35. Rozas, J.L., Paternain, A.V., and Lerma, J. (2003). Noncanonical signaling by ionotropic kainate receptors. Neuron *39*, 543-553.

36. Schepers, R.J., and Ringkamp, M. (2010). Thermoreceptors and thermosensitive afferents. Neurosci Biobehav Rev *34*, 177-184.

37. Speese, S., Petrie, M., Schuske, K., Ailion, M., Ann, K., Iwasaki, K., Jorgensen, E.M., and Martin, T.F. (2007). UNC-31 (CAPS) is required for dense-core vesicle but not synaptic vesicle exocytosis in Caenorhabditis elegans. The Journal of neuroscience : the official journal of the Society for Neuroscience *27*, 6150-6162.

38. Story, G.M., Peier, A.M., Reeve, A.J., Eid, S.R., Mosbacher, J., Hricik, T.R., Earley, T.J., Hergarden, A.C., Andersson, D.A., Hwang, S.W.*, et al.* (2003). ANKTM1, a TRP-like channel expressed in nociceptive neurons, is activated by cold temperatures. Cell *112*, 819-829.

39. Suzuki, H., Thiele, T.R., Faumont, S., Ezcurra, M., Lockery, S.R., and Schafer, W.R. (2008). Functional asymmetry in Caenorhabditis elegans taste neurons and its computational role in chemotaxis. Nature *454*, 114-117.

40. Takasaki, J., Saito, T., Taniguchi, M., Kawasaki, T., Moritani, Y., Hayashi, K., and Kobori, M. (2004). A novel Galphaq/11-selective inhibitor. J Biol Chem *279*, 47438-47445.

41. Tomioka, M., Adachi, T., Suzuki, H., Kunitomo, H., Schafer, W.R., and Iino, Y. (2006). The Insulin/PI 3-Kinase Pathway Regulates Salt Chemotaxis Learning in Caenorhabditis elegans. Neuron *51*, 613-625.

42. Traynelis, S.F., Wollmuth, L.P., McBain, C.J., Menniti, F.S., Vance, K.M., Ogden, K.K., Hansen, K.B., Yuan, H., Myers, S.J., and Dingledine, R. (2010). Glutamate receptor ion channels: structure, regulation, and function. Pharmacological reviews *62*, 405-496.

43. Valbuena, S., and Lerma, J. (2016). Non-canonical Signaling, the Hidden Life of Ligand-Gated Ion Channels. Neuron *92*, 316-329.

44. Vandewauw, I., De Clercq, K., Mulier, M., Held, K., Pinto, S., Van Ranst, N., Segal, A., Voet, T., Vennekens, R., Zimmermann, K*., et al.* (2018). A TRP channel trio mediates acute noxious heat sensing. Nature *555*, 662-666.

45. Wang, F., Flanagan, J., Su, N., Wang, L.C., Bui, S., Nielson, A., Wu, X., Vo, H.T., Ma, X.J., and Luo, Y. (2012a). RNAscope: a novel in situ RNA analysis platform for formalin-fixed, paraffin-embedded tissues. The Journal of molecular diagnostics : JMD *14*, 22-29.

46. Wang, R., Mellem, J.E., Jensen, M., Brockie, P.J., Walker, C.S., Hoerndli, F.J., Hauth, L., Madsen, D.M., and Maricq, A.V. (2012b). The SOL-2/Neto auxiliary protein modulates the function of AMPA-subtype ionotropic glutamate receptors. Neuron *75*, 838-850.

47. Wang, X., Li, G., Liu, J., Liu, J., and Xu, X.Z. (2016). TMC-1 Mediates Alkaline Sensation in C. elegans through Nociceptive Neurons. Neuron *91*, 146-154.

48. Ward, A., Liu, J., Feng, Z., and Xu, X.Z. (2008). Light-sensitive neurons and channels mediate phototaxis in C. elegans. Nature Neurosci *11*, 916-922.

49. Winter, Z., Gruschwitz, P., Eger, S., Touska, F., and Zimmermann, K. (2017). Cold Temperature Encoding by Cutaneous TRPA1 and TRPM8-Carrying Fibers in the Mouse. Frontiers in molecular neuroscience *10*, 209.

50. Xiao, R., Zhang, B., Dong, Y., Gong, J., Xu, T., Liu, J., and Xu, X.Z.S. (2013). A genetic program promotes C. elegans longevity at cold temperatures via a thermosensitive TRP channel. Cell *152*, 806-817.
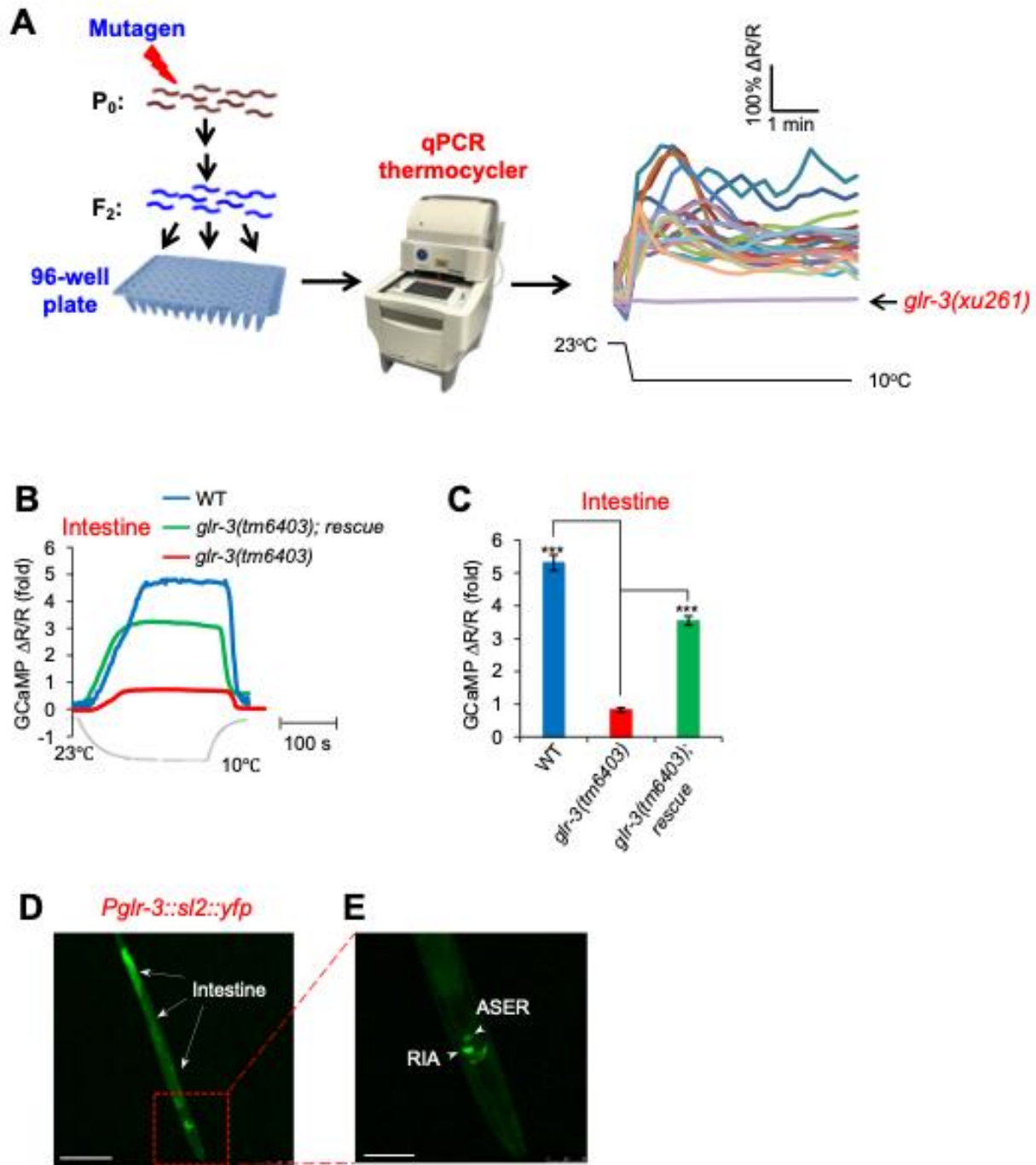
Figure 2.1. An unbiased activity-based genetic screen identifies a key role for

GLR-3 in cold sensation.

(A) Schematic describing the design of the screen. Worms carrying a transgene

co-expressing GCaMP3 and DsRed in the intestine were mutagenized with EMS and

their progeny was screened using a real-time PCR thermocycler for candidates defective in cooling-evoked calcium increase in the intestine. Sample traces were shown to the right, highlighting *glr-3(xu261)* mutant. The temperature was cooled from 23 to 10°C.

(B-C) Calcium imaging shows that the *glr-3(tm6403)* deletion mutant exhibited a severe defect in cooling-evoked calcium response in the intestine. This phenotype was rescued by expressing wild-type *glr-3* gene specifically in the intestine using the *ges-1* promoter. (B) Sample traces. (C) Bar graph. Error bars: SEM. n≥13. ***p<0.0001 (ANOVA with Bonferroni test).

(D-E) *glr-3* is expressed in the intestine and the ASER sensory neuron, in addition to the central interneurons RIA. A genomic DNA fragment encompassing 3.2 kb of 5'UTR and the entire coding region of *glr-3* was used to drive YFP expression. (D) Low magnification image. (E) High magnification image highlighting neuronal expression in the head. (D) and (E) are two independent images taken with different objectives. Arrow heads point to ASER and RIAR (RIAL not visible on this focal plane). Scale bars: 100 μm (D); 20 μm (E).

Figure 2.2. GLR-3 acts in ASER neuron to mediate cold sensation and cold-avoidance behavior.

(A-B) ASER neuron is cold-sensitive and requires GLR-3 for cold sensation. Cooling evoked robust calcium response in ASER neuron, which is defective in *glr-3(tm6403)* mutant worms. Transgenic expression of wild-type *glr-3* cDNA in ASER using the ASER-specific *gcy-5* promoter rescued the mutant phenotype. (A) Sample traces. (B) Bar graph. Error bars: SEM. n≥12. ***p<0.0001 (ANOVA with Bonferroni test).

(C-D) Loss of GLR-3 does not affect the sensitivity of ASER neuron to salt. *glr-3(tm6403)* mutant worms showed normal response to NaCl gradient compared to WT, while *che-2(e1033)* mutant worms were defective in this response. (C) Sample traces. (B) Bar graph. Error bars: SEM. n≥11. ***p<0.0001 (ANOVA with Bonferroni test).

(E-F) Cooling-evoked calcium response persists in *unc-13, unc-31* and *eat-4* mutant backgrounds. (C) Sample traces. (D) Bar graphs. Error bars: SEM. n≥11. ***p<0.0001 (ANOVA with Bonferroni test).

(G) GLR-3 mediates cooling-evoked avoidance behavior in ASER neuron. Cooling triggered turns in worms during swimming, and *glr-3* mutant worms showed a strong defect in this behavioral response, which was rescued by transgenic expression of *glr-3* cDNA in ASER. Error bars: SEM. n≥15.

(H) *glr-3(tm6403)* mutant worms show normal salt chemotaxis behavior, while *che-2(e1033)* mutant worms are defective in this behavior. The chemotaxis assay was run in triplicates, and the experiment was repeated four times. Error bars: SEM. ***p<0.0001 (ANOVA with Bonferroni test).
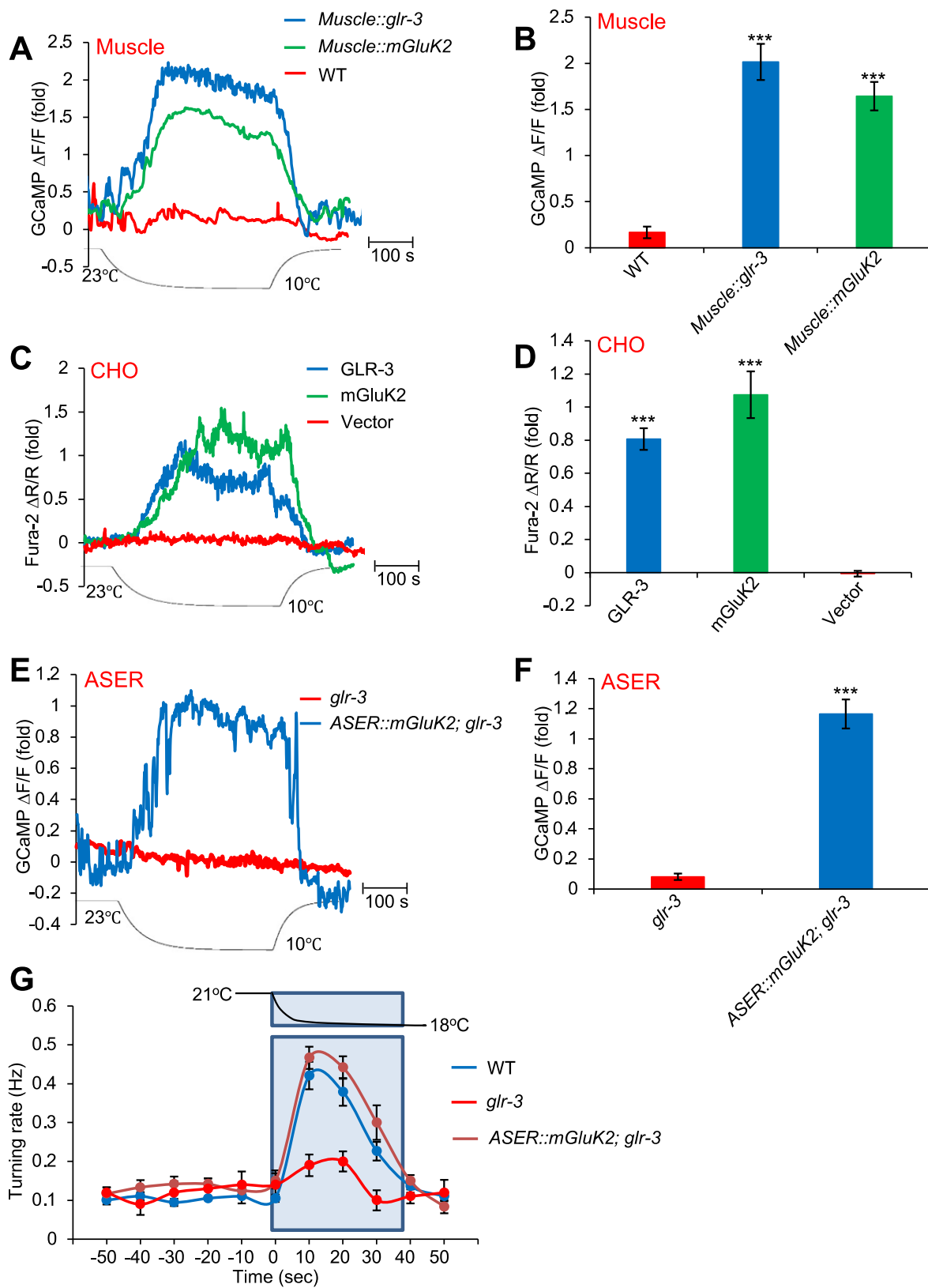
Figure 2.3. GLR-3 and mouse GluK2 function as a cold senor *in vitro,* and mouse GluK2 can functionally substitute for GLR-3 in cold sensation *in vivo.*

(A-B) Ectopic expression of GLR-3 and mouse GluK2 in worm muscle cells confers cold-sensitivity to these cells. GLR-3 and mouse GluK2 were expressed as a transgene in worm body-wall muscles using the *myo-3* promoter. Cooling evoked calcium response in muscle cells of transgenic worms. All genotypes carried a transgene expressing GCaMP6. (A) Sample traces. (B) Bar graph. Error bars: SEM. n≥11. ***p<0.0001 (ANOVA with Bonferroni test).

(C-D) Heterologous expression of GLR-3 and mouse GluK2 in CHO cells confers cold sensitivity to these cells. GLR-3 and mouse GluK2 were transfected into CHO cells, and cooling evoked calcium response in these cells as shown by Fura-2 imaging. (C) Sample traces. (D) Bar graph. Error bars: SEM. n≥20. ***p<0.0001 (ANOVA with Bonferroni test).

(E-F) Mouse GluK2 can functionally substitute for GLR-3 in cold sensation in ASER neuron. Transgenic expression of mouse GluK2 in ASER neuron of *glr-3* mutant worms rescued the *glr-3* mutant phenotype in cooling-evoked calcium response in ASER neuron. (E) Sample traces. (F) Bar graph. Error bars: SEM. n≥12. ***p<0.0001 (ANOVA with Bonferroni test).

(G) Mouse GluK2 can functionally substitute for GLR-3 in cold-avoidance behavior mediated by ASER neuron. Transgenic expression of mouse GluK2 in ASER neuron of *glr-3* mutant worms rescued the *glr-3* mutant phenotype in cooling-evoked avoidance behavior. Error bars: SEM. n≥15. See also Figure 2.9-2.10.
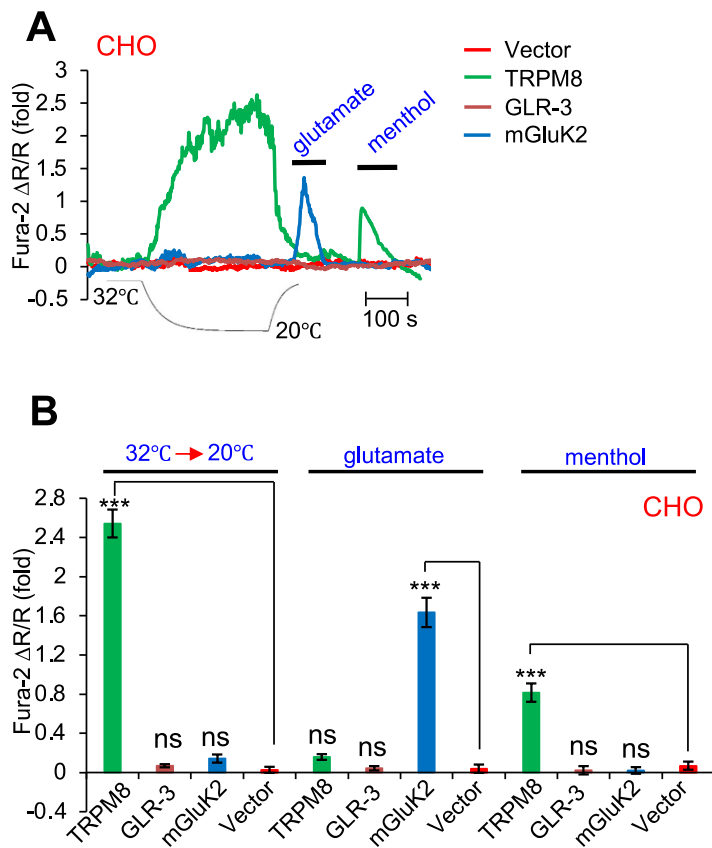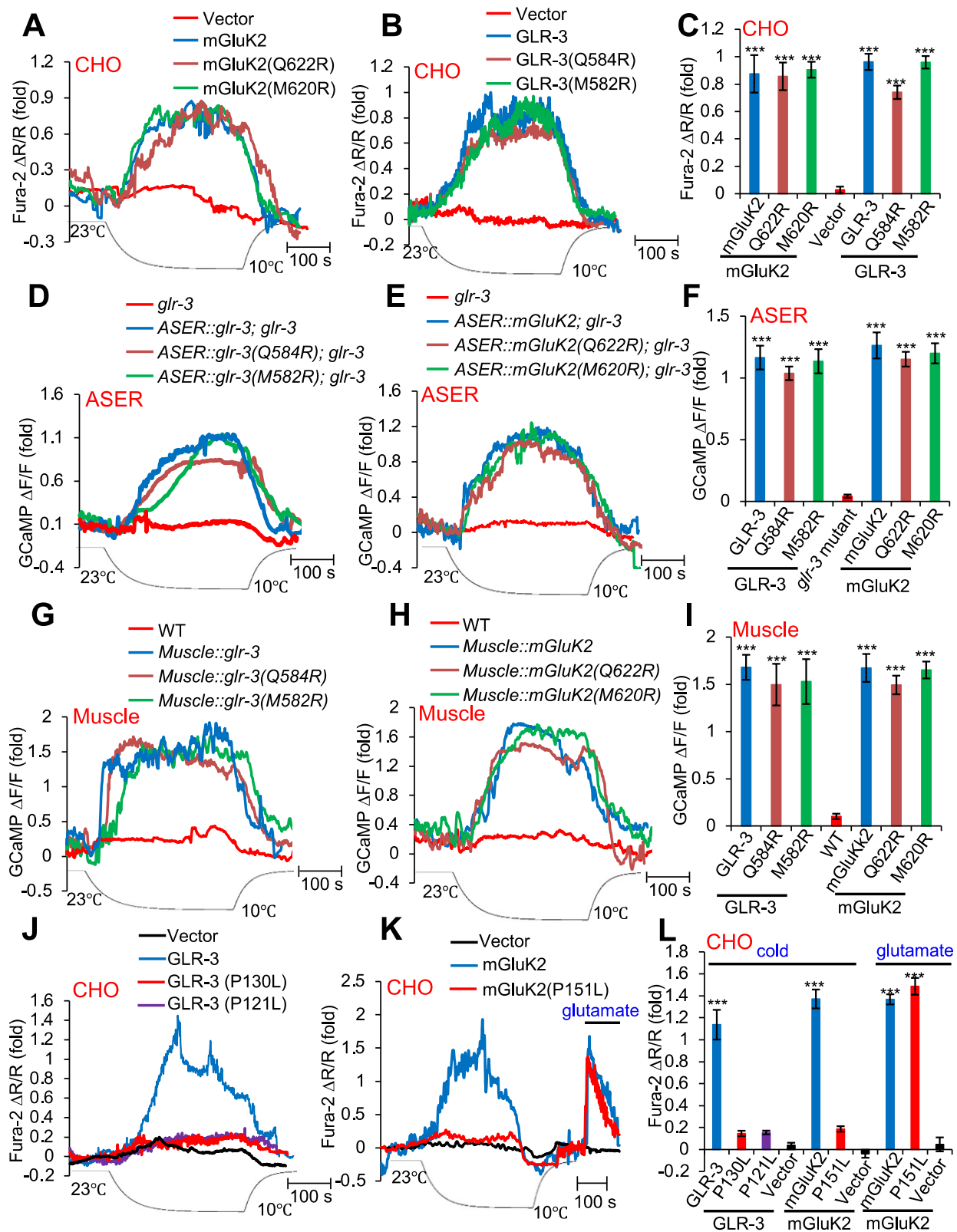
Figure 2.4. The sensitivity of GLR-3/GluK2 and TRPM8 to cold, glutamate and menthol. Cooling from 32°C to 20°C activated TRPM8 but not GLR-3 or mouse GluK2 when transfected in CHO cells. Mouse GluK2, but not GLR-3 or TRPM8, can be activated by glutamate (10 mM), while TRPM8 was also sensitive to menthol (100 μM) but not glutamate (10 mM). (A) Sample traces. (B) Bar graph. Error bars: SEM. n≥20. ***p<0.0001 (ANOVA with Bonferroni test).

See also Figure 2.11-2.12.

Figure 2.5. The cold sensitivity of GLR-3/GluK2 is independent of its channel function.

(A-C) Channel-dead GLR-3/GluK2 variants show normal cold sensitivity in CHO cells. The two channel-dead variants for mouse GluK2 (A), as well as GLR-3 (B), showed similar cold sensitivity compared to wild-type GluK2/GLR-3 when transfected in CHO cells. (A-B) Sample trances. (C) Bar graph. Error bars: SEM. n≥20. ***p<0.0001 (ANOVA with Bonferroni test).

(D-F) Channel-dead GLR-3/GluK2 variants show normal cold sensitivity in ASER neuron *in vivo*. The two channel-dead variants for GLR-3 (D), as well as mouse GluK2 (E), showed similar cold sensitivity compared to wild-type GluK2/GLR-3 when expressed as a transgene in ASER neuron of *glr-3* mutant worms. (D-E) Sample traces. (F) Bar graph. Error bars: SEM. n≥12. ***p<0.0001 (ANOVA with Bonferroni test).

(G-I) Channel-dead GLR-3/GluK2 variants show normal cold sensitivity in worm muscle cells. The two channel-dead variants for GLR-3 (G), as well as mouse GluK2 (H), showed similar cold sensitivity compared to wild-type GluK2/GLR-3 when expressed as a transgene in worm muscle cells. (G-H) Sample traces. (I) Bar graph. Error bars: SEM. n≥12. ***p<0.0001 (ANOVA with Bonferroni test).

(J-L) Cold-insensitive GLR-3/GluK2 mutants display glutamate-gated channel activity. (J) GLR-3(P121L) and GLR-3(P130L) were no longer sensitive to cold. (K) GluK2(P151L) was insensitive to cold but sensitive to glutamate. (L) Bar graph. Error bars: SEM. n≥22. ***p<0.0001 (ANOVA with Bonferroni test).

See also Figure 2.12.
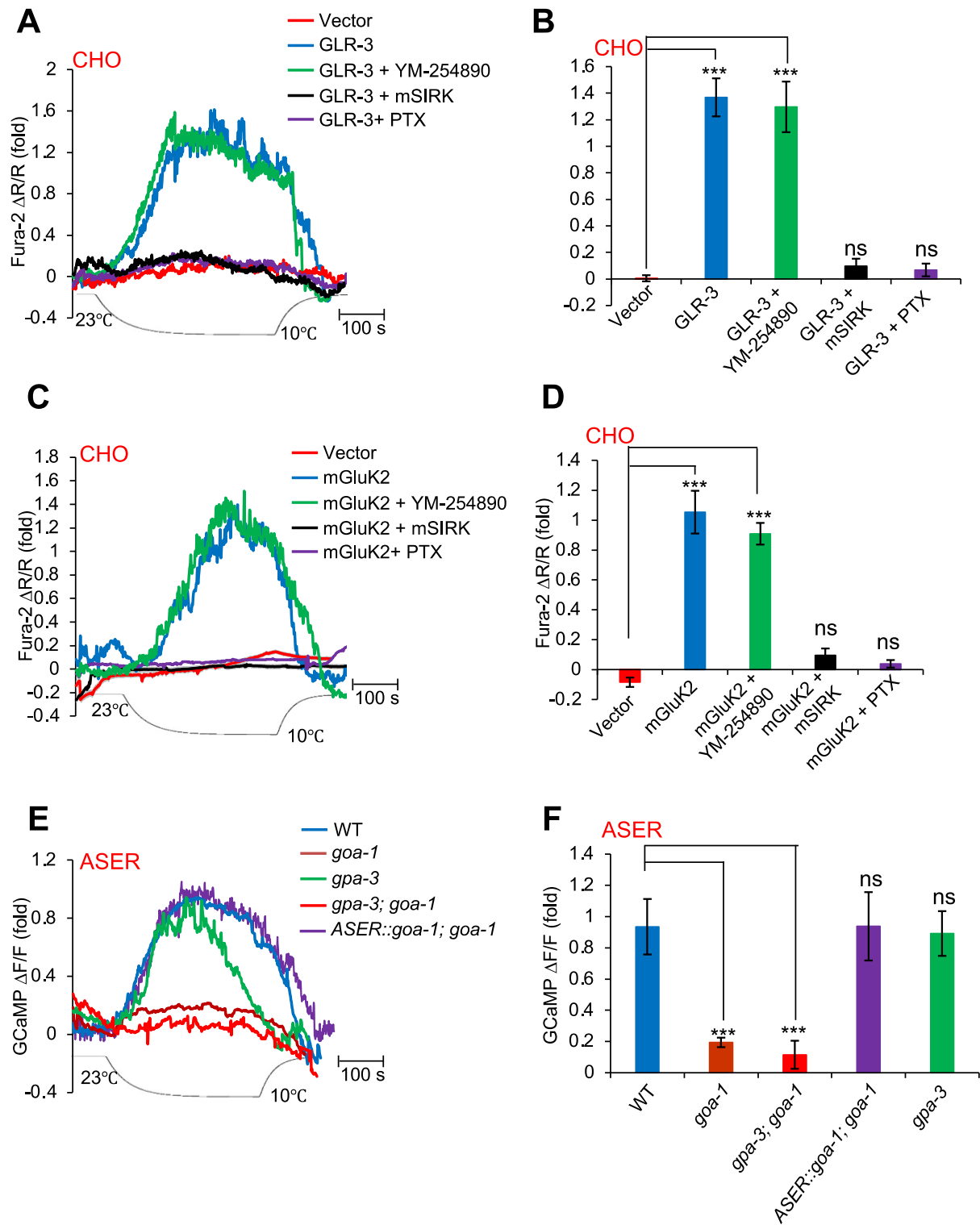
Figure 2.6. GLR-3 relies on G protein signaling to transmit cold signals.

(A-B) G protein inhibitors blocked the cold sensitivity of GLR-3 in CHO cells. The

pan-G protein inhibitor mSIRK (50 µM), the Gi/o inhibitor PTX (100 ng/ml), but not the

Gq/11 inhibitor YM-254890 (10 µM), blocked cooling-evoked calcium response

mediated by GLR-3 in CHO cells. (A) Sample traces. (B) Bar graph. Error bars: SEM.

n≥20. ***p<0.0001 (ANOVA with Bonferroni test).

(C-D) G protein inhibitors blocked the cold sensitivity of mouse GluK2 in CHO

cells. The pan-G protein inhibitor mSIRK (50 mM), the Gi/o inhibitor PTX (100 ng/ml),

but not the Gq/11 inhibitor YM-254890 (10 mM), blocked cooling-evoked calcium

response mediated by mouse GluK2 in CHO cells. (C) Sample traces. (D) Bar graph.

Error bars: SEM. n≥20. ***p<0.0001 (ANOVA with Bonferroni test).

(E-F) The cold sensitivity of ASER neuron requires the Gi/o protein gene *goa-1*.

goa-1(n1134) mutant worms showed a strong defect in cooling-evoked calcium

response in ASER neuron, a phenotype that was rescued by transgenic expression of

wild-type *goa-1* gene specifically in ASER neuron. (E) Sample traces. (F) Bar graph.

Error bars: SEM. n≥11. ***p<0.0001 (ANOVA with Bonferroni test).

See also Figure 2.13.
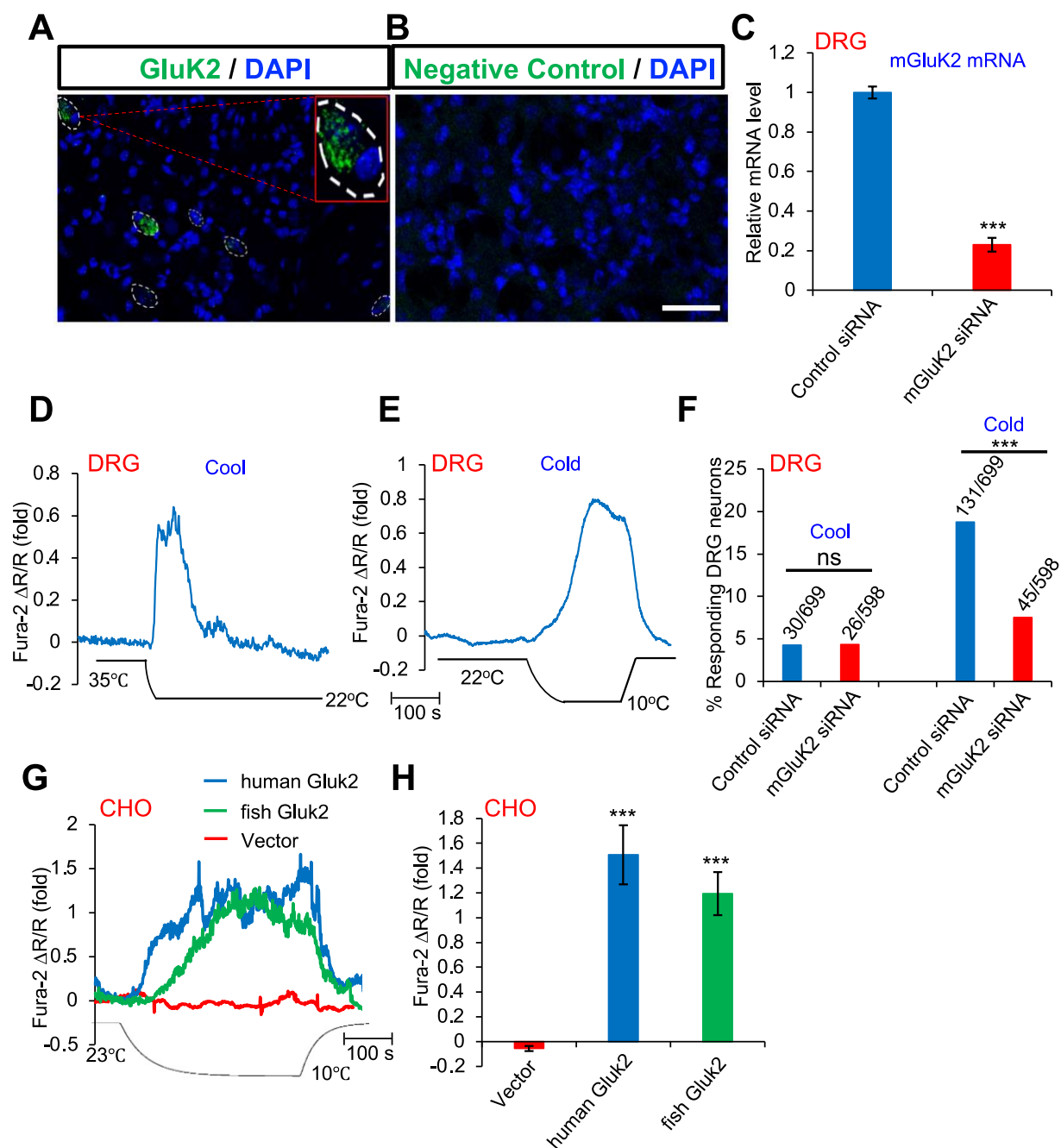
Figure 2.7. Mouse DRG neurons express GluK2 and knockdown of GluK2 in DRG neurons suppresses their sensitivity to cold but not cool temperatures.

(A-B) Mouse DRG neurons express GluK2 mRNA transcripts. (A) In situ hybridization using RNAscope assay detected GluK2 mRNA signals (puncta) in DRG

105

tissue. The dotted ovals denote the shape of the soma of the neurons expressing GluK2 transcripts. Only those neurons with at least 4 puncta inside the soma were scored positive, as the background signals detected by the control probe varied between 0-2 puncta/cell. The inset image in (A) highlights one GluK2-positive neuron. Green: GluK2 transcripts. Blue: DAPI. (B) Negative control probe staining (provided by Advanced Cell Diagnostics). Scale bar: 50 μm.

(C) Real-time quantitative RT-PCR (qPCR) analysis shows that siRNA knockdown of GluK2 in mouse DRG neurons greatly reduced the mRNA level of GluK2. qPCR reactions were run in triplicates. The experiment was repeated five times. Error bars: SEM. ***$p < 0.0001$ (t test).

(D-F) siRNA knockdown of GluK2 in mouse DRG neurons greatly reduces the sensitivity of these neurons to cold but not cool temperatures. (D) Sample trace showing calcium response to cool temperature (cooling to 22°C). (E) Sample trace showing calcium response to cold temperature (cooling to 10°C). (F) Bar graph. Sample sizes were shown on top of each bar. ***$p < 0.0001$ (χ^2 test).

(G-H) Fish and human GluK2 can also function as a cold receptor *in vitro*. Heterologous expression of fish and human GluK2 in CHO cells confers cold sensitivity to these cells. (E) Sample traces. (F) Bar graph. Error bars: SEM. n≥20. ***$p < 0.0001$ (ANOVA with Bonferroni test).
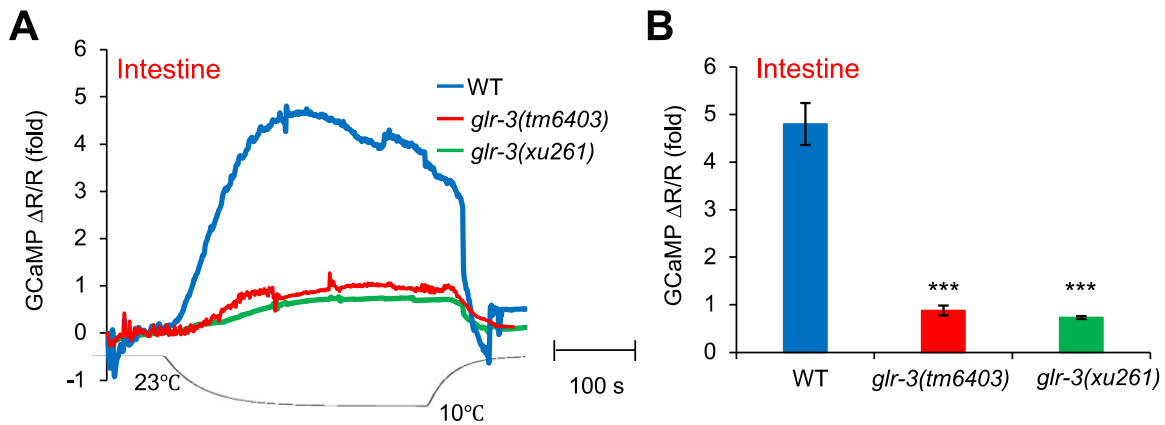
Figure 2.8. Additional data regarding cooling-evoked calcium response in the intestine. Both *glr-3(tm6403)* and *glr-3(xu261)* mutant worms showed a severe defect in cooling-evoked calcium response in the intestine. **(A)** Sample traces. **(B)** Bar graph. Error bars: SEM. n≥10. ***p<0.0001 (ANOVA with Bonferroni test).
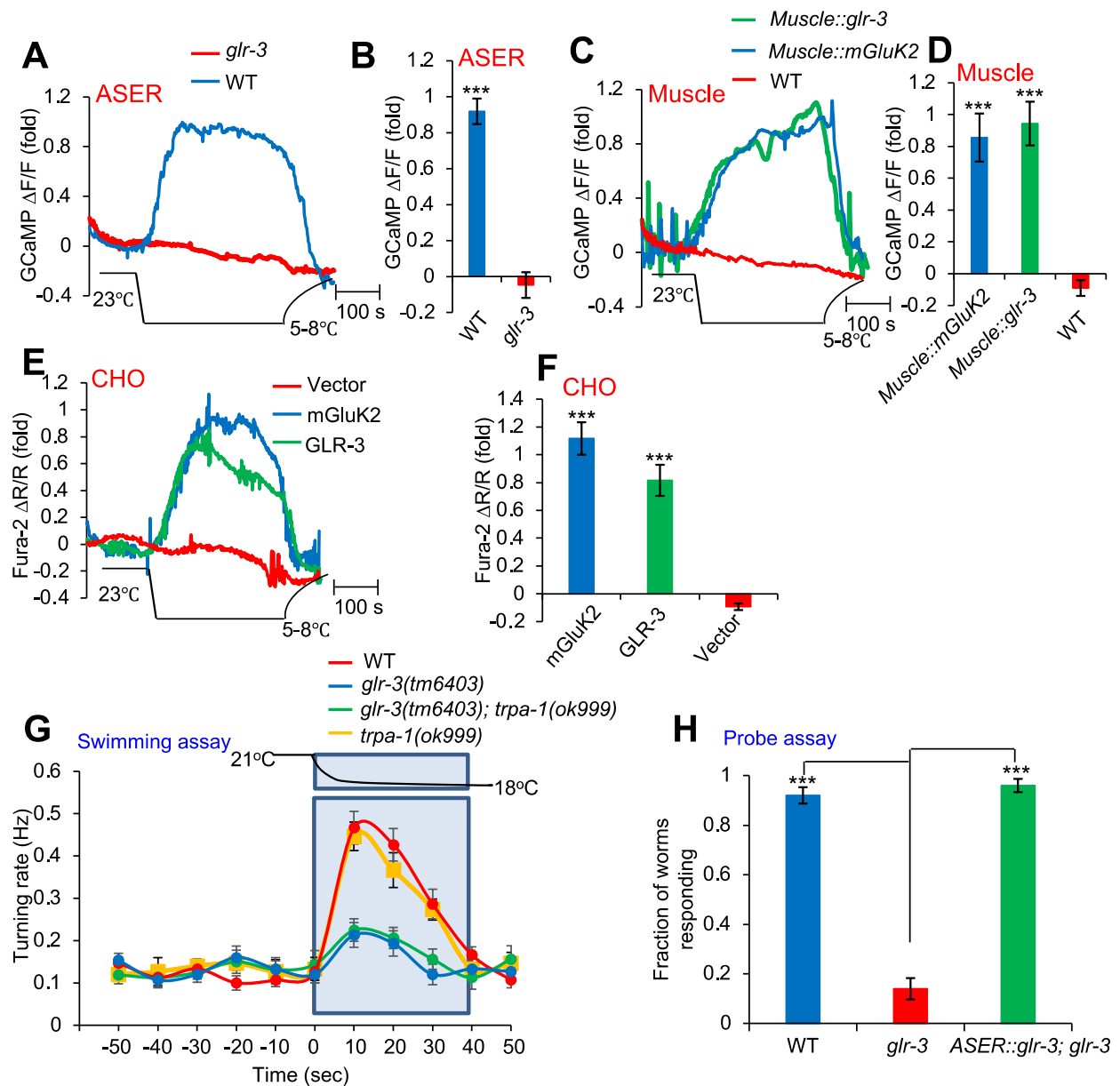
Figure 2.9. Rapid cooling evokes GLR-3/GluK2-dependent calcium response in *C. elegans* (ASER neuron and muscles) and CHO cells, and additional data on cold-avoidance behavior.

(A-F) Rapid cooling was achieved by perfusing pre-cooled solution towards the worm or CHO cells that express GLR-3/GluK2. We observed cooling-evoked calcium response similar to that described in the main figures. But since this protocol did not permit

precise control of the end temperature from experiment to experiment (varying from 5-8°C), we focused on the use of the conventional cooling protocol. Error bars: SEM. n≥12. ***p<0.0001 (ANOVA with Bonferroni test).

(G) TRPA-1 is not involved in cold-avoidance behavior in a swimming assay.

(H) *glr-3(tm6403)* mutant worms are defective in cold-avoidance behavior in a probe assay, which was rescued by an ASER-specific *glr-3* transgene. A pre-cooled probe, which cooled the air temperature near the head of the worm crawling on an agar plate, triggered backward movement (reversals). Error bars: SEM. n≥10. ***p<0.0001 (ANOVA with Bonferroni test).
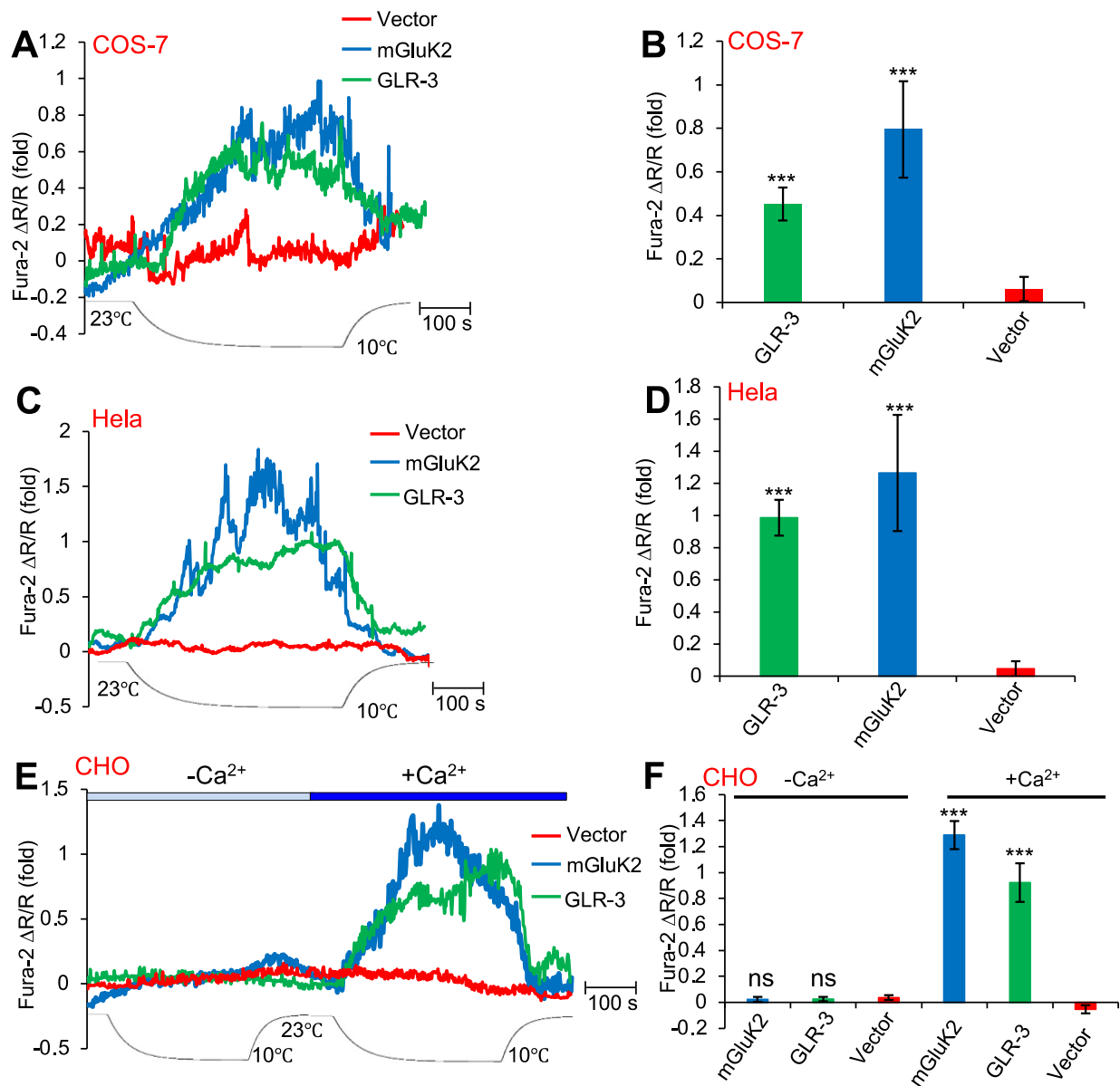
Figure 2.10. Heterologous expression of GLR-3 and mouse GluK2 in COS-7 and Hela cells confers cold sensitivity, and cooling-evoked calcium increase mediated by GLR-3/GluK2 primarily results from calcium influx.
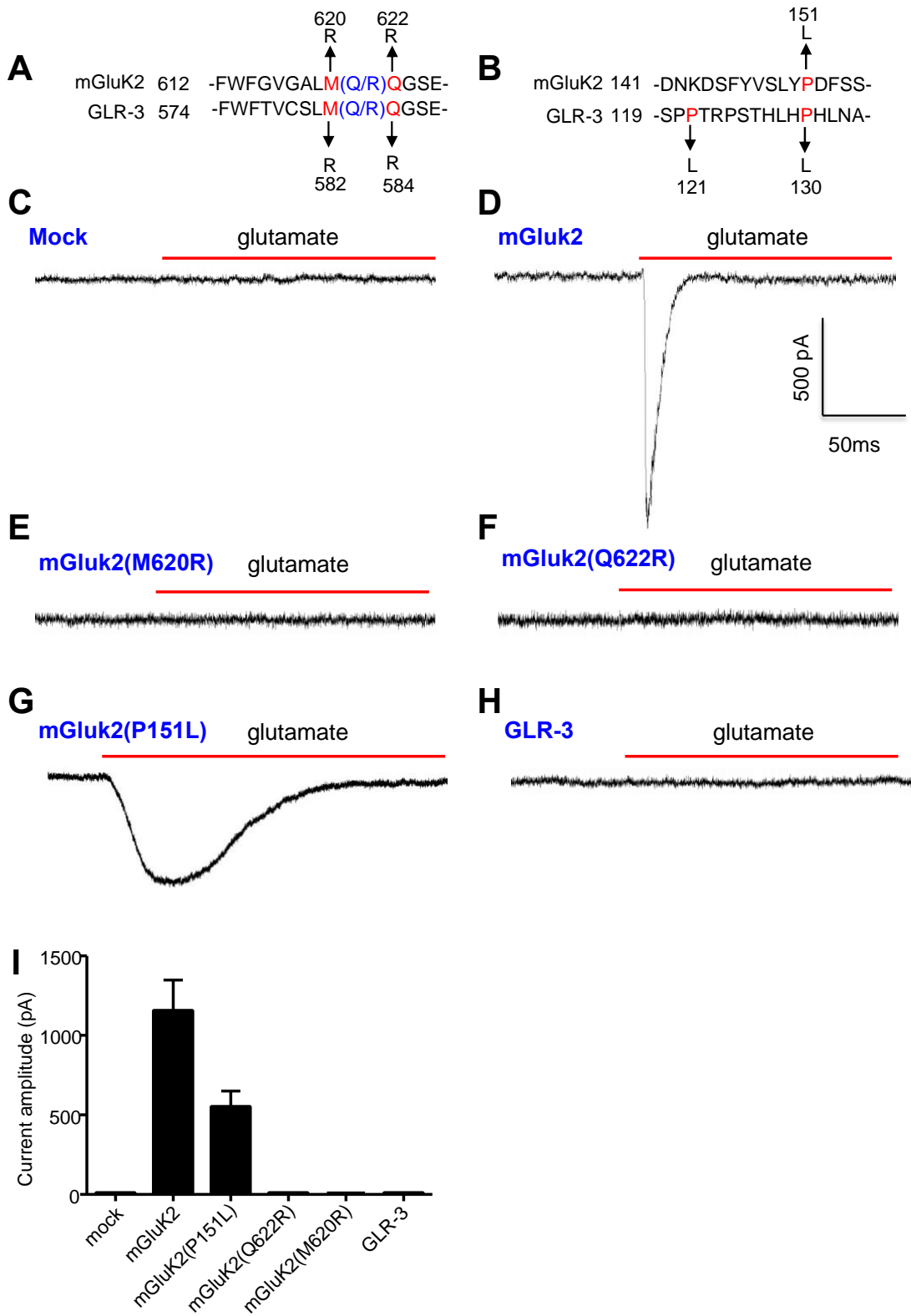
(A-D) COS-7 cells and Hela cells were transfected with GLR-3 and mGluK2 or vector control. Cooling evoked calcium response in GLR-3 and mGluK2 transfected cells but not control cells. **(A-B)** COS-7 cells. Error bars: SEM. n≥15. ***p<0.0001 (ANOVA with

Bonferroni test). **(C-D)** Hela cells. Error bars: SEM. n≥20. ***p<0.0001 (ANOVA with Bonferroni test).

(E-F) Cooling-evoked calcium increase mediated by GLR-3/GluK2 primarily results from calcium influx. Cooling evoked no or little calcium response in GLR-3/GluK2-expressing CHO cells in the absence of extracellular calcium, but evoked robust calcium increase when calcium was present in the bath solution. (E) Sample traces. (F) Bar graph. Error bars: SEM. n≥18. p=0.601, p=0.773, ***p<0.0001 (ANOVA with Bonferroni test).
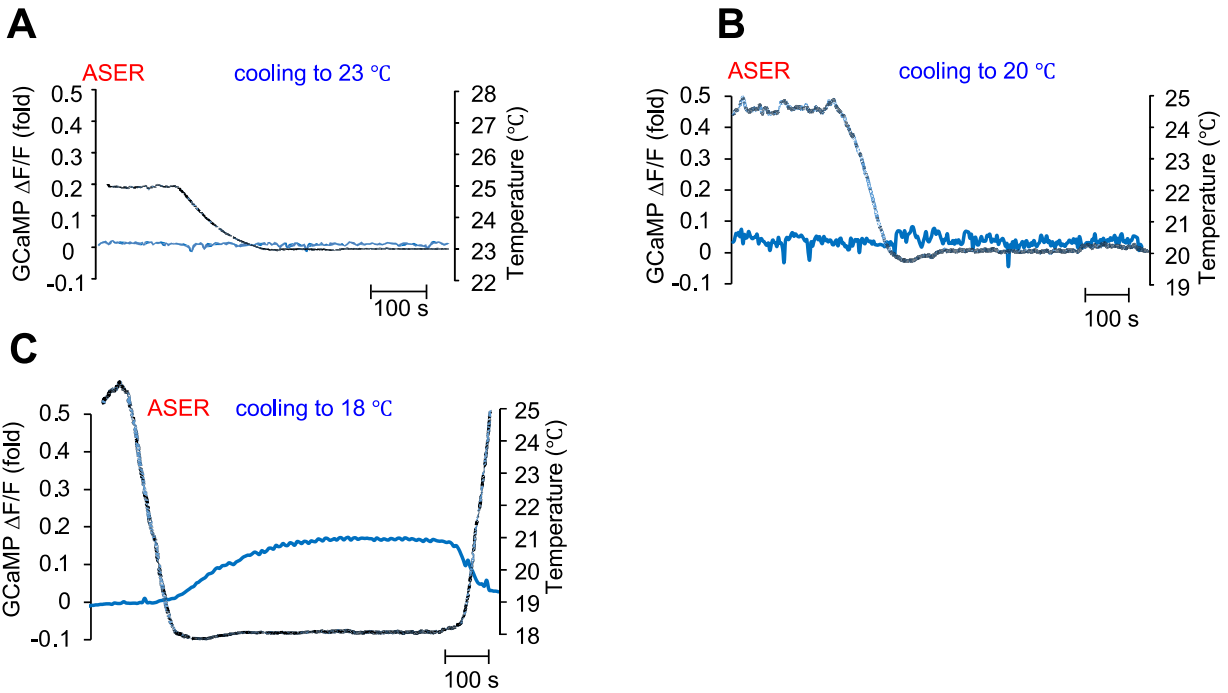
Figure 2.11. Cooling to 18°C evokes calcium response in ASER neuron. Sample

traces showing that the activation threshold of ASER neuron is around 18°C. Cooling to

23°C (A) and 20°C (B) failed to evoke calcium response in ASER neuron, while cooling

to 18°C did (C). The traces in blue represent calcium traces, while those in black denote

temperature changes.

A

620   622
R   R
↑   ↑

mGluK2 612 -FWFGVGAL**M**(Q/R)**Q**GSE-
GLR-3 574 -FWFTVCSL**M**(Q/R)**Q**GSE-

↓   ↓
R   R
582   584

B

151
L
↑

mGluK2 141 -DNKDSFYVSLY**P**DFSS-
GLR-3 119 -SP**P**TRPSTHLH**P**HLNA-

↓   ↓
L   L
121   130

C **Mock** glutamate

D **mGluk2** glutamate

500 pA

50ms

E **mGluk2(M620R)** glutamate

F **mGluk2(Q622R)** glutamate

G **mGluk2(P151L)** glutamate

**H** **GLR-3** glutamate

I

113

Figure 2.12. Glutamate-gated current is only detected in mouse GluK2 but not the channel-dead mouse GluK2 variants or GLR-3.

(A) Sequence alignment of mouse GluK2 and GLR-3 in the M2 pore region. The Q/R RNA editing site is denoted in blue. The residues mutated in this study are marked in red.

(B) Sequence alignment mouse GluK2 and GLR-3 in the N-terminal ATD domain where point mutations were generated in this study. The residues mutated are marked in red.

(C-I) Whole-cell recording of glutamate-gated currents of wild-type and various variants of mouse GluK2 as well as GLR-3 expressed in CHO cells. Glutamate: 10 mM. (C-H) Sample traces. (I) Bar graph. n≥4. Error bars: SEM.
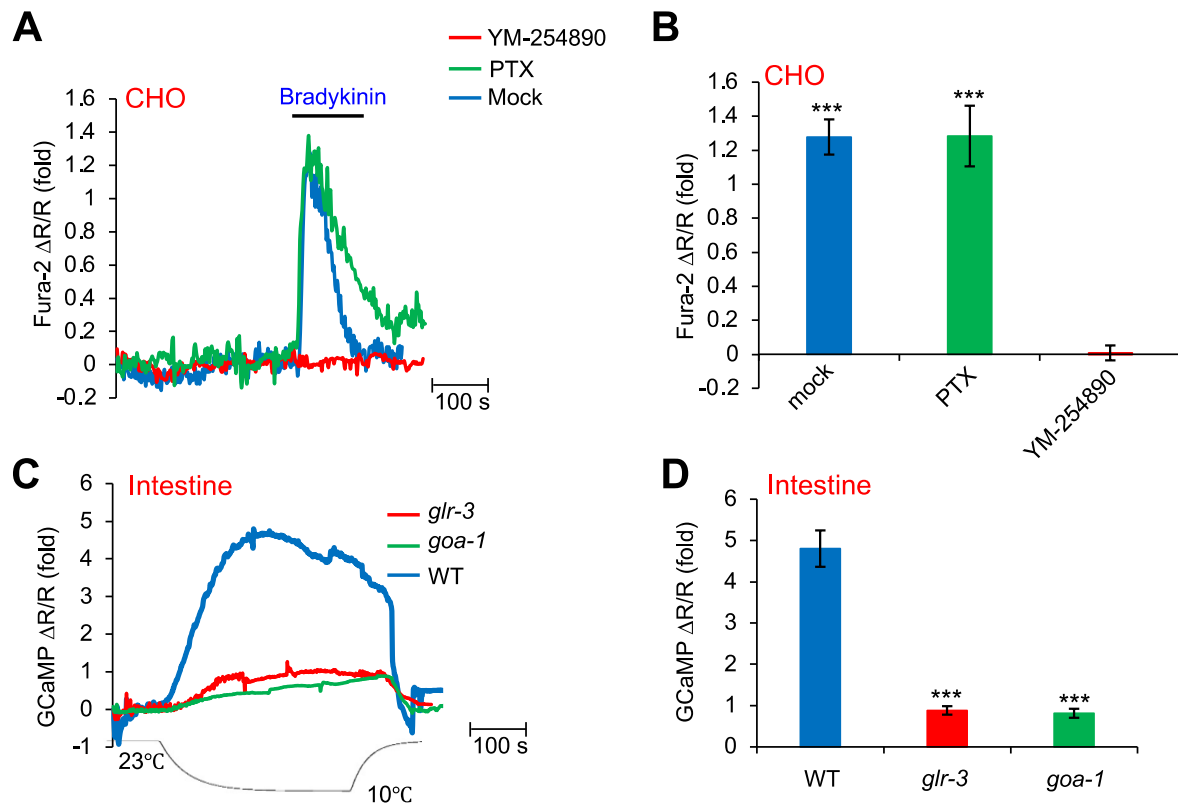
Figure 2.13. **Additional data on G protein signaling in CHO cells and cooling-evoked calcium response in *C. elegans* intestine.**

(A-B) Bradykinin-evoked calcium response in CHO cells is sensitive to the Gq/11 inhibitor YM-254890 but not the Gi/o inhibitor PTX. Bradykinin (10 μM) evoked robust calcium response in CHO cells, which was blocked by pre-incubation with YM-254890 (10 μM) but not by PTX (100 ng/ml). (A) Sample traces. (B) Bar graph. Error bars: SEM. n≥20. ***p<0.0001 (ANOVA with Bonferroni test).

(C-D) *goa-1(n1134)* mutant worms show a severe defect in cooling-evoked calcium response in the intestine. (C) Sample traces. (D) Bar graph. Error bars: SEM. n≥10. ***p<0.0001 (ANOVA with Bonferroni test).

CHAPTER III

The Nematode *C. Elegans* Senses Airborne Sound

3.1. Acknowledgements

3.2 Abstract

Unlike olfaction, taste, touch, vision and proprioception that are widespread across animal phyla, hearing is only found in vertebrates and some arthropods. The vast majority of invertebrate species are thus considered insensitive to sound. Here, we challenge this conventional view by showing that the earless nematode *C. elegans* senses airborne sound at frequencies reaching the kHz range. Sound vibrates *C. elegans* skin that acts as a pressure-to-displacement transducer similar to vertebrate eardrum, activates sound-sensitive FLP/PVD neurons attached to the skin, and evokes phonotaxis behavior. We identified two nAChRs that transduce sound signals independently of ACh, revealing an unexpected function of nAChRs in mechanosensation. Thus, the ability to sense airborne sound is not restricted to vertebrates and arthropods as previously thought, and might have evolved multiple times independently in the animal kingdom, suggesting convergent evolution. Our studies also demonstrate that animals without ears may not be presumed to be sound-insensitive.

3.3 Introduction

To sense the external and internal world, animals and humans have evolved a wide array of sensory systems. Among the six common sensory modalities, the sense of vision, touch, olfaction, taste, and proprioception are all widespread in the animal kingdom and found in most, if not all, animal phyla (Ache and Young, 2005; Gehring, 2014; Mill, 1976; Prescott and Dürr, 2015; Wicher, 2012). For example, even simple

organisms like cnidarians are capable of sensing light, touch, and chemicals, and also possess the sense of proprioception (Katsuki and Greenspan, 2013). Strikingly, the sense of hearing is only found in vertebrates and some arthropods (Budelmann, 1992; Faure et al., 2009; Webster, 1992). Most invertebrate species are, however, considered sound-insensitive (Budelmann, 1992; Faure *et al.*, 2009; Webster, 1992).

While hearing facilitates intraspecies communications, a more fundamental function of this sensory modality is to help the animal to locate predators/preys (Gans, 1992; Webster, 1992), which would benefit the survival of the animal, thereby increasing its fitness. As such, one might envision that hearing should have evolved more widely across animal phyla. However, it is difficult to test this concept, particularly in aquatic invertebrates, as it is technically challenging to distinguish between behavioral responses evoked by sound waves, substrate-borne vibrations, and local water movements (Budelmann, 1992).

The nematode *C. elegans* is widely used as a model for the study of sensory biology, owing to its amenability to genetic manipulations and its small and well annotated nervous system (Iliff and Xu, 2020). Furthermore, to survive the harsh environment, worms have evolved a rich repertoire of sensory systems. For example, worms are long known to have the sense of touch, olfaction and taste (Bargmann et al., 1993; Bargmann and Horvitz, 1991; Chalfie et al., 1985; Ward, 1973). We and others recently reported that worms also possess the sense of light (Edwards et al., 2008; Ward et al., 2008), as well as proprioception (Li et al., 2006). However, as worms do not have morphologically distinct ear organs, these animals are presumed to be insensitive

to airborne sound and thereby lack auditory sensation, which represents the only primary sensory modality absent in *C. elegans*.

Here, we found that despite the lack of ears, worms respond robustly to airborne sound at frequencies reaching the kHz range. Sound vibrates *C. elegans* skin that act as a sound pressure-to-displacement transducer similar to insect and vertebrate tympanum (eardrum), triggering the activation of sound-sensitive FLP and PVD neurons attached to the skin and evoking phonotaxis behavior. Interestingly, TRP and TMC mechanotransduction channels that mediate auditory sensation in insects and vertebrates, respectively, are not required to transduce sound signals in FLP/PVD neurons in *C. elegans*. In an activity-based forward genetic screen, we instead identified two nAChR (nicotinic acetylcholine receptor) subunits that are required for transducing sound signals, and surprisingly, this role of nAChRs is independent of their function as acetylcholine (ACh) receptors. Further analysis suggests that these two nAChRs function as essential subunits of the sound transduction channel. Thus, the ability to sense airborne sound is not restricted to vertebrates and arthropods as previously thought, suggesting that hearing might have evolved multiple times independently in the animal kingdom. Our work also uncovers an unexpected, ACh-independent function of nAChRs in mechanosensation and indicates that animals without ears may not be presumed to be insensitive to sound. This raises the intriguing possibility that other invertebrate animals with a soft body similar to *C. elegans* – such as terrestrial mollusks, annelids, and flatworms – might also be capable of sensing airborne sound.

3.4 Materials and Methods

EXPERIMENTAL MODEL AND SUBJECT DETAILS

Animals

C. elegans strains were cultured at 20°C on standard nematode growth medium (NGM) plates seeded with OP50 bacteria. In general, day 1 adult hermaphrodites were used for experiments unless specified otherwise. Please see below in METHODS DETAILS for further details. The specific genotypes of the strains used this study can be found in Table 3.1. Transgenic lines were generated by injecting plasmid DNA directly into the gonad of hermaphrodite worms. Mutant strains and integrated transgenic strains were outcrossed at least four times before use.

Cell lines

HEK293T cells were cultured in DMEM medium containing 10% fetal bovine serum (heat inactivated) in a 37˚C incubator containing 5% CO_2. This cell line was obtained from the ATCC. See Table 3.1 for details.

METHOD DETAILS

Molecular biology and genetics

For the experiments using transgenes, at least two independent transgenic lines were examined to confirm findings. *des-2* and *deg-3* cDNA were cloned by RT-PCR from total RNA isolated from WT (N2) worms. Transgene expression was verified by expression of a fluorescent marker (CFP, YFP or mCherry), which was driven by SL2 from the same transcript.

Genetic screen and genome editing

EMS was used to mutagenize worms carrying a transgene expressing GCaMP6(f) and mCherry in FLP neurons, which enables real-time visual detection of changes in GCaMP fluorescence in response to sound (2 sec, 1 kHz at 80 dB SPL) using a fluorescent stereomicroscope under a 10x objective (Zeiss Discovery V8 with M2Bio). ~2000 F1 parents were plated on individually seeded NGM plates as L4 for ~12 hours prior to removal, and the offspring on each individual plate were tested (~20,000 F2). Those candidates that failed to exhibit increased fluorescence in FLP in response to sound were recovered and outcrossed to the parental strain at least five times, and both parental and candidate strains underwent whole-genome sequencing (WGS). Sequencing results were analyzed as described previously (Gong et al., 2019). By comparing the WGS data between parental and mutant strains, we obtained density maps for each candidate and mapped the mutations in three candidate strains. Molecular lesion: *xu119* carries a G259E mutation in *des-2*; *xu126* carries a nonsense mutation (W396Stop) in *des-2*; *xu121* carries a mutation in the 5'UTR of *deg-3*, and complementation tests showed that *xu121* is an allele for *deg-3*.

des-2(xu461), deg-3(xu462), and *des-2 deg-3(xu482)* are deletion mutants generated by CRISPR/Cas9-based genome editing using standard protocol as described previously (Arribere et al., 2014). No repair template was included to facilitate isolation of deletion alleles. *des-2::mNG* and *deg-3::mNG* knockin alleles were generated using standard protocol as described (Dickinson et al., 2015). The mNG::3xFLAG tag was inserted at the C-terminal end of *des-2* and *deg-3*. To generate

des-2(G277K)::mNG, des-2(S292R)::mNG, and *des-2(L282S)::mNG deg-3(L310S)* knockin strains, the genome editing was performed in *des-2::mNG* background using standard protocol (Arribere *et al.*, 2014). In the case of *des-2(L282S)::mNG deg-3(L310S)* knockin strain, the two point mutants were introduced sequentially. All knockout and knockin strains were outcrossed at least four times prior to use.

Sound generation, delivery and measurement

Sinusoidal tones were generated by a computer sound card using Multi-Instrument (MI) audio software (Virtins Technology). The signal from the computer was amplified (Parasound Zamp v.3) and generated by a multi-field magnetic speaker (Tucker-Davis Technologies MF-1) with the internal parabolic cone attached. The computer output (via a 3.5mm stereo audio jack) was connected to the + and – terminals on a single channel of the amplifier. The amplifier is connected to the speaker via an RCA cable. The speaker tip was connected to a shortened pipette tip via a short length of ⅛" PVC tubing (see Figure 3.1A). To protect the speaker, the amplifier gain was fixed to produce a maximum output of 10 V peak voltage at 1 kHz. In some cases, sine waves were generated by a function generator (Brüel & Kjær type 4052) connected directly to the speaker via BNC to RCA cable.

The speaker is mounted to a manual micromanipulator arm (Narishige NMN-21). An 8-32 threaded rod attached to the back of the speaker is clamped to the manipulator and positioned 30 degrees downward. The manipulator and speaker are mounted to a block to bring it up to the microscope stage level and stabilize the entire setup.

The acoustic properties of the generated sound fields emanating from the output port were determined with a small diameter analog electret condenser omnidirectional microphone (1 mm inner diameter; Knowles, FG-23329-P07) in combination with MI audio software and an external sound card (Focusrite Scarlett Solo 2x2 USB Audio Interface) connected to the computer. This miniature microphone (mini-microphone) was powered by a custom power supply (Figure 3.14), and connected to the external sound card via a BNC to ¼" stereo jack adapter. The external sound card was connected to the computer via a USB connection. Sound pressure level (SPL), total harmonic distortion, and audio spectra were collected periodically throughout the duration of the presented experiments.

Initial calibration of the mini-microphone was performed by Kresge Hearing Research Institute sound engineers against a 1/8 inch microphone (Brüel & Kjær type 4138; type 2619 preamp, and type 2804 power supply) using a sound source (Krohn-Hite model 4400A Ultra-Low Distortion Oscillator) and spectrum analyzer (Stanford Research Systems Model SR760). The calibration parameters were input in MI audio software following the developer's instructions. Subsequently, calibration parameters were routinely verified using a sound level calibrator standard (1KHz 94 dB SPL; REED Instruments #R8090). We also verified the acoustic properties of the generated sounds using two additional microphone systems: (1) 6 mm omni-directional electret condenser USB microphone (Virtins VT RTA-168B) with the Multi-Instrument audio software; (2) 1/8" CCP Pressure Standard Microphone Set (GRAS 46DE) with APx517B amplifier (Audio Precision) and APx500 v6.0 Audio Measurement Software (Audio Precision). Both methods gave rise to the same measurement values. We recommend using a

calibrated microphone via USB in combination with Multi-Instrument software for the ease of use. We would be pleased to provide technical assistance to those who are interested in establishing this system.

Behavioral assays

Sound-evoked phonotaxis behavior was performed on day 1 adult hermaphrodite worms unless otherwise specified. Animals were tested on NGM plates freshly poured within 1-5 days or stored at 4°C before use. 50 µl of fresh OP50 bacteria was seeded onto the testing plates and dried with the lid off immediately prior to all behavior and calcium imaging experiments. Hermaphrodite worms were transferred to the seeded testing NGM plates 10 minutes before testing to stabilize behavior. Sound was delivered to the worm head or tail using the sound-delivering system described above. We typically stimulated worms with a 2 sec pulse of 80 dB SPL sound (1 kHz). No extra hearing protection is necessary when performing such experiments, as only prolonged exposure (≥8 hours) to audible sounds at ≥85 dB SPL is considered harmful to human ears (Rabinowitz, 2000). As shown in Figure 3.1A, the output port of the speaker (0.4-0.5 mm inner diameter) was set 0.5 mm above the agar surface. Once the height was set, the output port of the speaker was then aimed at the head or tail of a slowly-moving worm and was positioned at 1-1.5 body lengths away from the worm in the X-Y plane. This was achieved by slowly and gently moving the NGM plate by hand while the speaker was held fixed in place. This protocol did not appear to affect behavior, as the converse experiment, in which we moved the speaker with the manipulator while holding the NGM plate in place, yielded a similar result (Figure 3.8A). The sound

stimulus was carefully calibrated with a mini-microphone (1 mm inner diameter) described above by mimicking the actual experimental conditions. To do so, we placed the mini-microphone on the surface of an NGM assay plate at a location where a worm would normally reside during the behavioral test, and pointed the output port of the speaker at the mini-microphone in a way similar to that described above for the behavioral test. For head-avoidance assays, the response was scored if the worm reversed at least half of one head-swing within 3 seconds upon the cessation of sound stimulus (typically 2 sec pulse of 1 kHz at 80 dB SPL unless otherwise indicated). For tail-avoidance assays, the sound stimulus was directed from the side at the tail of worms who were moving very slowly. A response was scored if upon sound stimulation, the worm increased forward locomotion within 3 second upon the cessation of sound stimulus (2 sec pulse, 1 kHz at 89dB SPL). Under the same stimulus condition, the head of the worm appears to be more sensitive to sound than the tail in behavioral tests. To tabulate percent responding, each worm was tested five times with a 10-minute interval between trials. We focused on assaying the head-avoidance response, as it is much easier to score this response.

To assay osmotic avoidance behavior, day 1 hermaphrodite worms were transferred to the testing plates 10 minutes before testing to stabilize behavior. The test was performed by using a glass needle to drop glycerol (2 M in M13) in front of a forward-moving animal on the agar surface. An avoidance response was scored if the worm ceased forward movement and reversed backwards at least half of a head-swing upon the worm nose tip reaching the glycerol drop. To quantify percent responding, we tested each worm five times with a 10-minute interval between trials. For both the

osmotic avoidance and head-avoidance phonotaxis assays related to *bli* strains, young

day 2 animals were used, as *bli* mutants exhibit variable penetrance of blister

phenotype at day 1, but exhibit larger and more frequent blisters by day 2 of adulthood.

During assays with these strains, care was taken to select worms with large blisters

covering the head but not the nose tip.

The tap response was assayed using day 1 hermaphrodite worms on freshly

seeded NGM plates (prepared as described for phonotaxis behavior). Briefly, the NGM

plate (with lid off) was gently lifted 3 cm above the microscope surface and released to

administer a plate tap. An avoidance response was scored if the worm reversed at least

half of one head swing within 3 seconds of the tap. Percent responding was calculated

by testing each worm five times with a 10-minute interval between trials.

Histamine-induced neuronal silencing was performed as previously described

(Pokala *et al.*, 2014). Briefly, full-length cDNA encoding *Drosophila* HisCl1 (a gift from

Cori Bargmann) was cloned under the *sto-5* or *ser-2(prom3)* promoter to drive

expression in FLP or PVD, respectively (Russell *et al.*, 2014; Tsalik *et al.*, 2003), and

injected into N2 animals. For behavior assays, NGM plates were treated overnight with

either histamine (10 mM) or vehicle (ddH$_2$O). For testing, plates were freshly seeded

with a thin lawn of OP50 bacteria, and worms were allowed to habituate for 10 min

before the phonotaxis assay. Laser ablation was performed on L1-L2 larvae using a

laser microbeam (Andor) as described previously (Li *et al.*, 2006), and day 1 adult

worms were then tested for phonotaxis behavior.

Laser Doppler vibrometry

Contactless surface vibrations were measured using a laser Doppler vibrometer (LDV; OFV-303, Polytec USA) with a spot size of 10 μm. An NI PCI-6123 card was used to measure the LDV response. For all vibration measurements, 55 mm NGM plates were allowed to dry overnight at room temperature and were used immediately or stored in a cold room wrapped in parafilm to prevent desiccation for up to one week. Worms showed normal sound-evoked phonotaxis responses under this condition. To prepare for measurements, a group of five worms were first paralyzed in 10 mM NaN3 (in M13) solution, transferred to an unseeded NGM plate to remove excess liquid, and then moved to a testing NGM plate containing 10 mM NaN3. LDV measurements were taken by focusing the laser beam spot on each worm at the anterior region of the animal right behind the pharynx. The sound stimulus from the speaker output port (1.5 mm inner diameter) was delivered to the worm as described for the behavior assay. For vibration measurements in Figure 2B-E, day 1 adult worms were used, while for those in Figure 3.2F-G, day 2 worms were analyzed as the penetrance of *bli* mutant phenotype was more pronounced at day 2. During assays with *bli* strains, care was taken to select worms with blisters large enough in the anterior region to allow the laser to focus on the area with a disrupted cuticle. Vibration measurements were taken by acquiring voltage (mm/s/V) for 1 sec at a sampling rate of 10 kHz for sound frequencies <5 kHz, and at a sampling rate of 15 kHz with a 20 kHz velocity filter for sound frequencies ≥5 kHz. Voltage data underwent post-processing in Matlab using custom scripts and a set conversion factor of 10 mm/s/V to obtain displacement and velocity measurements with respect to frequency. Ten measurements were taken for each plate on the anterior

regions of the worm body to obtain the worm surface measurements and on the agar surface close to the worms for the agar substrate measurements.

Calcium imaging

Calcium imaging was performed on freely-moving animals using the CARIBN system as previously described (Piggott et al., 2011). Briefly, imaging was performed in an environmentally controlled room (20°C, 30% humidity) on day 1 adult hermaphrodites using assay plates prepared as described for the phonotaxis assay. Hermaphrodite worms were picked one day before the experiment at L4 stage. Prior to testing, worms were transferred to freshly seeded NGM plates 10 minutes before testing. Sound stimulus (10 sec) from the output port of the speaker (1.5 mm inner diameter) was delivered using the device described above. The speaker was adjusted to be 0.5 mm above the agar surface using a micromanipulator and at a distance of approximately four body lengths away from the worm. The sound stimulus from the speaker was calibrated as described for the phonotaxis assay using a mini-microphone (1 mm inner diameter) situated in a similar position to the worm on the NGM plate. Ratiometric imaging was performed on worms co-expressing GCamp6(f) and mCherry, and ΔR/R was used to quantify changes in fluorescence. We quantified the peak calcium response, as peak responses are more consistent between experiments.

Electrophysiology

HEK293T cells were cultured in DMEM medium containing 10% fetal bovine serum (heat inactivated) in a 37˚C incubator containing 5% CO_2. Cells were transferred

into 35 mm dishes one day prior to transfection. *C. elegans* cDNA for *des-2, deg-3* and *ric-3* were cloned into mammalian expression vector pcDNA3. Cells were transfected with Lipofectamine2000 (ThermoFisher) for 4 hours. EGFP and *ric-3* was co-transfected with the genes of interest. EGFP functioned as a marker, and RIC-3 is a chaperone to facilitate DES-2/DEG-3 trafficking to the cell membrane. The DNA amount ratio for *des-2/deg-3/ric-3* was 1:1:1. Cells were recorded at 12~18 hours post-transfection.

Whole-cell patch-clamping was carried out using an Olympus IX73 inverted microscope with a Multiclamp 700B amplifier. Transfected cells were identified by green fluorescence signal. Choline (10 mM) was diluted in the bath solution and perfused toward the cell using a rapid perfusion system (RSC-200, Bio-Logic). Pipette resistance was 2-5 MΩ when filled with pipette solution. Cell capacitance and series resistance were compensated during recording. Voltage was clamped at -70 mV. Bath solution (in mM): 140 NaCl, 3 KCl, 2 CaCl2, 1.5 MgCl2, 10 glucose, and 10 HEPES (pH adjusted to 7.3). Pipette solution (in mM): 145 KCl, 1 MgCl2, 5 EGTA and 10 HEPES (pH adjusted to 7.2).

Confocal microscopy

Images were captured on a Nikon spinning-disk confocal microscope using a 60x objective as previously described (Wang et al., 2021). Briefly, late L4 or young adult worms were mounted on a 2% agarose pad (in M13) containing 5 mM levamisole to paralyze the worms. Excitation intensity was enhanced to clearly show the quaternary branches, which required slightly over-exposing the cell body. For each image,

approximately 30 Z steps of 0.5 µm/step were taken to ensure all branches of the

PVD/FLP neuron could be clearly observed.

QUANTIFICATION AND STATISTICAL ANALYSIS

Statistics were performed using GraphPad Prism. P values <0.05 were

considered significant. The statistical method, error bars, and n number were all

described in the figure legends. Specifically, for those involving multi-group

comparisons, we applied ANOVA followed by a post hoc analysis. t test was applied to

those involving two sample groups.

Table 3.1 Chapter 3 Key Resource Table

REAGENT or RESOURCE	SOURCE	IDENTIFIER
Bacterial and virus strains		
E. coli: OP50	Caenorhabditis Genetics Center	OP50
Experimental models: Cell lines		
HEK293T	ATCC	ACS-4500
Experimental models: Organisms/Strains		
Wild type: N2.	Caenorhabditis Genetics Center	WB strain: N2.
mec-4(e1611).	Caenorhabditis Genetics Center	TQ528
bli-1(e769).	Caenorhabditis Genetics Center	TQ10560
bli-2(e768).	Caenorhabditis Genetics Center	TQ10419
bli-6(sc16).	Caenorhabditis Genetics Center	TQ10421
mec-3(e1338).	Caenorhabditis Genetics Center	TQ526
xuEx3483[Psto-5::dHisCl::YFP].	This paper	TQ10245
xuEx3484[Pser-2(prom3)::dHisCl::YFP].	This paper	TQ10246

xuEx2708[Psto-5::GCaMP6(f)+Psto-5::mCherry2].	This paper	TQ9905
xuIs531[Pser-2(prom3)::GCaMP6(f) + Pser-2(prom3)::mCherry].	This paper	TQ9910
unc-13(e51); xuEx2708[Psto-5::GCaMP6(f)+Psto-5::mCherry2].	This paper	TQ9193
unc-31(e169); xuEx2708[Psto-5::GCaMP6(f)+Psto-5::mCherry2].	This paper	TQ9197
unc-13(e51); xuIs531[Pser-2(prom3)::GCaMP6(f) + Pser-2(prom3)::mCherry].	This paper	TQ9372
unc-31(e169); xuIs542[Pser-2(prom3)::GCaMP6(f) + Pser-2(prom3)::mCherry].	This paper	TQ10558
pezo-1(xu112)	This paper	TQ4342
trp-4(sy695).	(Li *et al.*, 2006)	TQ109
tmc-1(ok1859) tmc-2(ok1302).	This paper	TQ3369
osm-9(ky10).	Caenorhabditis Genetics Center	TQ472
del-1(ok150); mec-10(tm1552); unc-8(tm2071).	(Tao *et al.*, 2019)	TQ10553
degt-1(ok3307).	Caenorhabditis Genetics Center	TQ9155
pezo-1(xu112); xuEx2708[Psto-5::GCaMP6(f)+Psto-5::mCherry2].	This paper	TQ9866
trp-4(sy695); xuEx2708[Psto-5::GCaMP6(f)+Psto-5::mCherry2].	This paper	TQ10429
tmc-1(ok1859) tmc-2(ok1302); xuEx2708[Psto-5::GCaMP6(f)+Psto-5::mCherry2].	This paper	TQ10425
osm-9(ky10); xuEx2708[Psto-5::GCaMP6(f)+Psto-5::mCherry2].	This paper	TQ10475
del-1(ok150); mec-10(tm1552); unc-8(tm2071); xuEx2708[Psto-5::GCaMP6(f)+Psto-5::mCherry2].	This paper	TQ9590
degt-1(ok3307); xuEx2708[Psto-	This paper	TQ9199

5::GCaMP6(f)+Psto-5::mCherry2].		
des-2(xu461).	This paper	TQ7712
deg-3(xu462).	This paper	TQ7713
des-2 deg-3(xu482).	This paper	TQ7723
des-2 deg-3(xu482); xuEx3317[Psto-5::des-2::sl2::CFP+Psto-5::deg-3::sl2::CFP].	This paper	TQ9922
des-2 deg-3(xu482); xuEx2708[Psto-5::GCaMP6(f) + Psto-5::mCherry2].	This paper	TQ8026
des2 deg3(xu482); xuEx2708[Psto-5::GCaMP6(f)+Psto 5::mCherry2]; xuEx3317[Psto-5::des-2::sl2::CFP+Psto-5::deg-3::sl2::CFP].	This paper	TQ9909
des-2::mNeonGreen::flag.	This paper	TQ10430
deg-3::mNeonGreen::flag.	This paper	TQ9812
unc-17(e245); xuEx2708[Psto-5::GCaMP6(f)+Psto-5::mCherry2].	This paper	TQ9597
cha-1(p1152); xuEx2708[Psto-5::GCaMP6(f)+Psto-5::mCherry2].	This paper	TQ9596
des-2 deg-3(xu482); xuEx3355[Psto-5::des2(S292R)::sl2::CFP+Psto-5::deg3(S320R)::sl2::CFP].	This paper	TQ9973
des-2 deg-3(xu482); xuEx3378[Psto-5::des2(G277K)::sl2::CFP+Psto-5::deg3(G305K)::sl2::CFP].	This paper	TQ9975
des-2(S292R)::mNeonGreen::flag.	This paper	TQ10438
des-2(G277K)::mNeonGreen::flag.	This paper	TQ10433
des-2(G277K)::mNeonGreen; xuEx2708[Psto-5::GCaMP6(f)+Psto-5::mCherry2].	This paper	TQ10338
des-2(S292R)::mNeonGreen; xuEx2708[Psto-	This paper	TQ10339

5::GCaMP6(f)+Psto-5::mCherry2].		
des-2::mNeonGreen; xuEx2708[Psto-5::GCaMP6(f)+Psto-5::mCherry2].	This paper	TQ10337
des-2(L282S)::mNeonGreen; deg-3(L310S).	This paper	TQ10434
des-2(L282S)::mNeonGreen;deg-3(L310S); xuEx2708[Psto-5::GCaMP6(f)+Psto-5::mCherry2].	This paper	TQ10340
des-2 deg-3(xu482); xuIs531[Pser-2(prom3)::GCaMP6(f) + Pser-2(prom3)::mCherry].	This paper	TQ8918
deg-3::mNeonGreen; xuEx2708[Psto-5::GCaMP6(f)+Psto-5::mCherry2].	This paper	TQ10552
Oligonucleotides		
Primer: for des-2 mNeongreen knockin: guide RNA fwd: CAAGCTGGTGTTGAATATGG GTTTTAGAGCTAGAAATAGC	This paper	N/A
Primer: for des-2 mNeongreen knockin: 5' arm fwd: acgttgtaaaacgacggccagtcgccggcaa tctactagaacaatccaac	This paper	N/A
Primer: for des-2 mNeongreen knockin: 5' arm rev: CATCGATGCTCCTGAGGCTCCC GATGCTCCTCCTCCGTACTCTA CTCCTGCTTG ATGCCAGTGAATGAAACCAATG	This paper	N/A
Primer: for des-2 mNeongreen knockin: 3' arm fwd: CGTGATTACAAGGATGACGATG ACAAGAGA TGAacattctcattttcatc	This paper	N/A
Primer: for des-2 mNeongreen knockin: 3' arm rev: ggaaacagctatgaccatgttatcgatttc gagtctgggaatactcaccg	This paper	N/A

Primer: for deg-3 mNeongreen knockin: guide RNA fwd: CACAATACAGTTATGACCACCG TTTTAGAGCTAGAAATAGC	This paper	N/A
Primer: for deg-3 mNeongreen knockin: 5' arm fwd: acgttgtaaaacgacggccagtcgccggcaa atttcagGTCCACATTGCG	This paper	N/A
Primer: for deg-3 mNeongreen knockin: 5' arm rev: CATCGATGCTCCTGAGGCTCCC GATGCTCC GACATTAAAGAATCGGTCATCT	This paper	N/A
Primer: for deg-3 mNeongreen knockin: 3' arm fwd: CGTGATTACAAGGATGACGATG ACAAGAGA TAAaacttatctcttttttcc	This paper	N/A
Primer: for deg-3 mNeongreen knockin: 3' arm rev: ggaaacagctatgaccatgttatcgatttcctga actaacaatacggaag	This paper	N/A
Recombinant DNA		
Plasmid: pcDNA3.0::Flag::deg-3(cDNA)	This paper	pSX2507
Plasmid: pcDNA3.0::Flag::des-2(cDNA)	This paper	pSX3236
Plasmid: pBS77::Psto-5::des-2(c)::sl2::CFP	This paper	pSX2782
Plasmid: Psto-5::deg-3(c)::sl2::CFP	This paper	pSX2829
Plasmid: pcDNA3.0::flag::des-2(L282S)	This paper	pSX2905
Plasmid: pcDNA3.0::flag::des-2(G277K)	This paper	pSX2908
Plasmid: pcDNA3.0::flag::des-2(S292R)	This paper	pSX2910
Plasmid: pcDNA3.0::flag::deg-3(L310S)	This paper	pSX2914
Plasmid: pcDNA3.0::flag::deg-3(G305K)	This paper	pSX2917
Plasmid: pcDNA3.0::flag::deg-3(S320R)	This paper	pSX2919
Plasmid: Psto-5::des-2(G277K)::sl2::CFP	This paper	pSX2954
Plasmid: Psto-5::deg-3(G305K)::sl2::CFP	This paper	pSX2955
Plasmid: Psto-5::des-2(S292R)::sl2::CFP	This paper	pSX2958
Plasmid: Psto-5::deg-3(S320R)::sl2::CFP	This paper	pSX2959
Plasmid: Psto-5::dHicCL::sl2::YFP	This paper	pSX3116

Plasmid: Pser-2(3)::dHisCl::sl2::YFP	This paper	pSX3235
Plasmid: pBS77::pSto-5::GCaMP6f	This paper	pSX1788
Plasmid: pBS77:: Psto-5::SL2::mCherry2	This paper	pSX1784
Software and algorithms		
GraphPad	GraphPad Software, Inc	N/A
Multi-Instrument Standard 3.9 audio software	Virtins Technology	https://www.virtins.com/multi-instrument.shtml
Matlab	MathWorks	R2017b
APx500 v6.0 Audio Measurement Software	Audio Precision	https://www.ap.com/download/apx500-measurement-software-18/
Other		
Multi-field speakers	Tucker-Davis Technologies (TDT)	MF-1
Audio amplifier	Parasound	Zamp v.3
Function Arbitrary Waveform Generator	Brüel & Kjær	Type 4052
1/8 inch microphone	Brüel & Kjær	Type 4183
Microphone preamp	Brüel & Kjær	Type 2619
Microphone power supply	Brüel & Kjær	Type 2804
Analog electret condenser omnidirectional microphone	Knowles	FG-23329-P07
USB Audio Interface	Focusrite	SCARLETT-SOLO-3G
Ultra-Low Distortion Oscillator	Krohn-Hite	Model 4400A
Spectrum analyzer	Stanford Research Systems	Model SR760
6 mm omni-directional electret condenser USB microphone	Virtins	VT RTA-168B
1/8 inch CCP Pressure Standard Microphone Set	GRAS	46DE
Sound level calibrator	REED Instruments	R8090
Acoustic audio analyzer/amplifier	Audio Precision	APx517B

3.5 Results

Sound evokes aversive phonotaxis behavior in a frequency-dependent manner

C. elegans was previously thought to live in the soil. However, recent work

showed that *C. elegans* in fact lives in composts and rotting materials above ground

(Felix and Braendle, 2010), suggesting that they are more vulnerable to some of their

predators (e.g. arthropods) (Kiontke and Fitch, 2013), whose activities produce audible sound. We thus reasoned that worms might exhibit aversive behavioral responses to audible sound. Given the small size of the worm, we developed a system that allowed us to deliver sound stimuli from a speaker to specific body parts of the worm, for example, head vs. tail (Figure 3.1A). We found that worms responded robustly to sound stimuli (Figure 3.1B-C and 3.8A). Specifically, sound stimuli (2 sec, 1 kHz, 80 dB SPL) delivered to the head stopped worms from moving forward and triggered backward movement (reversals) (Figure 3.1B-C, 3.8A). When we aimed the speaker at the tail of the worm, sound stimuli stimulated forward movement (Figure 3.1C, 3.8A). Thus, worms avoid sound sources, exhibiting aversive phonotaxis behavior. This also demonstrates that worms are able to locate sound sources. As it is much easier to score reversals, we decided to focus on characterizing the head-avoidance phonotaxis behavior (sound-evoked reversals).

We examined phonotaxis responses triggered by different frequencies of sound (Figure 3.1D). Worms responded to sound at frequencies spanning from 100 Hz to 5 kHz (Figure 3.1D), a range that is even broader than some vertebrate animals (e.g. most fishes and turtles) (Christensen-Dalsgaard et al., 2012; Schellart and Popper, 1992). The activation threshold, which is defined as the sound intensity needed to trigger phontotaxis responses, varied with sound frequencies, reaching the range of 50-60 dB SPL at low frequencies (Figure 3.1D). We did not test frequencies below 100 Hz due to limitations of the speaker setup. At frequencies above 5 kHz, no response was detected at the maximum stimulus intensity possible in our setup (~110 dB SPL). We

thus conclude that worms respond to sound stimuli in a frequency-dependent manner. For convenience, we chose to use 1 kHz sound in further characterizations.

Phonotaxis behavior is activated by airborne sound rather than substrate-borne vibrations

As worms were tested on the surface of an agar plate, the substrate on which they navigate, one potential concern is that sound might vibrate the surface of the agar plate, and such substrate-borne vibrations would then trigger behavioral responses in worms. If so, worms might have responded to sound-evoked substrate-borne vibrations rather than airborne sound. Indeed, it is well known that substrate-borne vibrations trigger behavioral responses in worms (Holbrook and Mortimer, 2018; Wicks and Rankin, 1995). This mechanosensory behavior (i.e. tap responses) has been well characterized, which is mediated by touch receptor neurons (Wicks and Rankin, 1995). We thus tested *mec-4(e1611)* mutant worms in which touch receptor neurons are degenerated (Driscoll and Chalfie, 1991). *mec-4* mutant worms lacked substrate-borne vibration-activated behavior (Figure 3.8B); yet, they exhibited normal phonotaxis behavior (Figure 3.1E), suggesting that phonotaxis is evoked by airborne sound rather than substrate-borne vibrations.

To provide further evidence, we directly measured sound-evoked substrate vibrations by laser Doppler vibrometry (Figure 3.2A). Specifically, we quantified the vibration parameters (i.e. displacement and velocity) of the surface layer of the agar plate. A displacement in the micrometer (μm) range is required to activate touch receptor neurons that mediate substrate-borne vibration-activated behavior (Eastwood

137

et al., 2015). However, we detected minimal, if any, sound-evoked vibrations on the surface of the agar plate (Figure 3.2B-C). This provides further evidence suggesting that phonotaxis behavior is activated by airborne sound rather than substrate-borne vibrations.

Sound vibrates *C. elegans* skin to trigger phonotaxis behavior

We then asked how airborne sound activates phonotaxis behavior. In vertebrates and some insects, sound vibrates the tympanum (eardrum), triggering a wide range of auditory behavioral responses (Christensen-Dalsgaard and Carr, 2008; Gopfert and Hennig, 2016). In this case, the eardrum functions as a pressure-to-displacement transducer, converting sound pressure waves into mechanical motion. *C. elegans* body is covered by the cuticle, a thin (<1 μm thickness), elastic membrane primarily composed of collagen (Bercher et al., 2001; Cohen and Sundaram, 2020). Using laser Doppler vibrometry, we found that the surface of worm cuticle was actively vibrated by sound (Figure 3.2B-C and Figure 3.9A-D). For example, in response to 1 kHz sound stimulus, the cuticle vibrated at the same 1 kHz frequency (Figure 3.9A-B). Further analysis showed that the displacement and velocity of sound-evoked cuticle vibrations decreased as the sound frequency increased (Figure 3.2D-E). No vibrations were detected in the cuticle in response to sound at frequencies of >5 kHz (Figure 3.2D-E), consistent with our phonotaxis behavior data (Figure 3.1D). These results demonstrate that sound waves can actively vibrate *C. elegans* cuticle.

It should be noted that although sound vibrates the cuticle, this type of mechanical stimulus is rather mild, as the cuticle displacement caused by sound

stimulation is in the nanometer (nm) range (Figure 3.2D). Notably, when evoked by high

frequency sounds (e.g. 3 kHz, 80 dB SPL sound, Figure 3.2D), a cuticle displacement

as small as ~5 nm was sufficient to trigger phonotaxis responses (Figure 3.1D). By

contrast, a micrometer (µm) range of cuticle displacement is required for other types of

mechanical stimuli, such as gentle touch, to activate mechanosensory behavioral

responses in *C. elegans* (Eastwood *et al.*, 2015).

Are sound-evoked cuticle vibrations important for phonotaxis behavior? To

address this question, we set out to test mutants with aberrant cuticle structure, as they

may display a defect in sound-evoked vibrations in the cuticle. We focused on *bli-1, 2*

and *6* mutants. Unlike other cuticle mutants that largely maintain normal layered cuticle

structure, these three cuticle mutants lack struts in the intermediate layer of the cuticle

and display disrupted cuticle structure with the cortical and basal layers detached from

each other (Cohen and Sundaram, 2020). We found that *bli-1, 2* and *6* mutants

exhibited a strong defect in sound-evoked vibrations in the cuticle (Figure 3.2F-G).

Importantly, these cuticle mutants were severely defective in sound-evoked phonotaxis

behavior (Figure 3.2H), though they responded to other aversive cues such as osmotic

shock (Figure 3.9E). These results together demonstrate that sound vibrates *C. elegans*

cuticle, which is essential for triggering phonotaxis behavior.

FLP and PVD neurons are sound-sensitive neurons mediating phonotaxis
behavior

Sound is expected to activate sound-sensitive mechanosensory neurons to drive

phonotaxis behavior. To identify such sound-sensitive neurons, we examined *mec-3*

mutant worms in which several classes of mechanosensory neurons fail to differentiate properly (Way and Chalfie, 1989), and found that these mutant worms were defective in phonotaxis behavior (Figure 3A). Notably, *mec-4* mutants did not express such a phonotaxis phenotype (Figure 3.1E). The difference between *mec-3* and *mec-4* mutants is that the former but not the latter affects FLP and PVD neurons (Way and Chalfie, 1989), two mechanosensory neurons known to be activated by noxious touch and body stretch (Albeg et al., 2011; Li et al., 2011; Tao et al., 2019). Activation of FLP and PVD neurons triggers reversals and forward movement, respectively (Husson et al., 2012; Li *et al.*, 2011). These features together suggest FLP and PVD neurons as candidate sound-sensitive neurons mediating sound-evoked reversals and forward movement, respectively. Indeed, worms with FLP and PVD neurons ablated using a laser micro-beam exhibited a severe defect in sound-evoked reversals and forward movement, respectively (Figure 3.2B), suggesting that these neurons are required for phonotaxis behavior. To provide additional evidence, we acutely silenced FLP and PVD neurons with a HisCl transgene, which encodes a histamine-gated Cl$^-$ channel (Pokala et al., 2014), and found that such acute silencing of FLP and PVD yielded a similar defect (Figure 3.2C). These results demonstrate that FLP and PVD neurons are required for mediating phonotaxis behavior, suggesting that they are sound-sensitive neurons.

To garner further evidence, we recorded the activity of FLP and PVD neurons in response to sound stimuli by calcium imaging. Considering the mechanosensory nature of FLP and PVD neurons, we imaged freely-moving rather than immobilized worms, as immobilization may generate mechanical stresses affecting these neurons. We found that sound evoked robust calcium responses in FLP and PVD neurons (Figure 3.2D-E).

We repeated the experiments in *unc-13* and *unc-31* mutant worms that are devoid of neurotransmission mediated by exocytosis from synaptic vesicles (SV) and dense core vesicles (DCV), respectively (Richmond et al., 1999; Speese et al., 2007). Sound-evoked calcium responses persisted in FLP neurons of *unc-13* and *unc-31* mutant worms (Figure 3.2F-G). A similar result was obtained with PVD neurons, though the response was slightly reduced in *unc-13* worms (Figure 3.2H-I). Thus, the observed responses in FLP and PVD neurons likely arose cell-autonomously, suggesting that FLP and PVD neurons are primary sound-sensitive neurons mediating phonotaxis behavior. As we focused on the head-avoidance phonotaxis behavior (sound-evoked reversals) mediated by FLP neurons, we decided to focus on recording FLP neurons in further characterizations.

Known mechanotransduction channels are not required for sound sensing in *C. elegans*

Having identified sound-sensitive neurons driving phonotaxis behavior, we next sought to identify the mechanotransduction channel(s) that transduces sound signals in these neurons. In insects and vertebrates, TRP (TRPN/NOMPC and TRPV) and TMC mechanotransduction channels transduce sound signals in sound-sensitive chordotonal neurons and inner ear hair cells, respectively (Gopfert and Hennig, 2016; Jia et al., 2020; Pan et al., 2013). Mutant worms lacking the *C. elegans* TRPN/NOMPC channel TRP-4 and TRPV channel OSM-9 showed normal phonotaxis behavior (Figure 3.4A). FLP neurons also responded normally to sound stimulation in *trp-4* and *osm-9* mutant worms (Figure 3.4C-D). *C. elegans* encodes two TMC channels: TMC-1 and TMC-2

(Wang et al., 2016); however, no defect in phonotaxis behavior or sound-evoked calcium responses was detected in *tmc-1 tmc-2* double mutant worms (Figure 3.4A, 4C and 4D). Thus, *C. elegans* sound sensing in FLP neurons appears to require mechanotransduction channels distinct from those found in insects and vertebrates.

We also examined several other mechanotransduction channels, for example, the Piezo channel PEZO-1, but did not observe any defect in *pezo-1* mutant worms (Figure 3.4A, 4C and 4D). As FLP/PVD neurons are also activated by harsh touch and body stretch, we tested the corresponding mechanotransduction channels DEGT-1 and UNC-8/MEC-10/DEL-1 that are activated by these two types of mechanical stimuli, respectively (Tao *et al.*, 2019). No defect in sound sensing was observed in *degt-1* and *unc-8; mec-10 del-1* mutant worms (Figure 3.4B, 4E and 4F). We thus conclude that *C. elegans* sound-sensitive FLP/PVD neurons require a distinct type of mechanotransduction channel(s) to transduce sound signals.

An unbiased, activity-based genetic screen identifies two nAChR subunits DES-2 and DEG-3 required for sound sensing

The failure to identify mechanotransduction channels mediating sound sensing in *C. elegans* with candidate gene approaches prompted us to consider an unbiased strategy. We thus opted to perform an unbiased forward genetic screen. We first followed the traditional strategy by performing a chemical-mutagenesis screen for mutants defective in phonotaxis behavior. However, this screen did not turn out to be very fruitful, as further characterizations of FLP neurons by calcium imaging revealed that the majority of isolated mutants did not show a defect in FLP neurons. This might

be explained by the fact that behavioral screens usually lack specificity. Thus, the phenotype observed in the mutants might simply result from defects in sensory processing mediated by downstream neural circuits rather than in sound sensing by FLP neurons. We thus sought to design an activity-based genetic screen by directly targeting the sound-sensitive neuron FLP.

We made the intriguing observation that FLP neurons maintained a low basal level of GCaMP fluorescence at the quiescent state, but responded robustly to sound stimulation by drastically increasing their GCaMP fluorescence intensity (Figure 3.5A). This enabled us to conduct a genetic screen by visually screening for mutants in which GCaMP fluorescence intensity in FLP failed to increase upon sound stimulation under a stereomicroscope. After screening ~20,000 F2 worms, we isolated 13 mutants. We focused on three strong mutants: *xu119, xu121,* and *xu126.* As expected, these mutants were also defective in phonotaxis behavior (Figure 3.5B). By whole-genome sequencing, we mapped *xu119* and *xu126* to the *des-2* gene, and *xu121* to the *deg-3* gene. *des-2* and *deg-3* encode two nicotinic acetylcholine receptor (nAChR) subunits that function together as a heteromeric channel (Treinin et al., 1998). These two genes are encoded by the same operon (Treinin *et al.*, 1998). To validate the phenotype, we examined null mutants (deletion alleles) generated by CRISPR-based genome editing. Null mutants, including *des-2* and *deg-3* single mutants [*des-2(xu461)* and *deg-3(xu462)*] as well as *des-2 deg-3* double mutant [*des-2 deg-3(xu482)*], all exhibited the same phonotaxis phenotype (Figure 3.5B). By contrast, *des-2 deg-3* mutant worms showed normal responses in other aversive behaviors, such as tap response, osmotic avoidance and nose touch response (Figure 3.8B and 3.11A-B). We then focused on

des-2 deg-3 double mutant for further characterizations. We recorded FLP neurons in *des-2 deg-3* mutant worms by calcium imaging, and found that they failed to respond to sound (Figure 3.5C-D). Transgenic expression of wild-type *des-2* and *deg-3* genes in FLP neurons rescued both the phonotaxis behavior and calcium imaging phenotypes (Figure 3.5B-D), indicating that DES-2/DEG-3 acts in FLP neurons to mediate sound sensing.

To determine the expression pattern of DES-2/DEG-3, we inserted a mNeonGreen (mNG) tag into the endogenous locus of *des-2* and *deg-3* by CRISPR-based genome editing. Both *des-2::mNG* and *deg-3::mNG* knockin alleles were functional, as they responded normally to sound stimuli (Figure 3.11C-E), indicating that the mNG tag does not interfere with the function of DES-2/DEG-3. As described previously (Albeg *et al.*, 2011), we found that DES-2 and DEG-3 were expressed throughout the sensory dendrites and soma of FLP neurons (Figure 3.5E). DES-2 and DEG-3 were also expressed strongly in PVD neurons and weakly in a few other neurons (Figure 3.5E and 3.11F). Indeed, similar to FLP neurons, PVD neurons in *des-2 deg-3* mutant worms also failed to respond to sound (Figure 3.11G-I). Among all the worm neurons, FLP and PVD are unique in that they are multi-dendritic neurons with their dendritic trees covering the head and body/tail of the worm, respectively, and together these two sound-sensitive neurons tile the entire body wall of the worm (Figure 3.5E) (Albeg *et al.*, 2011; Inberg et al., 2019; Sundararajan et al., 2019). Notably, FLP/PVD soma are positioned apposed to the epidermis, and their dendrites are physically attached to the epidermis (Inberg *et al.*, 2019; Sundararajan *et al.*, 2019), a morphological feature that is well suited to detect sound-evoked vibrations in the skin.

Thus, it appears that both the morphology of FLP/PVD neurons and the expression

pattern of DES-2/DEG-3 channels are consistent with their roles in mediating sound

sensing in *C. elegans*.

Acetylcholine (ACh) is not required for the function of DES-2/DEG-3 in sound sensing

The identification of the nAChR DES-2/DEG-3 as an essential player in sound

sensing raises the question about the specific role of DES-2/DEG-3 in this sensory

modality. As DES-2/DEG-3 is an acetylcholine (ACh)-gated ion channel (Treinin *et al.*,

1998), it is conceivable that sound stimuli might somehow stimulate ACh release, which

in turn would activate the nAChR DES-2/DEG-3. If so, DES-2/DEG-3 would play a

rather indirect role in sound sensing. Indeed, DES-2/DEG-3 has been reported to

indirectly regulate mechanosensation in an ACh-dependent manner (Cohen et al.,

2014). In this case, one would expect that ACh should be important for sound sensing,

and that inhibiting the synthesis or release of ACh shall recapitulate the *des-2 deg-3*

mutant phenotype. To test this model, we examined *cha-1* and *unc-17* mutant worms

that are deficient in ACh synthesis and release, respectively. Specifically, *cha-1* and

unc-17 encode the worm ortholog of choline acetyltransferase (ChAT) and vesicular

ACh transporter (VAChT), respectively, with the former being essential for ACh

synthesis and the latter required for uploading ACh to synaptic vesicles and hence ACh

release (Alfonso et al., 1993; Alfonso et al., 1994). To our surprise, both *cha-1* and *unc-17* mutants exhibited normal sound-evoked responses in FLP neurons (Figure 3.6A-B),

indicating that ACh is not required for sound sensing. Thus, though DES-2/DEG-3 has

the capacity to function as an ACh receptor, its ACh receptor function does not contribute to sound sensing, suggesting that DES-2/DEG-3 may play a more direct role in sound sensing in *C. elegans*. This also uncovers an ACh-independent function of nAChRs.

DES-2/DEG-3 is an essential component of the sound transduction channel

The lack of a role for the ACh receptor function of DES-2/DEG-3 in sound sensing prompted us to ask how DES-2/DEG-3 is involved. In addition to acting as an ACh receptor, nAChRs are also ion channels. We thus wondered if the ion channel function of DES-2/DEG-3 is important for sound sensing. The transmembrane segment M2 lines the channel pore of nAChRs. The point mutations G243K and A258R in the M2 segment in mammalian nAChRs (e.g. α7 nAChR) are known to abolish the channel conductance (Criado et al., 2011). The corresponding point mutations are G277K and S292R in DES-2, and G305K and S320R in DEG-3 (Figure 3.12A). We recorded agonist-evoked currents of DES-2/DEG-3 expressed in HEK293T cells, and verified that these mutant forms of DES-2/DEG-3 lacked channel activity even in response to prolonged agonist application (Figure 3.12B and 3.12D). No reliable mechanically-activated currents were recorded in DES-2/DEG-3 expressed in HEK293T cells (Figure 3.12C). This *in vitro* data, however, does not necessarily indicate that this channel is mechano-insensitive, as some of the auxiliary proteins required for DES-2/DEG-3 mechanosensitivity *in vivo* may be absent in HEK293T cells *in vitro*. A similar phenomenon was observed with the mechanosensitive ENaC/DEG channel subunits MEC-4/MEC-10 when expressed *in vitro* (Bounoutas and Chalfie, 2007; Goodman et

al., 2002). We then tested those channel-dead mutant forms of DES-2/DEG-3 in worms by expressing them as a transgene in FLP neurons, and found that they failed to rescue the phonotaxis phenotype of *des-2 deg-3* mutant worms (Figure 3.7A), while a transgene expressing wild-type DES-2/DEG-3 did (Figure 3.5B). This suggests that the ion-conducting activity of DES-2/DEG-3 is required for its function in sound sensing.

To provide additional evidence, we introduced the channel-dead mutations G277K and S292R into the endogenous *des-2* locus by CRISPR-based genome editing to generate two knockin alleles: *des-2(G277K)* and *des-2(S292R)*. We performed the genome editing in the *des-2::mNG* background, as the mNG (mNeonGreen) tag did not affect DES-2 function (Figure 3.11C-E), yet offered an opportunity to assess the potential effect of G277K and S292R mutations on DES-2 expression. As expected, these two channel-dead mutations did not notably affect the expression of the endogenous DES-2 protein (Figure 3.13). Importantly, *des-2(G277K)* and *des-2(S292R)* knockin worms, both of which carried channel-dead mutations, were severely defective in phonotaxis behavior (Figure 3.7B), and also completely lacked sound-evoked calcium responses in FLP neurons (Figure 3.7C-D), a phenotype identical to *des-2 deg-3* null mutant worms. This result provides strong evidence that the ion channel function of DES-2/DEG-3 is essential for transducing sound signals, suggesting that DES-2/DEG-3 is an essential component of the sound transduction channel.

To provide further evidence, we sought to perform the converse experiment by potentiating the channel activity of DES-2/DEG-3. We reasoned that if DES-2/DEG-3 is an essential component of the sound transduction channel, then potentiating its channel activity should potentiate the phonotaxis behavior and the sound-evoked activity of

sound-sensitive neurons. The L-S point mutation (L248S in Figure 3.12A) in the pore-lining M2 segment of mammalian □7 nAChR is known to slow down the channel's desensitization/inactivation kinetics, thereby prolonging the open duration of the channel (Labarca et al., 1995; Revah et al., 1991). We first verified this result in HEK293T cells, and found that DES-2/DEG-3 carrying the corresponding L-S mutation [DES-2(L282S)/DEG-3(L310S)] inactivated much more slowly and thus remained open much longer than WT channel, though its amplitude was slightly reduced (Figure 3.12B, 3.12D-E). We then introduced this L-S point mutation into the endogenous *des-2 deg-3* locus by CRISPR-based genome editing. In phonotaxis behavior tests, knockin worms carrying the L-S mutation in DES-2/DEG-3, albeit displaying a response rate similar to wild-type worms (Figure 3.7E), responded with more head-swings (i.e. longer reversal distance) in each reversal event (Figure 3.7F), indicating that these knockin worms responded more robustly to sound stimuli. A similar phenomenon was observed in sound-evoked calcium responses in FLP neurons. Specifically, though the amplitude of sound-evoked calcium responses was reduced in L-S knockin worms (Figure 3.7G-H), upon the cessation of sound stimuli, the responses deactivated at a much slower pace than wild-type worms (Figure 3.7G and 7I). This provides a neural basis underlying the enhanced phonotaxis behavioral responses in L-S knockin worms. Thus, enhancing the channel activity of DES-2/DEG-3 potentiated the phonotaxis behavior as well as the sound-evoked activity of sound-sensitive neurons. These results, together with those from channel-dead knockin worms, suggest that DES-2/DEG-3 functions as an essential component of the sound transduction channel and might do so by forming the

channel pore. This reveals an unexpected, ACh-independent function of nAChRs in mechanosensation.

3.6 Discussion

Among the six primary sensory modalities, hearing is unique in that it is only found in vertebrates and some arthropods. This has led to the view that all non-arthropod invertebrate species are insensitive to sound (Budelmann, 1992; Faure *et al*., 2009; Webster, 1992). On the other hand, given that the primary function of hearing is believed to detect predators/preys (Gans, 1992; Webster, 1992), the ability to sense sound would be expected to have evolved more widely across animal phyla. However, the search for such sound-sensitive animals has not been very successful (Budelmann, 1992; Faure *et al*., 2009; Webster, 1992). Here, we show that the nematode *C. elegans*, an animal that lacks ear organs, senses airborne sound. Interestingly, worms can locate sound sources and engage in aversive phonotaxis behavior to avoid sound sources. Thus, the ability to sense airborne sound is not restricted to vertebrates and arthropods. Our results also show that animals without morphologically distinct ear organs may not be presumed to be insensitive to sound.

C. elegans primarily live in composts and rotting materials above ground (Felix and Braendle, 2010), and are vulnerable to their predators such as insects and centipedes (Kiontke and Fitch, 2013). In addition, as worms feed on and inhabit decaying materials such as rotting fruits and insect host cadavers (for parasitic nematodes), they may fall prey to omnivores and scavenger insects (e.g. beetles and ants) indirectly (Ulug et al., 2014). Many such predatory animals generate loud audible

sounds through stridulation (e.g. insects and centipedes) and/or wing beating (e.g.

insects) (Bennet-Clark, 1975; Masters, 1980), as well as produce loud rustling sounds

during foraging (e.g. insects and centipedes) (Goerlitz and Siemers, 2007; Siemers and

Guttinger, 2006). The ability to detect sound sources and engage in aversive

phonotaxis behavior might potentially help worms to evade such predatory animals.

Nevertheless, whether this behavior is ecologically relevant in the wild remains to be

tested.

One striking observation is that sound actively vibrates worm skin, which is

essential for the activation of phonotaxis behavior. In this case, worm skin functions as

a sound pressure-to-displacement transducer in a manner similar to vertebrate/insect

tympanum (eardrum). Notably, the displacement values of sound-evoked vibrations in

worm skin are similar to those reported for human eardrum measured at similar

frequencies (Goode et al., 1993; Goode et al., 1996). While the exact mechanisms are

unclear, the fact that worm cuticle and mammalian eardrum both have collagen as a

core component might contribute to this phenomenon (Cohen and Sundaram, 2020;

Stenfeldt et al., 2006). Interestingly, the sound-sensitive neurons FLP and PVD are

closely associated with the skin, with their soma and sensory dendrites attached to the

epidermis (Albeg *et al.*, 2011; Inberg *et al.*, 2019; Sundararajan *et al.*, 2019). In addition,

their sensory dendrites form an elaborate net-like structure that tiles and envelopes the

entire body wall of the worm (Albeg *et al.*, 2011; Inberg *et al.*, 2019; Sundararajan *et al.*,

2019). These morphological features make FLP and PVD neurons well positioned for

detecting sound-evoked vibrations in the skin. Moreover, the receptive field of FLP and

PVD neurons covers distinct areas of the worm body, with the dendrites of FLP

enveloping the head and those of PVD occupying the body/tail (Albeg *et al.*, 2011; Inberg *et al.*, 2019; Sundararajan *et al.*, 2019). As FLP and PVD are coupled to distinct downstream interneuron circuits, their activation drives reversals and forward movements, respectively (Husson *et al.*, 2012; Li *et al.*, 2011). These characteristics may contribute to worms' ability to locate and avoid sound sources from different directions.

Interestingly, FLP/PVD sound-sensitive neurons can also be activated by other mechanical stimuli such as noxious touch and body stretch (Albeg *et al.*, 2011; Li *et al.*, 2011; Tao *et al.*, 2019). However, noxious touch represents a much more intense stimulus than sound waves (Cho et al., 2017; Tao *et al.*, 2019), and body stretch only weakly activates these sound-sensitive neurons (Tao *et al.*, 2019). For example, for noxious touch stimuli, a >20 μm cuticle displacement is required to activate PVD neurons (Cho *et al.*, 2017), whereas for sound waves, a cuticle displacement in the nanometer (nm) range is sufficient to activate the same PVD neurons (Figure 3.2D and 3E). As such, airborne sound likely represents the most effective mechanical stimulus that activates FLP/PVD neurons. Perhaps, these sound-sensitive neurons are geared to high-frequency mechanical stimuli like sound waves, which might underlie their relatively low sensitivity to other mechanical stimuli such as touch and stretch. Remarkably, by comparing their activation thresholds, worms might potentially be as sensitive or even more sensitive to airborne sound than many vertebrate animals such as salamanders, lungfish, and some turtles (Christensen-Dalsgaard *et al.*, 2012; Christensen et al., 2015a; Christensen et al., 2015b). Worms also respond to a wider

range of sound frequencies than these vertebrate animals (Christensen-Dalsgaard *et al.*, 2012; Christensen *et al.*, 2015a; Christensen *et al.*, 2015b).

One popular definition of hearing was proposed by Glen Wever as *"the response of an animal to sound vibrations by means of a special organ for which such vibrations are the most effective stimulus"* (Wever, 1974). In light of Wever's view, worm skin together with FLP/PVD sound-sensitive neurons would form a special sensory "organ" for sound detection, with sound being the most effective stimulus. We thus propose that this sound-sensing "organ", though morphologically distinct from vertebrate and insect ears, possesses functional features similar to its vertebrate and insect counterparts.

Despite notable similarities, auditory sensation in vertebrates, insects and *C. elegans* manifests clear distinctions. One of the most striking such distinctions probably lies at the molecular level. As a comparison, all animal species employ opsins to detect light (Suga et al., 2008; Terakita, 2005), with the exception of worms that sense light through LITE-1, a non-opsin type of photoreceptor (Ghosh et al., 2021; Gong et al., 2016). By contrast, auditory sensation in vertebrates, insects and *C. elegans* appear to rely on distinct classes of mechanotransduction channels. Specifically, vertebrates depend on TMC channels to transduce sound signals (Jia *et al.*, 2020; Pan *et al.*, 2013), while insects (e.g. *Drosophila*) require TRP family channels for sound sensing (Gopfert and Hennig, 2016). In *C. elegans*, we found that sound-sensitive FLP/PVD neurons do not require TMC or TRP family channels, but instead depend on a nAChR channel (DES-2/DEG-3). Surprisingly, this role of DES-2/DEG-3 is independent of its function as an ACh receptor, indicating that it plays a more direct role in the process. Indeed, further analysis shows that this nAChR functions as an essential component of the

sound transduction channel and might do so by forming the channel pore. We thus

propose that DES-2/DEG-3 might function as pore-forming subunits of a

mechanotransduction channel complex/apparatus that transduces sound stimuli in

sound-sensitive neurons. This role of DES-2/DEG-3 would be similar to that of the

ENaC/DEG channel subunits MEC-4/MEC-10 in the mechanotransduction channel

complex/apparatus that transduces touch stimuli in *C. elegans* touch receptor neurons

(Bounoutas and Chalfie, 2007). nAChRs are best known to function as ACh receptors

that mediate nicotine dependence in the brain and muscle contractions at the

neuromuscular junctions. Though nAChRs have been implicated in mechanosensation

in worms and mammalian cells, such a role is indirect, as it depends on ACh (Cohen *et

al.*, 2014; Pan et al., 2012). Our results unveil an unexpected, ACh-independent

function of nAChRs in mechanosensation.

3.7 Concluding remarks

In summary, we show that despite the lack of ears, the nematode *C. elegans*

senses airborne sound. Worms detect sound through their skin, which acts in a manner

similar to the eardrum in vertebrate and insect ears. At the molecular level, worms

transduce sound signals through a mechanotransduction channel apparatus that is

distinct from that employed by vertebrates and insects. Apparently, auditory sensation in

vertebrates, insects and *C. elegans* bears both similarities and distinctions. We thus

conclude that the ability to sense airborne sound is not restricted to vertebrates and

arthropods as believed previously. This supports the notion that hearing might have

evolved multiple times independently across animal phyla, suggesting convergent

153

evolution. This stands in sharp contrast to the evolution of vision, which as proposed by

Charles Darwin, occurred relatively early and probably only once with a monophyletic

origin (Gehring, 2014). Our studies also raise the intriguing possibility that other earless

invertebrates, particularly those with a soft body like *C. elegans* - such as terrestrial

mollusks, annelids and flatworms - might also possess the ability to sense airborne

sound.

References

1. Ache, B.W., and Young, J.M. (2005). Olfaction: diverse species, conserved principles. Neuron *48*, 417-430. 10.1016/j.neuron.2005.10.022.

2. Albeg, A., Smith, C.J., Chatzigeorgiou, M., Feitelson, D.G., Hall, D.H., Schafer, W.R., Miller, D.M., 3rd, and Treinin, M. (2011). C. elegans multi-dendritic sensory neurons: morphology and function. Mol Cell Neurosci *46*, 308-317.

3. Alfonso, A., Grundahl, K., Duerr, J.S., Han, H.P., and Rand, J.B. (1993). The Caenorhabditis elegans unc-17 gene: a putative vesicular acetylcholine transporter. Science *261*, 617-619.

4. Alfonso, A., Grundahl, K., McManus, J.R., and Rand, J.B. (1994). Cloning and characterization of the choline acetyltransferase structural gene (cha-1) from C. elegans. J Neurosci *14*, 2290-2300.

5. Arribere, J.A., Bell, R.T., Fu, B.X., Artiles, K.L., Hartman, P.S., and Fire, A.Z. (2014). Efficient marker-free recovery of custom genetic modifications with CRISPR/Cas9 in Caenorhabditis elegans. Genetics *198*, 837-846. 10.1534/genetics.114.169730.

6. Bargmann, C.I., Hartwieg, E., and Horvitz, H.R. (1993). Odorant-selective genes and neurons mediate olfaction in C. elegans. Cell *74*, 515-527.

7. Bargmann, C.I., and Horvitz, H.R. (1991). Chemosensory neurons with overlapping functions direct chemotaxis to multiple chemicals in C. elegans. Neuron *7*, 729-742.

8. Bennet-Clark, H.C. (1975). Sound production in insects. Sci Prog *62*, 263-283.

9. Bercher, M., Wahl, J., Vogel, B.E., Lu, C., Hedgecock, E.M., Hall, D.H., and Plenefisch, J.D. (2001). mua-3, a gene required for mechanical tissue integrity in Caenorhabditis elegans, encodes a novel transmembrane protein of epithelial attachment complexes. J Cell Biol *154*, 415-426. 10.1083/jcb.200103035.

10. Bounoutas, A., and Chalfie, M. (2007). Touch sensitivity in Caenorhabditis elegans. Pflugers Archiv : European journal of physiology *454*, 691-702.

11. Budelmann, B.U. (1992). Hearing in Nonarthropod Invertebrates. In The Evolutionary Biology of Hearing, D.B. Webster, R.R. Fay, and A.N. Popper, eds. (Springer-Verlag New York Inc.), pp. pp. 141-155.

12. Chalfie, M., Sulston, J.E., White, J.G., Southgate, E., Thomson, J.N., and Brenner, S. (1985). The neural circuit for touch sensitivity in Caenorhabditis elegans. J Neurosci *5*, 956-964.

13. Cho, Y., Porto, D.A., Hwang, H., Grundy, L.J., Schafer, W.R., and Lu, H. (2017). Automated and controlled mechanical stimulation and functional imaging in vivo in C. elegans. Lab Chip *17*, 2609-2618. 10.1039/c7lc00465f.

14. Christensen-Dalsgaard, J., Brandt, C., Willis, K.L., Christensen, C.B., Ketten, D., Edds-Walton, P., Fay, R.R., Madsen, P.T., and Carr, C.E. (2012). Specialization for underwater hearing by the tympanic middle ear of the turtle, Trachemys scripta elegans. Proc Biol Sci *279*, 2816-2824. 10.1098/rspb.2012.0290.

15. Christensen-Dalsgaard, J., and Carr, C.E. (2008). Evolution of a sensory novelty: tympanic ears and the associated neural processing. Brain Res Bull *75*, 365-370. 10.1016/j.brainresbull.2007.10.044.

16. Christensen, C.B., Christensen-Dalsgaard, J., and Madsen, P.T. (2015a). Hearing of the African lungfish (Protopterus annectens) suggests underwater pressure detection and rudimentary aerial hearing in early tetrapods. J Exp Biol *218*, 381-387. 10.1242/jeb.116012.

17. Christensen, C.B., Lauridsen, H., Christensen-Dalsgaard, J., Pedersen, M., and Madsen, P.T. (2015b). Better than fish on land? Hearing across metamorphosis in salamanders. Proc Biol Sci *282*. 10.1098/rspb.2014.1943.

18. Cohen, E., Chatzigeorgiou, M., Husson, S.J., Steuer-Costa, W., Gottschalk, A., Schafer, W.R., and Treinin, M. (2014). Caenorhabditis elegans nicotinic acetylcholine receptors are required for nociception. Mol Cell Neurosci *59*, 85-96. 10.1016/j.mcn.2014.02.001.

19. Cohen, J.D., and Sundaram, M.V. (2020). C. elegans Apical Extracellular Matrices Shape Epithelia. J Dev Biol *8*. 10.3390/jdb8040023.

20. Criado, M., Svobodova, L., Mulet, J., Sala, F., and Sala, S. (2011). Substitutions of amino acids in the pore domain of homomeric alpha7 nicotinic receptors for analogous residues present in heteromeric receptors modify gating, rectification and binding properties. J Neurochem *119*, 40-49. 10.1111/j.1471-4159.2011.07398.x.

21. Dickinson, D.J., Pani, A.M., Heppert, J.K., Higgins, C.D., and Goldstein, B. (2015). Streamlined Genome Engineering with a Self-Excising Drug Selection Cassette. Genetics *200*, 1035-1049. 10.1534/genetics.115.178335.

22. Driscoll, M., and Chalfie, M. (1991). The mec-4 gene is a member of a family of Caenorhabditis elegans genes that can mutate to induce neuronal degeneration. Nature *349*, 588-593.

23. Eastwood, A.L., Sanzeni, A., Petzold, B.C., Park, S.J., Vergassola, M., Pruitt, B.L., and Goodman, M.B. (2015). Tissue mechanics govern the rapidly adapting and symmetrical response to touch. Proc Natl Acad Sci U S A *112*, E6955-6963. 10.1073/pnas.1514138112.

24. Edwards, S.L., Charlie, N.K., Milfort, M.C., Brown, B.S., Gravlin, C.N., Knecht, J.E., and Miller, K.G. (2008). A novel molecular solution for ultraviolet light detection in Caenorhabditis elegans. PLoS Biol *6*, e198.

25. Faure, P.A., Mason, A.C., and Yack, J.E. (2009). Invertebrate Ears and Hearing. In Encyclopedia of the Neuroscience, L.R. Squire, ed. (Elsevier), pp. pp. 2035-2042.

26. Felix, M.A., and Braendle, C. (2010). The natural history of Caenorhabditis elegans. Curr Biol *20*, R965-969. 10.1016/j.cub.2010.09.050.

27. Gans, C. (1992). An Overview of the Evolutionary Biology of Hearing. In The Evolutionary Biology of Hearing, D.B. Webster, R.R. Fay, and A.N. Popper, eds. (Springer-Verlag New York Inc.), pp. pp. 3-13.

28. Gehring, W.J. (2014). The evolution of vision. Wiley Interdiscip Rev Dev Biol *3*, 1-40. 10.1002/wdev.96.

29. Ghosh, D.D., Lee, D., Jin, X., Horvitz, H.R., and Nitabach, M.N. (2021). C. elegans discriminates colors to guide foraging. Science *371*, 1059-1063. 10.1126/science.abd3010.

30. Goerlitz, H.R., and Siemers, B.M. (2007). Sensory ecology of prey rustling sounds: acoustical features and their classification by wild Grey Mouse Lemurs. Funct Ecol *21*, 143-153. 10.1111/j.1365-2435.2006.01212.x.

31. Gong, J., Liu, J., Ronan, E.A., He, F., Cai, W., Fatima, M., Zhang, W., Lee, H., Li, Z., Kim, G.H., et al. (2019). A Cold-Sensing Receptor Encoded by a Glutamate Receptor Gene. Cell *178*, 1375-1386 e1311. 10.1016/j.cell.2019.07.034.

32. Gong, J., Yuan, Y., Ward, A., Kang, L., Zhang, B., Wu, Z., Peng, J., Feng, Z., Liu, J., and Xu, X.Z. (2016). The C. elegans Taste Receptor Homolog LITE-1 Is a Photoreceptor. Cell *167*, 1252-1263 e1210. 10.1016/j.cell.2016.10.053.

33. Goode, R.L., Ball, G., and Nishihara, S. (1993). Measurement of umbo vibration in human subjects--method and possible clinical applications. Am J Otol *14*, 247-251.

34. Goode, R.L., Ball, G., Nishihara, S., and Nakamura, K. (1996). Laser Doppler vibrometer (LDV)--a new clinical tool for the otologist. Am J Otol *17*, 813-822.

35. Goodman, M.B., Ernstrom, G.G., Chelur, D.S., O'Hagan, R., Yao, C.A., and Chalfie, M. (2002). MEC-2 regulates C. elegans DEG/ENaC channels needed for mechanosensation. Nature *415*, 1039-1042.

36. Gopfert, M.C., and Hennig, R.M. (2016). Hearing in Insects. Annu Rev Entomol *61*, 257-276. 10.1146/annurev-ento-010715-023631.

37. Holbrook, R.I., and Mortimer, B. (2018). Vibration sensitivity found in Caenorhabditis elegans. J Exp Biol *221*. 10.1242/jeb.178947.

38. Husson, S.J., Costa, W.S., Wabnig, S., Stirman, J.N., Watson, J.D., Spencer, W.C., Akerboom, J., Looger, L.L., Treinin, M., Miller, D.M., 3rd, et al. (2012). Optogenetic analysis of a nociceptor neuron and network reveals ion channels acting downstream of primary sensors. Curr Biol *22*, 743-752. 10.1016/j.cub.2012.02.066.

39. Iliff, A.J., and Xu, X.Z.S. (2020). C. elegans: a sensible model for sensory biology. J Neurogenet *34*, 347-350. 10.1080/01677063.2020.1823386.

40. Inberg, S., Meledin, A., Kravtsov, V., Iosilevskii, Y., Oren-Suissa, M., and Podbilewicz, B. (2019). Lessons from Worm Dendritic Patterning. Annu Rev Neurosci *42*, 365-383. 10.1146/annurev-neuro-072116-031437.

41. Jia, Y., Zhao, Y., Kusakizako, T., Wang, Y., Pan, C., Zhang, Y., Nureki, O., Hattori, M., and Yan, Z. (2020). TMC1 and TMC2 Proteins Are Pore-Forming Subunits of Mechanosensitive Ion Channels. Neuron *105*, 310-321 e313. 10.1016/j.neuron.2019.10.017.

42. Katsuki, T., and Greenspan, R.J. (2013). Jellyfish nervous systems. Curr Biol *23*, R592-594. 10.1016/j.cub.2013.03.057.

43. Kiontke, K., and Fitch, D.H. (2013). Nematodes. Curr Biol *23*, R862-864. 10.1016/j.cub.2013.08.009.

44. Labarca, C., Nowak, M.W., Zhang, H., Tang, L., Deshpande, P., and Lester, H.A. (1995). Channel gating governed symmetrically by conserved leucine residues in the M2 domain of nicotinic receptors. Nature *376*, 514-516. 10.1038/376514a0.

45. Li, W., Feng, Z., Sternberg, P.W., and Xu, X.Z.S. (2006). A C. elegans stretch receptor neuron revealed by a mechanosensitive TRP channel homologue. Nature *440*, 684-687.

46. Li, W., Kang, L., Piggott, B.J., Feng, Z., and Xu, X.Z.S. (2011). The neural circuits and sensory channels mediating harsh touch sensation in Caenorhabditis elegans. Nature Communications *2*, 315.

47. Masters, W.M. (1980). Insect Disturbance Stridulation - Characterization of Airborne and Vibrational Components of the Sound. J Comp Physiol *135*, 259-268. Doi 10.1007/Bf00657254.

48. Mill, P.J. (1976). Structure and function of proprioceptors in the invertebrates (Chapman and Hall ; distributed by Halsted Press).

49. Pan, B., Geleoc, G.S., Asai, Y., Horwitz, G.C., Kurima, K., Ishikawa, K., Kawashima, Y., Griffith, A.J., and Holt, J.R. (2013). TMC1 and TMC2 are

components of the mechanotransduction channel in hair cells of the mammalian inner ear. Neuron *79*, 504-515. 10.1016/j.neuron.2013.06.019.

50. Pan, N.C., Ma, J.J., and Peng, H.B. (2012). Mechanosensitivity of nicotinic receptors. Pflugers Archiv : European journal of physiology *464*, 193-203. 10.1007/s00424-012-1132-9.

51. Piggott, B.J., Liu, J., Feng, Z., Wescott, S.A., and Xu, X.Z.S. (2011). The neural circuits and synaptic mechanisms underlying motor initiation in C. elegans. Cell *147*, 922–933.

52. Pokala, N., Liu, Q., Gordus, A., and Bargmann, C.I. (2014). Inducible and titratable silencing of Caenorhabditis elegans neurons in vivo with histamine-gated chloride channels. Proc Natl Acad Sci U S A *111*, 2770-2775. 10.1073/pnas.1400615111.

53. Prescott, T.J., and Dürr, V. (2015). The world of touch. Scholarpedia *10*, 32688. doi:10.4249/scholarpedia.32688.

54. Rabinowitz, P.M. (2000). Noise-induced hearing loss. American family physician *61*, 2749-2756, 2759-2760.

55. Revah, F., Bertrand, D., Galzi, J.L., Devillers-Thiery, A., Mulle, C., Hussy, N., Bertrand, S., Ballivet, M., and Changeux, J.P. (1991). Mutations in the channel domain alter desensitization of a neuronal nicotinic receptor. Nature *353*, 846-849. 10.1038/353846a0.

56. Richmond, J.E., Davis, W.S., and Jorgensen, E.M. (1999). UNC-13 is required for synaptic vesicle fusion in C. elegans. Nat Neurosci *2*, 959-964.

57. Russell, J., Vidal-Gadea, A.G., Makay, A., Lanam, C., and Pierce-Shimomura, J.T. (2014). Humidity sensation requires both mechanosensory and thermosensory pathways in Caenorhabditis elegans. Proc Natl Acad Sci U S A *111*, 8269-8274. 10.1073/pnas.1322512111.

58. Schellart, N.A.M., and Popper, A.N. (1992). Functional Aspects of the Evolution of the Auditory System of Actinopterygian Fish. In The Evolutionary Biology of Hearing, D.B. Webster, R.R. Fay, and A.N. Popper, eds. (Springer-Verlag New York Inc.), pp. pp. 295-322.

59. Siemers, B.M., and Guttinger, R. (2006). Prey conspicuousness can explain apparent prey selectivity. Curr Biol *16*, R157-R159. DOI 10.1016/j.cub.2006.02.056.

60. Speese, S., Petrie, M., Schuske, K., Ailion, M., Ann, K., Iwasaki, K., Jorgensen, E.M., and Martin, T.F. (2007). UNC-31 (CAPS) is required for dense-core vesicle but not synaptic vesicle exocytosis in Caenorhabditis elegans. J Neurosci *27*, 6150-6162. 10.1523/JNEUROSCI.1466-07.2007.

61. Stenfeldt, K., Johansson, C., and Hellstrom, S. (2006). The collagen structure of the tympanic membrane: collagen types I, II, and III in the healthy tympanic membrane, during healing of a perforation, and during infection. Arch Otolaryngol Head Neck Surg *132*, 293-298. 10.1001/archotol.132.3.293.

62. Suga, H., Schmid, V., and Gehring, W.J. (2008). Evolution and functional diversity of jellyfish opsins. Curr Biol *18*, 51-55. 10.1016/j.cub.2007.11.059.

63. Sundararajan, L., Stern, J., and Miller, D.M., 3rd (2019). Mechanisms that regulate morphogenesis of a highly branched neuron in C. elegans. Dev Biol *451*, 53-67. 10.1016/j.ydbio.2019.04.002.

64. Tao, L., Porto, D., Li, Z., Fechner, S., Lee, S.A., Goodman, M.B., Xu, X.Z.S., Lu, H., and Shen, K. (2019). Parallel Processing of Two Mechanosensory Modalities by a Single Neuron in C. elegans. Dev Cell *51*, 617-631 e613. 10.1016/j.devcel.2019.10.008.

65. Terakita, A. (2005). The opsins. Genome Biol *6*, 213.

66. Treinin, M., Gillo, B., Liebman, L., and Chalfie, M. (1998). Two functionally dependent acetylcholine subunits are encoded in a single Caenorhabditis elegans operon. Proc Natl Acad Sci U S A *95*, 15492-15495.

67. Tsalik, E.L., Niacaris, T., Wenick, A.S., Pau, K., Avery, L., and Hobert, O. (2003). LIM homeobox gene-dependent expression of biogenic amine receptors in restricted regions of the C. elegans nervous system. Dev Biol *263*, 81-102.

68. Ulug, D., Hazir, S., Kaya, H.K., and Lewis, E. (2014). Natural enemies of natural enemies: the potential top-down impact of predators on entomopathogenic nematode populations. Ecol Entomol *39*, 462-469. 10.1111/een.12121.

69. Wang, X., Li, G., Liu, J., Liu, J., and Xu, X.Z. (2016). TMC-1 Mediates Alkaline Sensation in C. elegans through Nociceptive Neurons. Neuron *91*, 146-154. 10.1016/j.neuron.2016.05.023.

70. Wang, X., Li, T., Hu, J., Feng, Z., Zhong, R., Nie, W., Yang, X., and Zou, Y. (2021). In vivo imaging of a PVD neuron in Caenorhabditis elegans. STAR Protoc *2*, 100309. 10.1016/j.xpro.2021.100309.

71. Ward, A., Liu, J., Feng, Z., and Xu, X.Z. (2008). Light-sensitive neurons and channels mediate phototaxis in C. elegans. Nature Neurosci *11*, 916-922.

72. Ward, S. (1973). Chemotaxis by the nematode Caenorhabditis elegans: identification of attractants and analysis of the response by use of mutants. Proc Natl Acad Sci U S A *70*, 817-821.

73. Way, J.C., and Chalfie, M. (1989). The mec-3 gene of Caenorhabditis elegans requires its own product for maintained expression and is expressed in three neuronal cell types. Genes Dev *3*, 1823-1833.

74. Webster, D.B. (1992). Epilogue to the Conference on The Evolutionary Biology of Hearing. In The Evolutionary Biology of Hearing, D.B. Webster, R.R. Fay, and A.N. Popper, eds. (Springer-Verlag New York Inc.), pp. pp. 787-793.

75. Wever, E.G. (1974). The evolution of vertebrate hearing. In Handbook of Sensory Physiology, W.D. Keidel, and W.D. Neff, eds. (Springer-Verlag), pp. pp. 423-454.

76. Wicher, D. (2012). Functional and evolutionary aspects of chemoreceptors. Front Cell Neurosci *6*, 48. 10.3389/fncel.2012.00048.

77. Wicks, S.R., and Rankin, C.H. (1995). Integration of mechanosensory stimuli in Caenorhabditis elegans. J Neurosci *15*, 2434-2444.
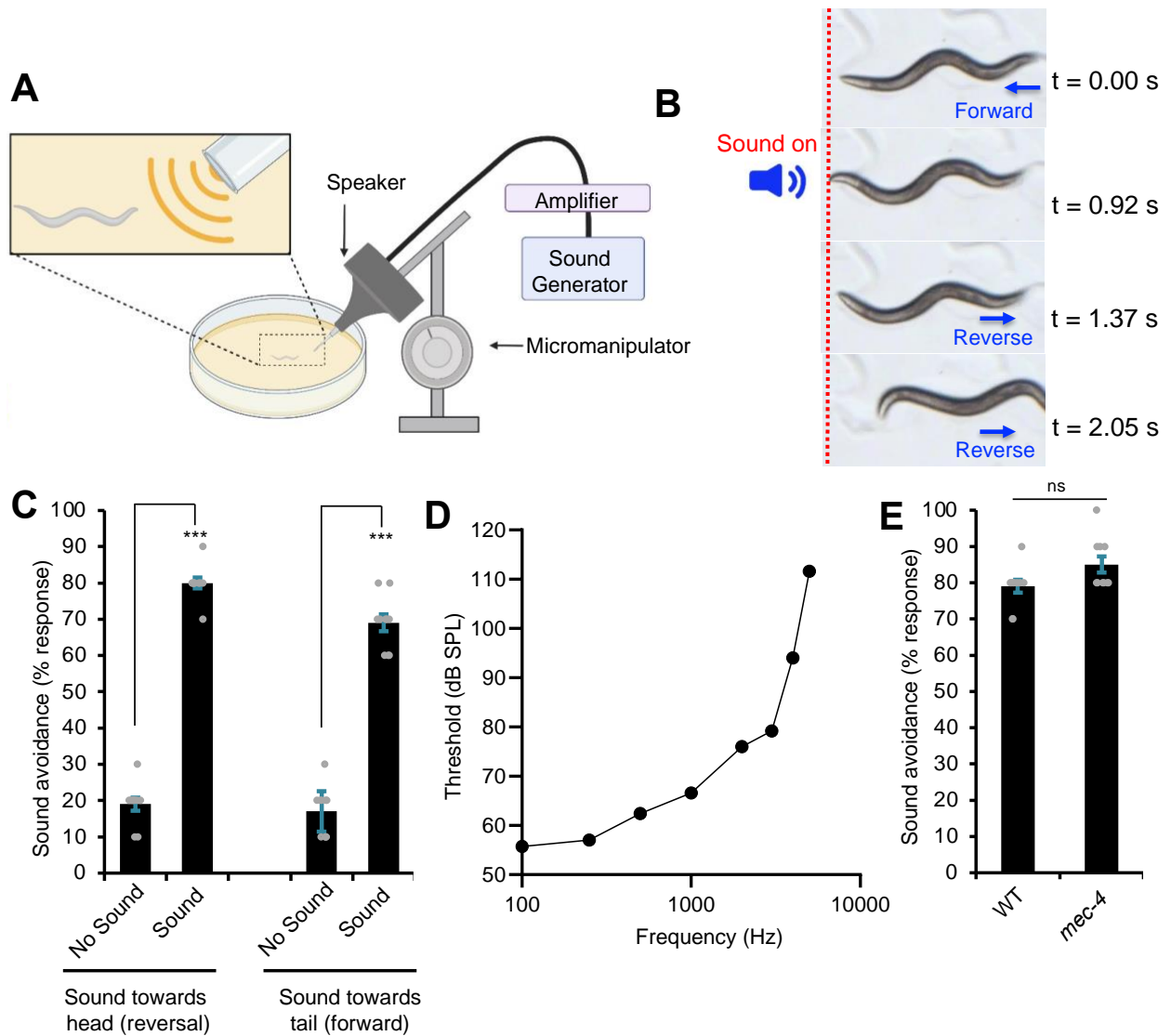
Figure 3.1. Sound evokes aversive phonotaxis behavior in *C. elegans* in a frequency-dependent manner.

(**A**) Schematic describing the assay. The speaker was mounted on a micromanipulator and fitted with an output port, a configuration that allows one to deliver sound stimuli to specific body parts of the worm (e.g. head vs. tail) under a stereomicroscope. Speaker

output was carefully calibrated with a mini-microphone to accurately reflect the sound pressure levels (SPL) received by the worm. See Methods for details.

(**B**) Snapshot images showing that sound stimuli triggered an avoidance response in a worm moving forward. A brief pulse of sound (2 sec, 1 kHz, 80 dB SPL) was delivered to the head of the worm. The animal immediately halted forward locomotion and initiated a reversal. The dotted red line indicates the position of the worm in the field.

(**C**) Worms avoid sound sources. The low basal response in the control groups arose from spontaneous reversals or acceleration of forward movement. ***$p < 0.0001$ (t-test). $n \geq 10$.

(**D**) Worms respond to sound in a frequency-dependent manner. Sound stimuli (2 sec) of varying frequency and SPL were tested for the head-avoidance phonotaxis behavior. Threshold was defined as the SPL of the stimulus that triggered a 50% response rate.

(**E**) *mec-4(e1611)* mutant worms show no defect in phonotaxis behavior. $p > 0.05$ (t-test) $n \geq 10$.

All error bars: SEM. See also Figure 3.8.
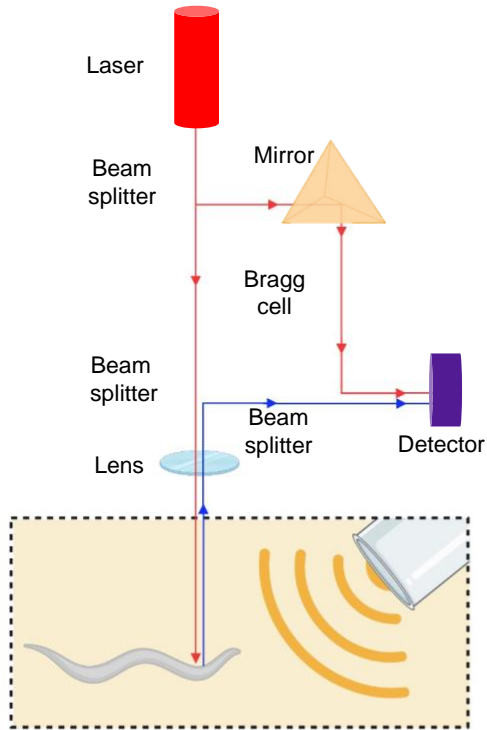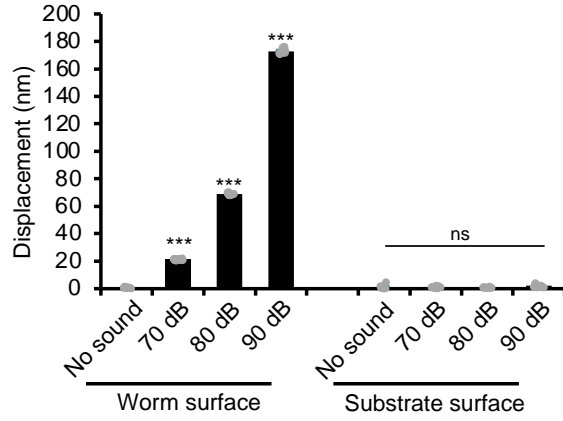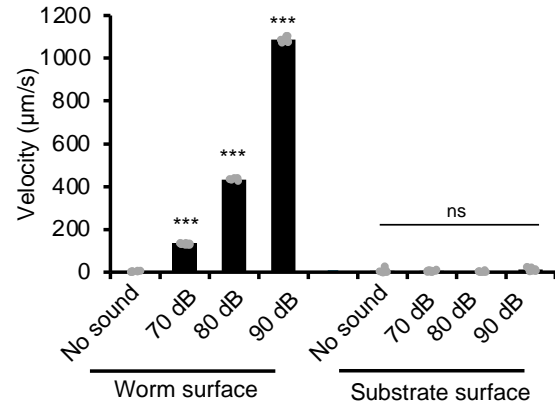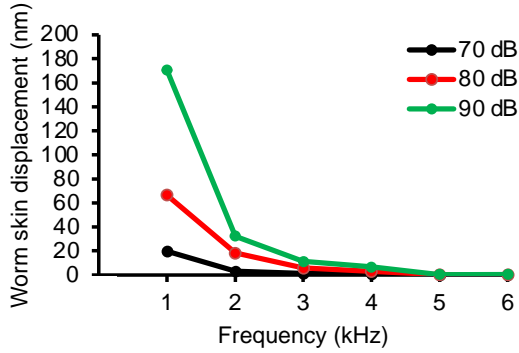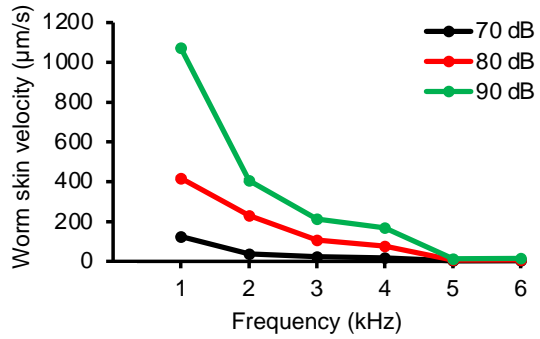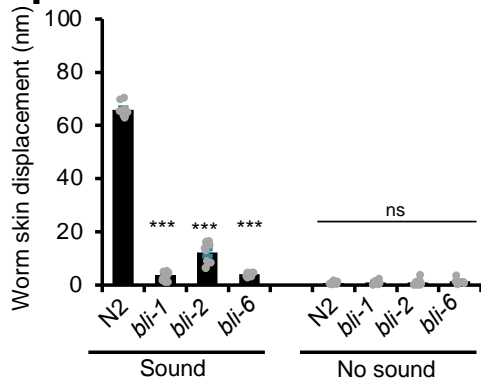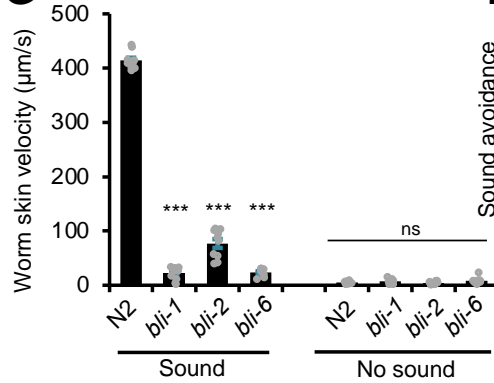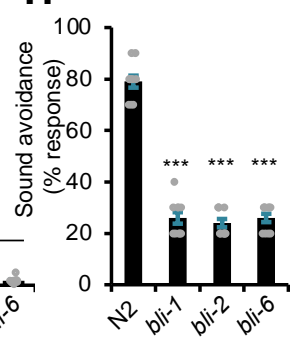
Figure 3.2. Airborne sound vibrates *C. elegans* skin to trigger phonotaxis behavior

(**A**) Schematic describing the laser Doppler vibrometry system used to measure non-contact surface vibration. The laser beam was directed at the surface of either the anterior region of the worm or the agar substrate. The vibration amplitude and frequency was extracted from the Doppler shift of the reflected laser beam frequency caused by surface vibration.

(**B-C**) Displacement and velocity values of sound-evoked vibrations. 1 kHz sound at the specified sound pressure levels (SPL) was applied. (B) Displacement graph. (C) Velocity graph. ***p<0.0001 (ANOVA with Bonferroni test). n≥10.

(**D-E**) Displacement and velocity values of agar surface vibrations evoked by sounds of varying frequencies. Sound frequencies lower than 1 kHz were not tested because of limitations of the system. (D) Worm skin displacement plot. (E) Worm skin velocity plot. n≥10.

(**F-G**) *bli* mutants show a strong defect in sound-evoked vibrations in the cuticle. Worms were tested with 1 kHz sound (80 dB SPL). (F) Worm skin displacement graph. (G) Worm skin velocity graph. ***p<0.0001 (ANOVA with Bonferroni test). n≥10

(**H**) *bli* mutants are defective in phonotaxis behavior. Head-avoidance responses were tested (2 sec, 1 kHz at 80 dB SPL). ***p<0.0001 (ANOVA with Bonferroni). n≥10.

All error bars: SEM. See also Figure 3.9.

A

B

C

D FLP Sound

E PVD Sound

F FLP Sound
WT
unc-31
unc-13

G

H PVD Sound
WT
unc-31
unc-13

I

171
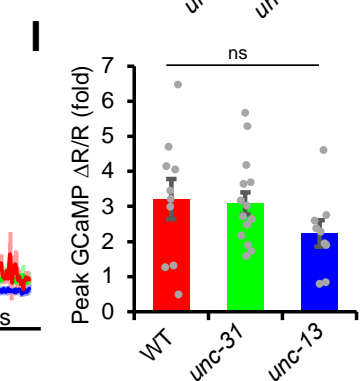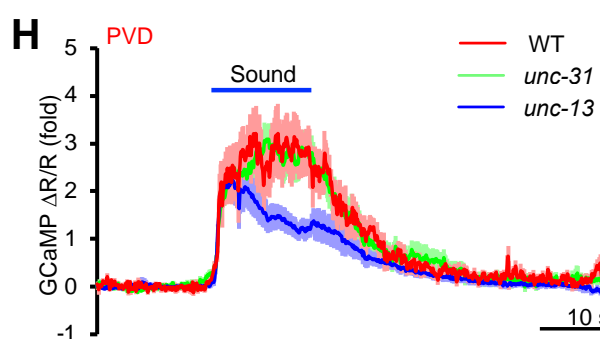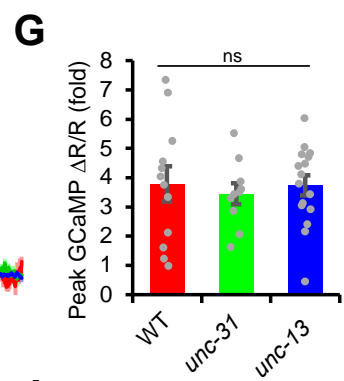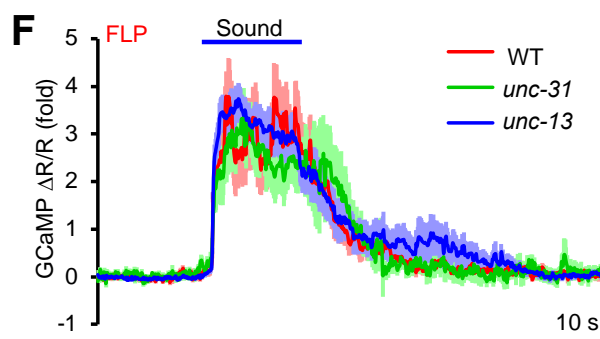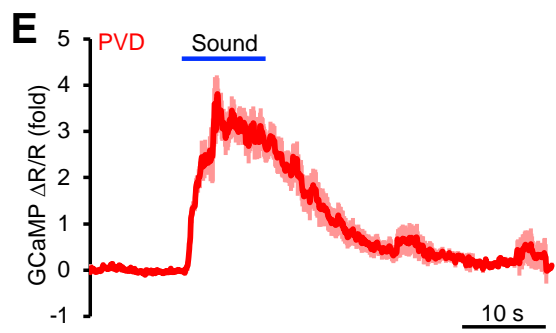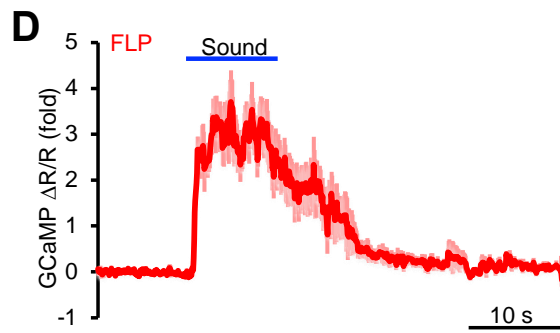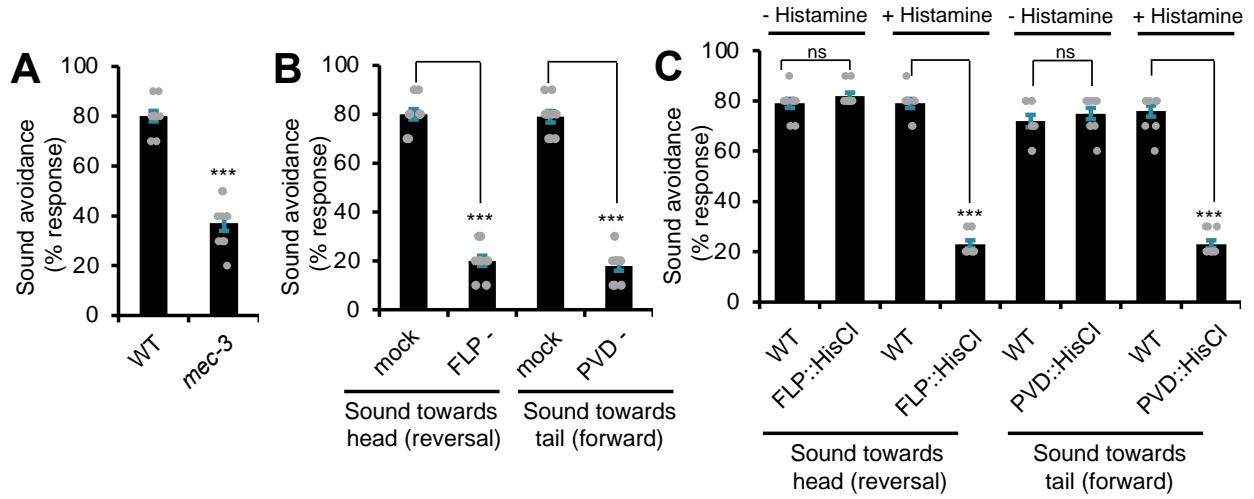
Figure 3.3. FLP and PVD neurons are sound-sensitive neurons mediating phonotaxis behavior.

(**A**) *mec-3(e1338)* mutant worms are defective in phonotaxis behavior. Head-avoidance response was tested. Sound stimulus: 2 sec, 1 kHz at 80 db SPL. ***p<0.0001 (t-test). n≥10.

(**B**) Laser ablation of FLP and PVD neurons leads to a severe defect in sound-evoked reversals and forward movement, respectively. ***p<0.0001 (t-test). n≥10.

(**C**) Acute silencing of FLP and PVD neurons with a HisCl transgene leads to a severe defect in sound-evoked reversals and forward movement, respectively. ***p<0.0001 (t-test). n≥10.

(**D-E**) FLP and PVD neurons are sound-sensitive. Sound evoked robust calcium responses in FLP (D), and PVD (E) neurons. Worms carried a transgene expressing GCaMP6 in FLP or PVD neurons using the *sto-5* or *ser-2(prom3)* promoter, respectively (Russell et al., 2014; Tsalik et al., 2003). mCherry was co-expressed with GCaMP6f to enable ratiometric imaging. Sound stimulus: 10 sec, 1 kHz at 89 dB SPL. Shown are averaged traces. Shades along the traces indicate error bars (SEM). n≥10.

(**F-G**) Sound-evoked FLP calcium responses persist in *unc-13,* and *unc-31* mutant backgrounds. (F) Average traces. (G) Bar graphs. p>0.05 (ANOVA with Bonferroni test). n≥10.

(**H-I**) Sound-evoked PVD calcium responses persist in *unc-13* and *unc-31* mutant backgrounds. (H) Average traces. (I) Bar graphs. Responses in *unc-13* mutant background were slightly reduced, though such a reduction was not statistically significant. p>0.05 (ANOVA with Bonferroni test). n≥10. All error bars: SEM. See also Figure 3.10.

173
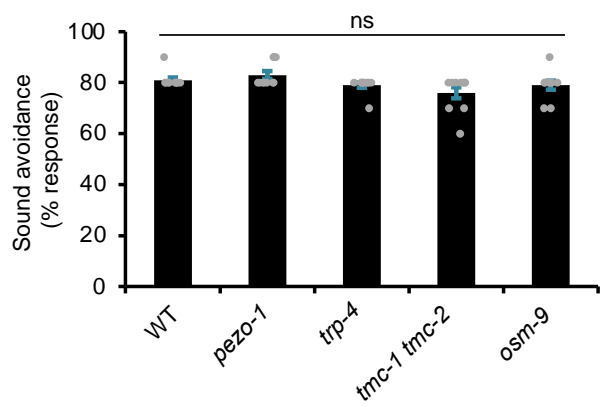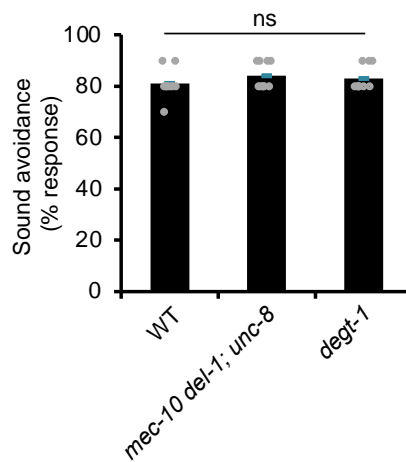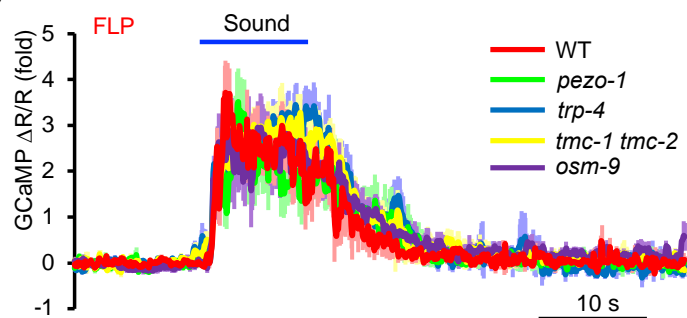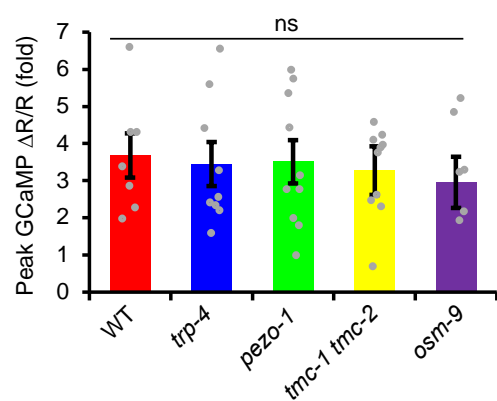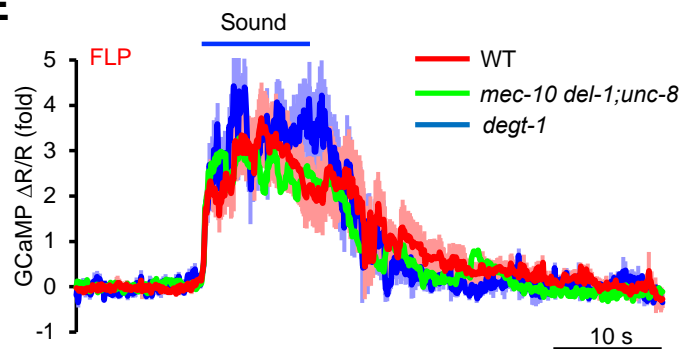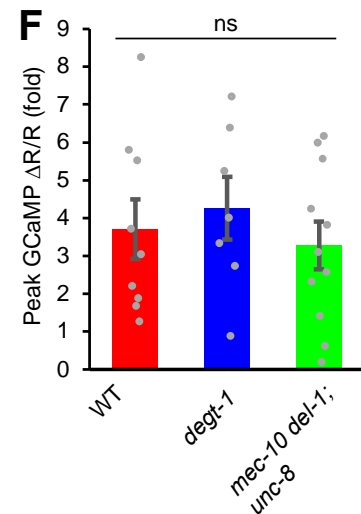
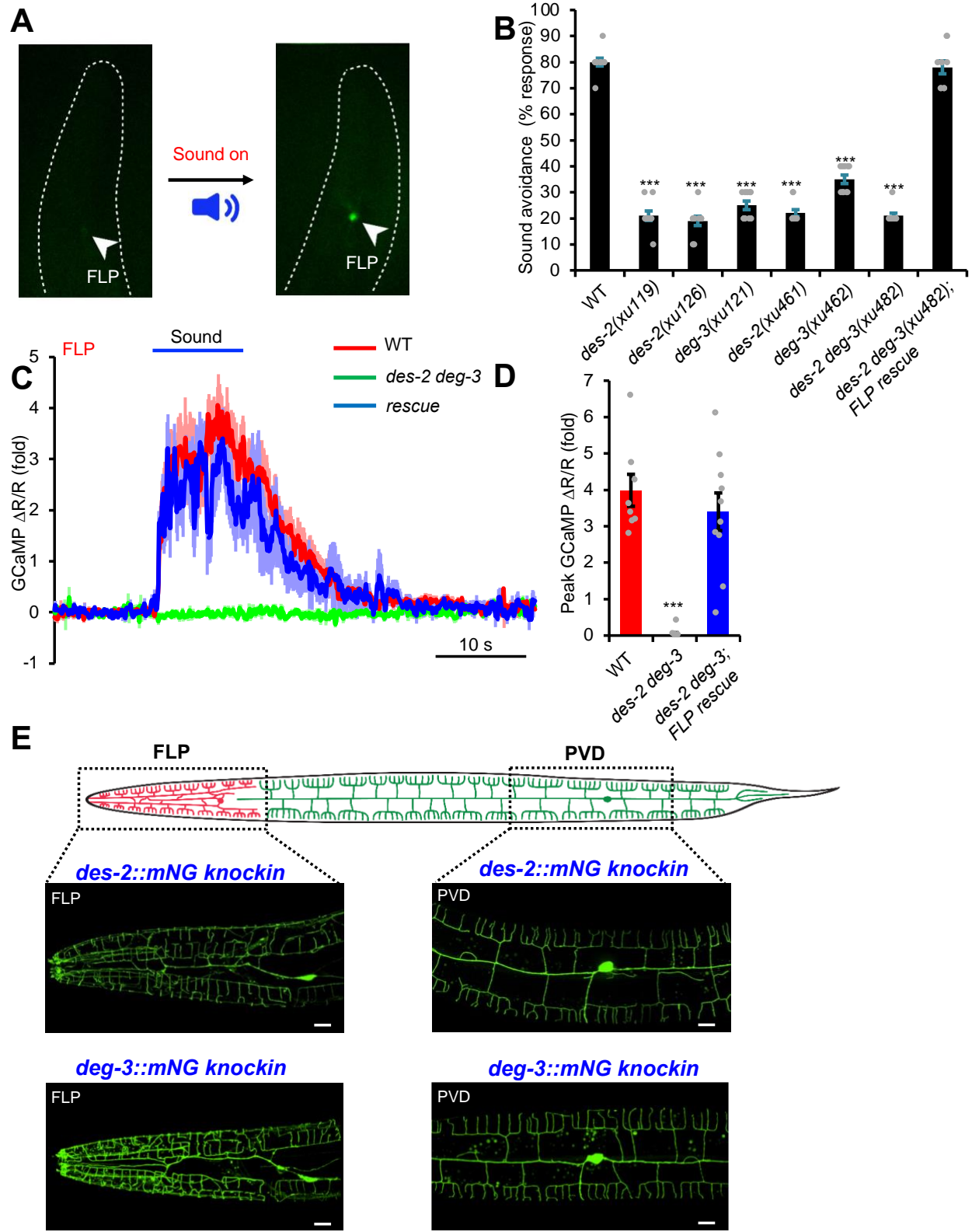**Figure 3.4. Known mechanotransduction channels are not required for sound sensing in *C. elegans.***

(**A**) TRP, TMC and Piezo channel mutants show no defect in phonotaxis behavior. Sound-evoked head-avoidance response was tested. Sound stimulus: 2 sec, 1 kHz at 80 dB SPL. p>0.05 (ANOVA with Bonferroni test). n≥10.

(**B**) Mutants lacking the harsh touch-sensitive DEGT-1 and stretch-sensitive MEC-10/DEL-1/UNC-8 channels do not show a defect in phonotaxis behavior. p>0.05 (ANOVA with Bonferroni test). n≥10.

(**C-D**) TRP, TMC and Piezo channel mutants show no defect in sound-evoked calcium responses in FLP neurons. (C) Average traces. (D) Bar graph. p>0.05 (ANOVA with Bonferroni test). n≥10

(**E-F**) DEGT-1 and MEC-10/DEL-1/UNC-8 channel mutants show no defect in sound-evoked calcium responses in FLP neurons. (E) Average traces. (F) Bar graphs. p>0.05 (ANOVA with Bonferroni test). n≥10

All error bars: SEM.

A

Sound on

FLP / FLP

B

Sound avoidance (% response)

WT / des-2(xu119) / des-2(xu126) / deg-3(xu121) / des-2(xu461) / deg-3(xu462) / des-2 deg-3(xu482) / des-2 deg-3(xu482); FLP rescue

C

FLP

Sound

GCaMP ΔR/R (fold)

WT
des-2 deg-3
rescue

10 s

D

Peak GCaMP ΔR/R (fold)

WT / des-2 deg-3 / des-2 deg-3; FLP rescue

E

FLP   PVD

des-2::mNG knockin   *des-2::mNG knockin*

FLP   PVD

deg-3::mNG knockin   *deg-3::mNG knockin*

FLP   PVD

175

Figure 3.5. An unbiased, activity-based genetic screen identifies two nAChR subunits DES-2 and DEG-3 that are required for sound sensing in *C. elegans*.
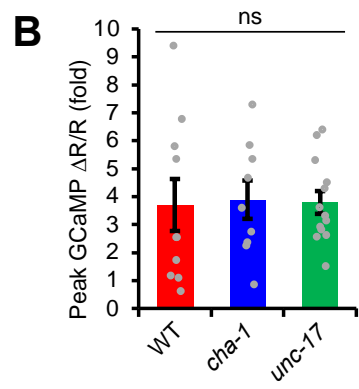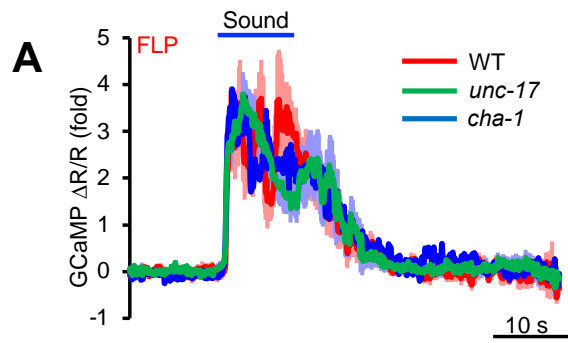
(**A**) Design of the screen. Left panel: a transgenic worm expressing GCaMP6 showed a very low level of basal fluorescence in FLP neuron. Right panel: upon sound simulation, FLP fluorescence intensity in the same worm increased drastically. Images were taken under a fluorescence stereomicroscope from a freely-moving worm placed in an NGM plate. Arrow heads point to FLP.

(**B**) *des-2 deg-3* mutant worms show a severe defect in phonotaxis behavior. Head-avoidance responses were tested. *des-2 deg-3* mutant phenotype was rescued with wild-type *des-2* and *deg-3* cDNA expressed as a transgene in FLP neurons. See Methods for the molecular lesions in mutant alleles. ***$p<0.0001$ (ANOVA with Bonferroni test). n≥10.

(**C-D**) FLP neurons in *des-2 deg-3* mutant worms do not show sound-evoked calcium responses, a phenotype rescued by transgenic expression of wild-type *des-2* and *deg-3* genes in FLP neurons. (C) Average traces. Shades along the traces indicated error bars (SEM). (D) Bar graph. ***$p<0.0001$ (ANOVA with Bonferroni test). n≥10.

(**E**) DES-2 and DEG-3 are expressed in FLP and PVD neurons. Shown in the top panel is a schematic illustrating the morphology of FLP and PVD neurons. Shown in the lower panels are confocal images of *des-2::mNG* and *deg-3::mNG* knockin worms. Scale bars, 10 μm.

All error bars: SEM. See also Figure 3.11.

A

FLP

Sound

GCaMP ΔR/R (fold)

— WT
— *unc-17*
— *cha-1*

10 s

B

ns

Peak GCaMP ΔR/R (fold)

WT   *cha-1*   *unc-17*

Figure 3.6. Acetylcholine (ACh) is not required for the function of DES-2/DEG-3 in sound sensing

(**A-B**) *cha-1* and *unc-17* mutants lack the synthesis and release of ACh, respectively.

FLP neurons in these two mutant worms responded normally to sound. (A) Average

calcium imaging traces. Shades along the traces denote error bars (SEM). (B) Bar

graphs. Error bars: SEM. $p > 0.05$ (ANOVA with Bonferroni test). $n \geq 10$.
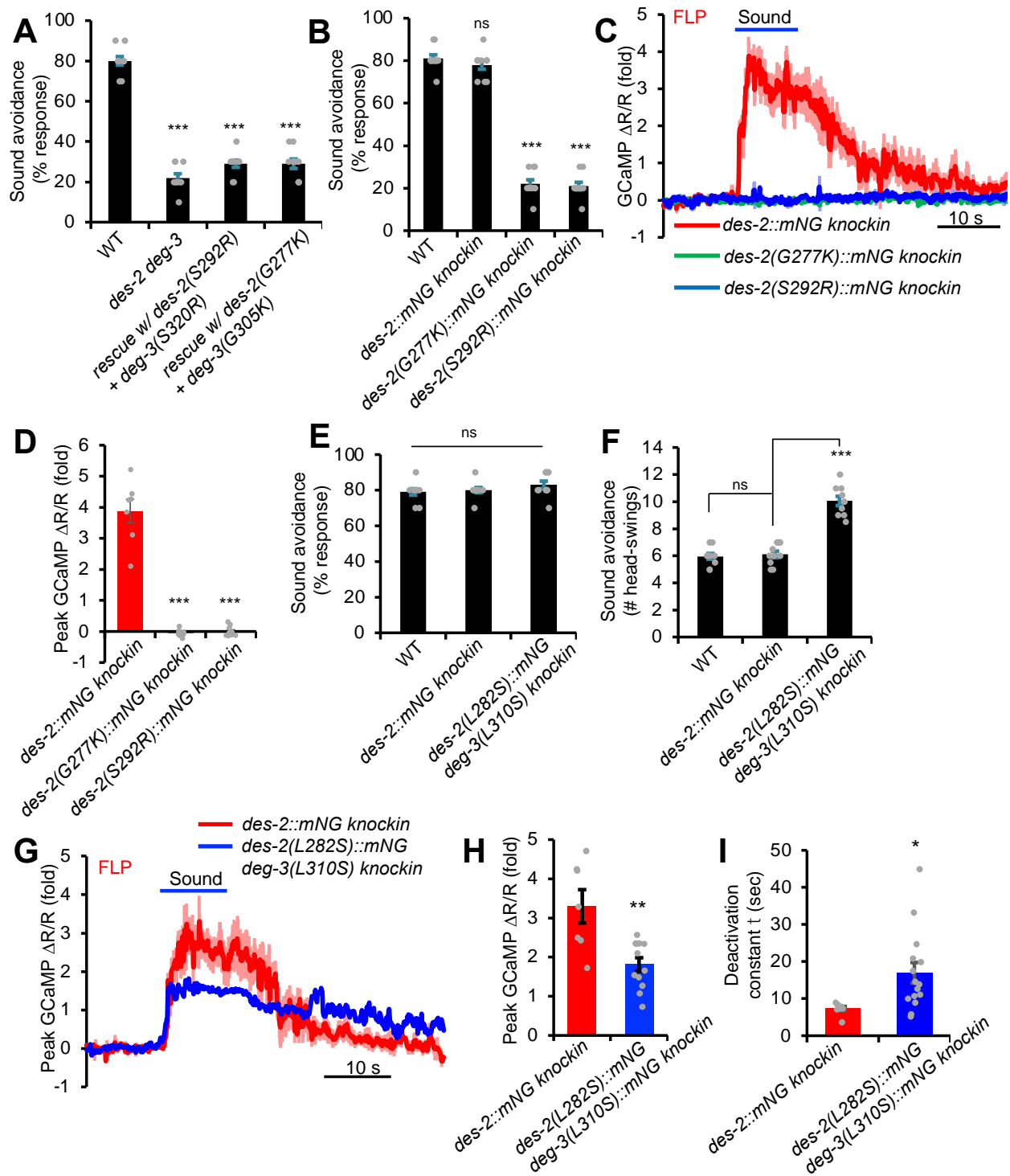
Figure 3.7. DES-2/DEG-3 is an essential component of the sound transduction channel.

(**A**) Channel-dead mutant forms of DES-2/DEG-3 fail to rescue *des-2 deg-3* phonotaxis mutant phenotype. Transgenes were expressed in *des-2 deg-3* mutant background. Head-avoidance phonotaxis behavior was tested. ***p<0.0001 (ANOVA with Bonferroni test). n≥10.

(**B**) *des-2(G277K)* and *des-2(S292R)* knockin worms carrying channel-dead mutations are severely defective in phonotaxis behavior. G277K and S292R mutations were introduced into *des-2::mNG* knockin background by CRISPR. ***p<0.0001 (ANOVA with Bonferroni test). n≥10. Note: in *des-2::mNG* knockin worms, the *deg-3* locus was left intact. *deg-3* should also be functionally expressed in *des-2::mNG* knockin worms, as these knockin worms and their FLP neurons responded normally to sound in phonotaxis behavior and calcium imaging assays, respectively (Figure 3.11C-E).

(**C-D**) FLP neurons in *des-2(G277K)* and *des-2(S292R)* knockin worms, which carry channel-dead mutations, do not respond to sound. (C) Average calcium imaging traces. Shades along the traces denote error bars (SEM). (D) Bar graph. ***p<0.0001 (ANOVA with Bonferroni test). n≥10

(**E-F**) Knockin worms carrying mutations that enhance the channel function of DES-2/DEG-3 respond more robustly to sound in phonotaxis behavior. The L-S mutation L282S and L310S was introduced into the endogenous *des-2* and *deg-3* locus by CRISPR, respectively. Though the response rate in L-S knockin mutant worms was similar to that in wild-type (E), mutant worms responded more robustly to sound by executing more head-swings (reversal duration) during reversal than wild-type worms (F). ***p<0.0001 (ANOVA with Bonferroni test). n≥10.

(**G-I**) Knockin worms carrying mutations that enhance the channel function of DES-2/DEG-3 show enhanced sound-evoked calcium responses in FLP neurons. (G) Average traces. (H) Bar graph showing the amplitude of calcium responses. (I) Bar graph showing the deactivation kinetics of calcium responses. *p<0.05; **p<0.005 (t-test). n≥10.

All error bars: SEM. See also Figure 3.12 and 3.13.
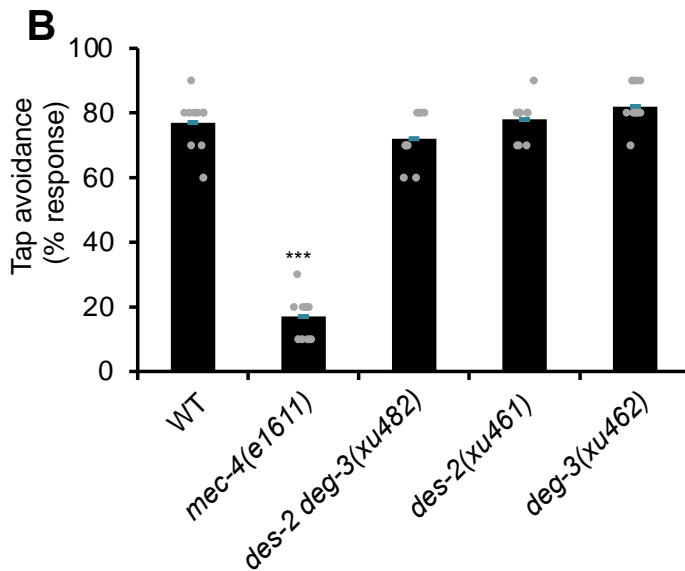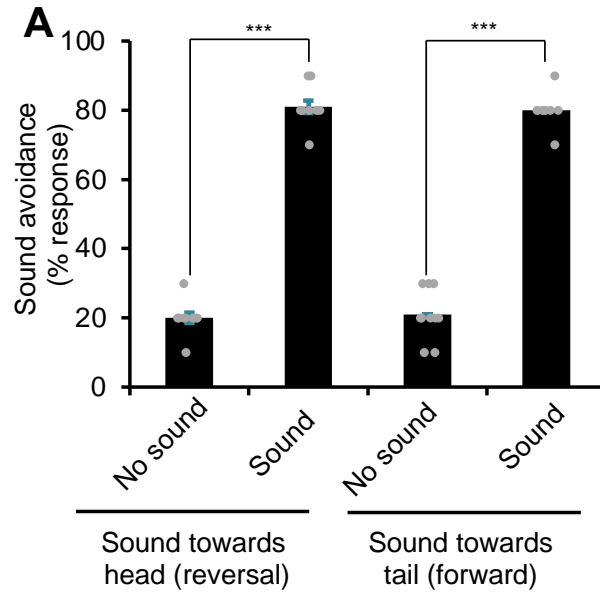
Figure 3.8. Additional data on phonotaxis behavior and substrate-borne vibration-activated behavior.

(A) Additional data on phonotaxis. In Figure 3.1C, we tested phonotaxis behavior by slowly and gently moving the NGM plate by hand while the speaker was held fixed in place. Here, we performed the converse experiment by moving the speaker with the

manipulator while holding the NGM plate in place. This yielded a similar result . Error bars: SEM. ****p<0.0001(t-test). n≥10.

(B) *mec-4* mutant shows a defect in tap avoidance, while *des-2* and *deg-3* mutant do not. Error bars: SEM. ****p<0.0001 (ANOVA with Bonferroni test). n≥10.
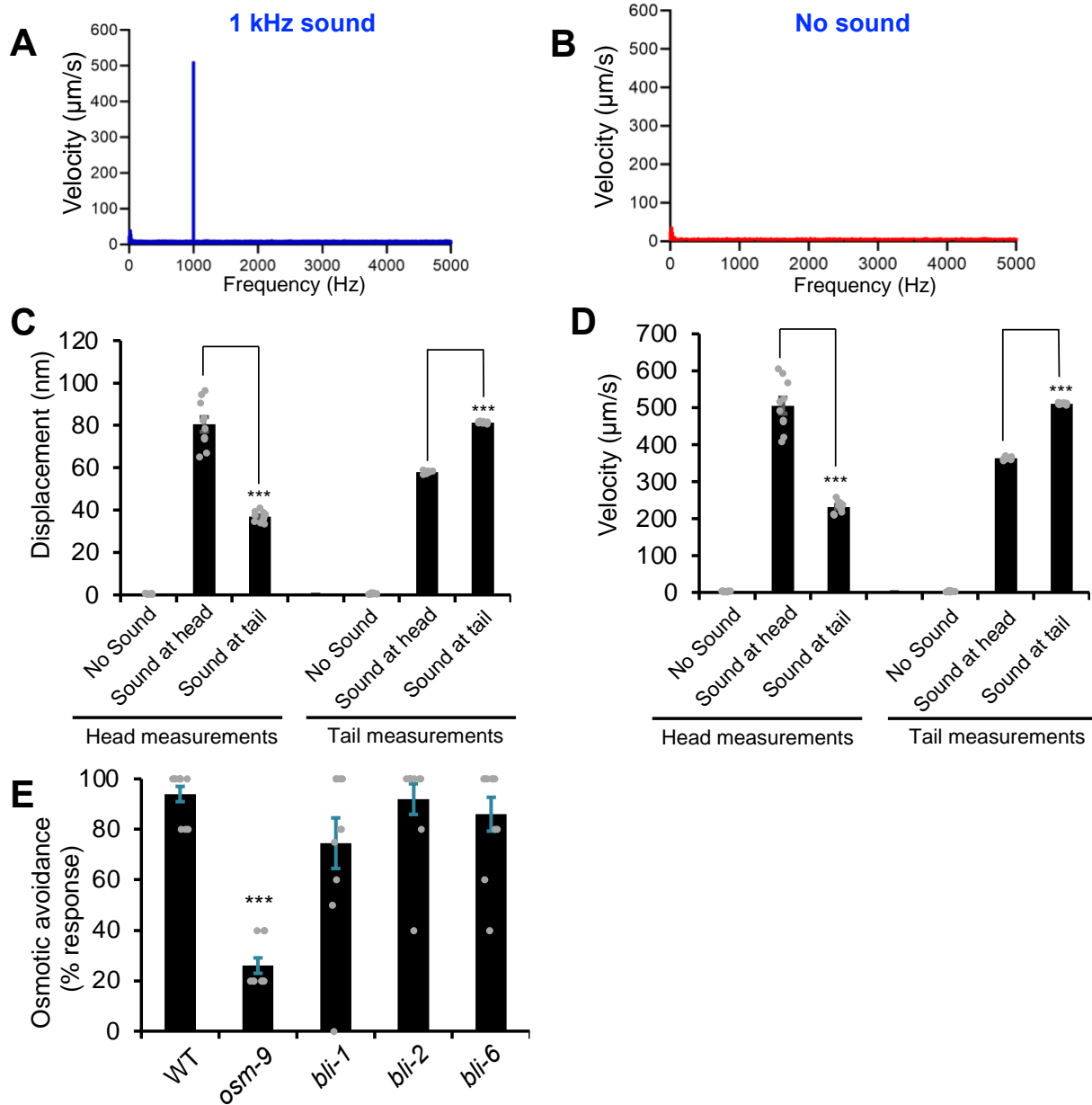
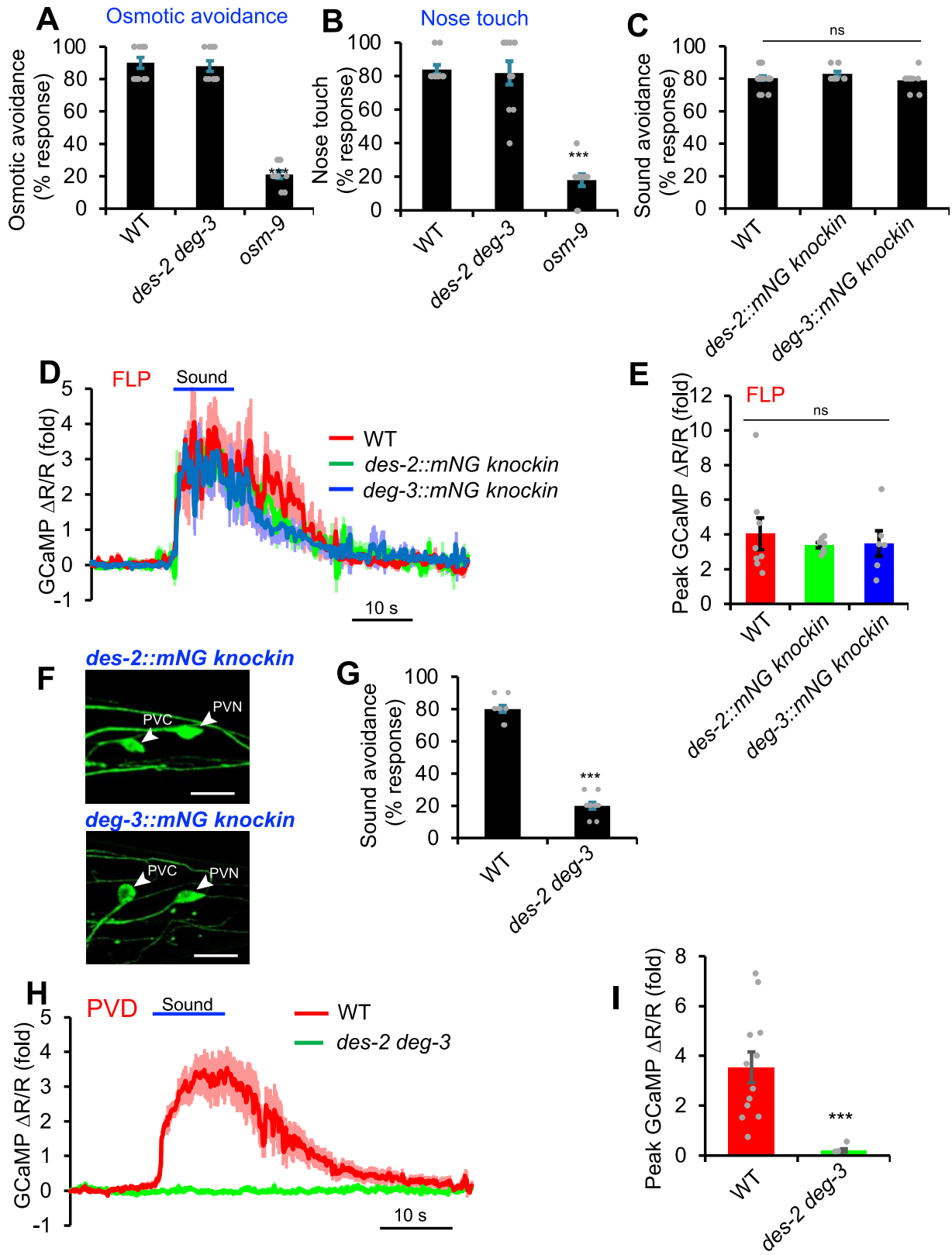**Figure 3.9. Additional data on sound-evoked cuticle vibrations in WT and cuticle mutants.**

(A-B) Worm cuticle vibrates at 1 kHz in response to 1 kHz sound stimulus (80 dB SPL). The small peak near 0 Hz arose from background building vibrations and was present in all recordings, including no sound control.

(C-D) Sound evokes a higher value of cuticle displacement in the head when the stimulus is applied to the head than to the tail, and *vice versa*. Sound stimulus: 1 kHz, 80 dB SPL. Error bars: SEM. ***p<0.0001 (ANOVA with Bonferroni test). n≥10.

(D) *bli* mutants show avoidance response to osmotic stimulus. Worms were tested with glycerol (2 M), which triggered reversals. *osm-9* mutant served as a positive control. Error bars: SEM. ***p<0.0001 (ANOVA with Bonferroni test). n≥10.
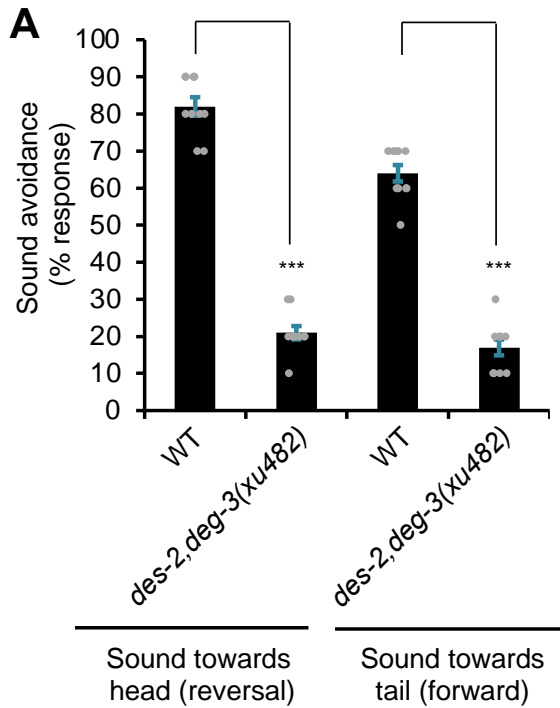
Figure 3.10. Additional data on phonotaxis behavior. The sound-delivery protocol used for calcium imaging of FLP/PVD neurons is slightly different from that for behavioral measurements, due to the setup of the calcium imaging system (see methods). We thus repeated the behavioral test using the condition adopted for the calcium imaging experiments. The scoring protocol remained the same. We obtained similar results using this protocol in WT worms, and *des-2 deg-3* mutant worms also showed a severe defect under this condition. Error bars: SEM. ****p<0.0001(t-test). n≥10.

A Osmotic avoidance

B Nose touch

C

D FLP | Sound | WT, *des-2::mNG knockin*, *deg-3::mNG knockin*

E FLP | ns

F *des-2::mNG knockin* — PVC, PVN

deg-3::mNG knockin — PVC, PVN

G

H PVD | Sound | WT, *des-2 deg-3*

I

Figure 3.11. Additional data on *des-2* and *deg-3*

(A-B) *des-2 deg-3(xu482)* mutant worms showed normal osmotic avoidance and nose touch avoidance behavioral responses. *osm-9* mutant worms, which were defective in both behaviors, were used as a control. Error bars: SEM. ***p<0.0001 (ANOVA with Bonferroni test). n≥10.

(C) *des-2::mNG* and *deg-3::mNG* knockin worms show no defect in phonotaxis behavior. Head-avoidance response was tested. Error bars: SEM. p>0.05 (ANOVA with Bonferroni test). n≥10.

(D-E) *des-2::mNG* and *deg-3::mNG* knockin worms show no defect in sound-evoked calcium responses in FLP neurons. (D) Average traces. Shades along the traces indicate error bars (SEM). (E) Bar graph. Error bars: SEM. P>0.05 (ANOVA with Bonferroni test). n≥10.

(F) *des-2* and *deg-3* are expressed in additional neurons in the tail area. *des-2* and *deg-3* were previously reported to be expressed in IL2 and PVC neurons besides FLP and PVD (Treinin et al., 1998). We did not detect reliable expression of *des-2* and *deg-3* in IL2 neurons in *des-2::mNG* and *deg-3::mNG* knockin worms. However, knockin worms expressed *des-2* and *deg-3* in additional neurons in the tail region (consistent expression in PVC and PVN and inconsistent expression in a few other tail neurons). Scale bars, 10 µm.

(G) *des-2 deg-3(xu482)* mutant worms are defective in sound-stimulated forward movement. Error bars: SEM. ***p<0.0001 (t test). n≥10.

(H-I) *des-2 deg-3(xu482)* mutant worms lack sound-evoked calcium responses in PVD neurons. (H) Average traces. Shades along the traces indicate error bars (SEM). (I) Bar graph. Error bars: SEM. ***p<0.0001 (t test). n≥10.

Figure 3.12. Electrophysiological characterization of wild-type and mutant forms of DES-2/DEG-3 in HEK293T cells.

(A) Sequence alignment of *C. elegans* DES-2 and DEG-3 and human nAChR7 in the pore-lining M2 segment. The residues in DES-2 and DEG-3 that were mutated in this study are marked in red.
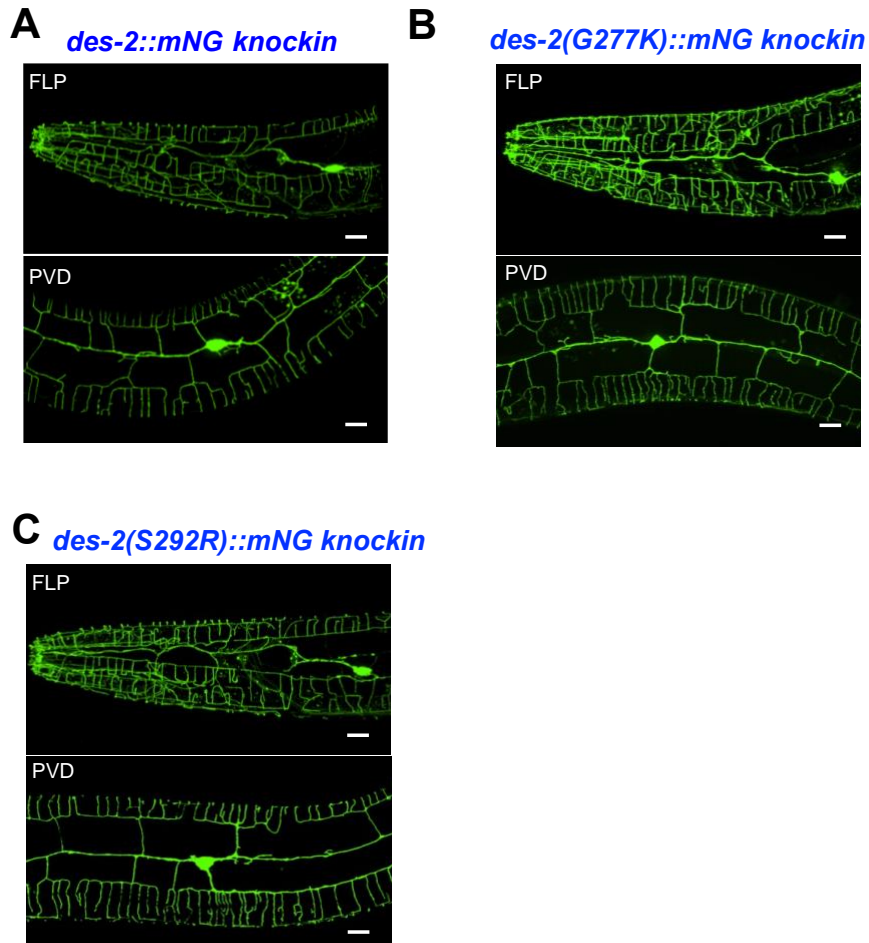
(B) Representative current traces from HEK293T cells expressing wild-type and mutant forms of DES-2/DEG-3. Horizontal bars above each trace indicate the application of choline (10 mM), which is known as a potent agonist for DES-2/DEG-3. Agonist was applied to mutant forms of DES-2/DEG-3 for a longer duration to ensure that no current was evoked (for channel-dead mutants) or the current was able to deactivate for a sufficient amount of time needed for data quantification (for L-S mutant). Holding potential: -70 mV. RIC-3, a chaperon for nAChRs, was co-transfected with DES-2 and DEG-3 into HEK293T cells.

(C) No notable mechanically-activated currents were detected in DES-2/DEG-3 expressed in HEK293T cells. Cells were stimulated with a glass probe driven by a piezo actuator as described previously (Li et al., 2011). The stimulus steps, ranging from 0 to 8 mm, were shown to the top.

(D) Bar graph summarizing the data in (B). Mock, DEG-3, DES-2(G277K)+DEG-3, DES-2(S292R)+DEG-3, DES-2(S292R)+DEG-3(S320R), and DES-2(G277K)+DEG-3(G305K) all showed no current (n≥5). DES-2: 8.0±3.4 (pA/pF) (n=10). DES-2+DEG-3: 267.4±145.3 (pA/pF) (n=17). DES-2(L282S)+DEG-3(L310S): 179.5±135.6 (pA/pF) (n=10).

(E) Bar graph showing that DES-2(L282S)/DEG-3(L310S) desensitizes/inactivates more slowly than wild-type DES-2/DEG-3 channel. The decay phase of the currents were

fitted with exponential function to calculate the decay constant t. For DES-2+DEG-3: 0.97±0.19 (s) (n=11); DES-2(L282S)+DEG-3(L310S): 21.76±5.51 (s) (n=9). Data are presented as mean±s.d. **$p<0.001$ (t test).

A *des-2::mNG knockin*

FLP

PVD

B *des-2(G277K)::mNG knockin*

FLP

PVD

C *des-2(S292R)::mNG knockin*

FLP

PVD

Figure 3.13. Knockin worms carrying channel-dead mutations show normal expression of DES-2. The channel-dead mutations G277K and S292R were introduced into the endogenous locus of *des-2* by CRISPR-based genome editing. Prior to introducing G277K and S292 point mutations, we first introduced the mNG (mNeonGreen) tag into the endogenous *des-2* locus to produce *des-2::mNG* knockin line by CRISPR-based genome editing. This mNG tag did not affect DES-2 function (Figure 3.11). We then performed genome editing in this *des-2::mNG* background to introduce the G277K and S292 channel-dead mutations. *des-2(G77K)::mNG* (B) and *des-2(S292R)::mNG* (C) knockin lines show normal expression of DES-2 in FLP and PVD neurons compared to the parental control (A). Scale bars, 10 μm.

A

RED 4832.1300

WHITE BLACK

BCAAW

335MWR050K 031-10-RFXG1
OUT
GND
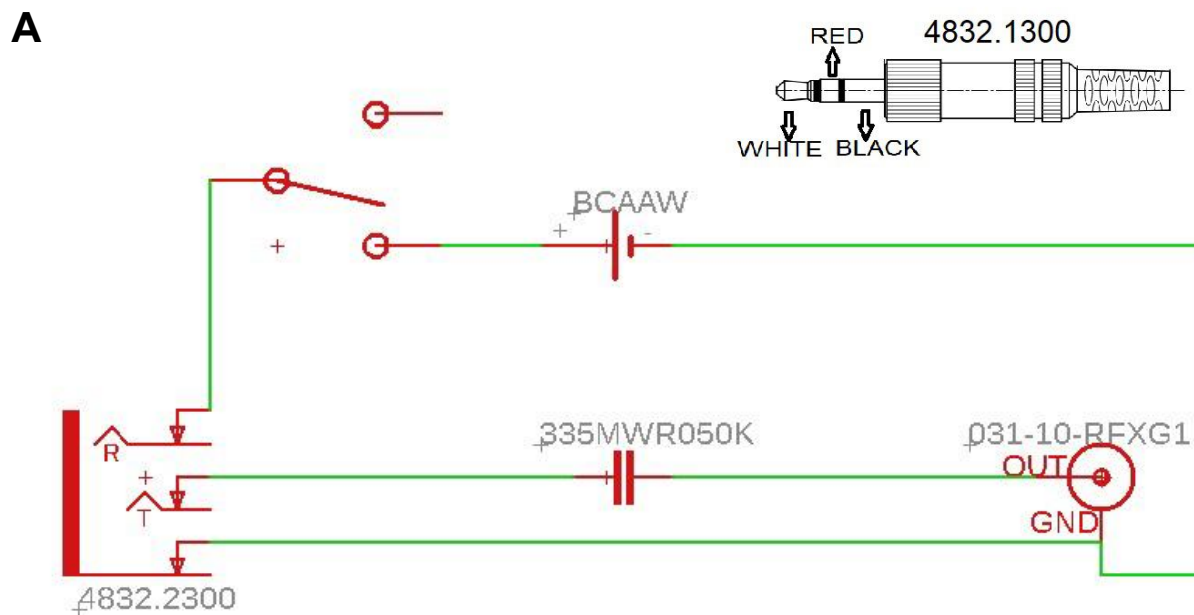
4832.2300

B

| Description	Part #	Source
SPDT Toggle switch	M2013SS1W01	Digi-Key Electronics
Panel mount TRS jack	4832.23	Digi-Key Electronics
Metalized film capacitor	335MWR050K	Digi-Key Electronics
AA Battery holder with leads	BCAAW	Digi-Key Electronics
Analog electret condenser microphone	FG-23329-P07	Digi-Key Electronics
TRRS phono cable	10-02153	Digi-Key Electronics
Aluminum enclosure	PRT-13839	Digi-Key Electronics
Panel mount BNC connector	031-10-RFXG1	Digi-Key Electronics
TRS plug (3.5mm)	4832.13	Digi-Key Electronics
BNC to 1/4" audio adapter	1297	Digi-Key Electronics
Focusrite Scarlett solo	SCARLETT-SOLO-3G	B&H Photo Video

Figure 3.14. Schematic and parts list for miniature microphone power supply. The miniature microphone requires its own power supply. (A) A schematic for the design of the custom power supply used to operate the Knowles miniature microphone. (B) The parts list for the items required for assembling the microphone power supply. This information is also shown in the STAR Methods section.

CHAPTER 4

Conclusions

C. elegans is a tiny roundworm in the Nematode phylum that has emerged as a popular model organism for studying sensory biology and neuroscience. Despite having a simple nervous system (~302 neurons), it has been shown to possess most of the major sensory modalities including thermosensation, mechanosensation, chemosensation, photosensation, and now, auditory sensation[1]. *C. elegans* ability to sense this broad range of sensations despite lacking specialized external organs represents their striking ability to sense stimuli by relying on their simple anatomy comprised of an exoskeleton, muscle, and nervous system. This dissertation research presents two major contributions to the field of sensory biology that shed new insight into the evolution and function of sensory systems.

The dissertation work described in Chapter 2 resulted in the discovery of novel thermosensitive neural responses and sensory pathways, which greatly aids in understanding how organisms detect and respond to thermal stimuli. Here, we identified a novel evolutionarily conserved cold receptor and uncovered the downstream signaling mechanisms leading to cold-induced neuronal activation (See Figure 4.1)
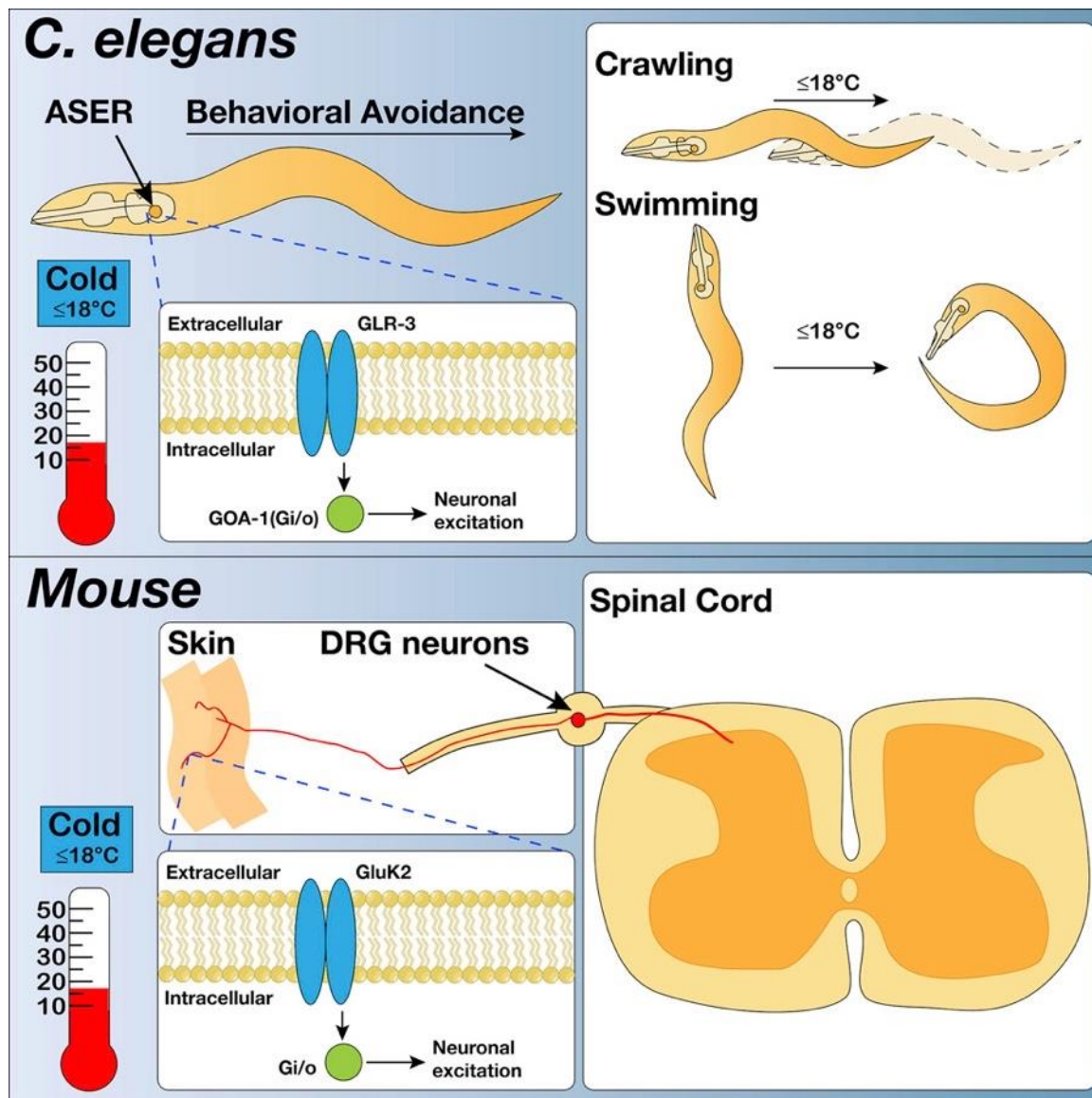
Figure 4.1. Graphical abstract of findings in Chapter 2.

Development of an unbiased activity-based genetic screen enabled us to identify a key

role for GLR-3 in mediating cold sensation[2]. GLR-3 is a member of the kainate-type

glutamate receptor family. We find that GLR-3 acts in the ASER sensory neuron to

mediate cold sensation and cold avoidance behavior. We also discovered that the cold

sensitivity of GLR-3 is independent of its ion channel function, as channel dead variants

showed normal cold sensitivity in ASER neurons. We also found that the cold sensitivity

of ASER neuron requires the Gi/o protein gene *goa-1*. This supports that GLR-3 functions as a metabotropic rather than ionotropic cold sensor. We find this function to be evolutionarily conserved, as the GLR-3 homolog GluK2 from fish, mouse, and human all function as a cold receptor *in vitro*. Additionally, mouse GluK2 can functionally substitute for GLR-3 in *C. elegans in vivo*. Intriguingly, this work illustrates the ability for a CNS chemoreceptor to perform a distinct role in peripheral somatosensation. The overall results of Chapter 2 provide critical insight into the neurons and neural circuitry underlying cold sensation in *C. elegans,* which may be conserved in higher organisms.

Many open questions remain as to whether and how GLR-3/GluK2 functions as a cold sensor across metazoa. How does GLR-3/GluK2 induce neuronal excitability downstream of G protein signaling? Our results reveal that GLR-3/GluK2 cold responses depend on Gi/o proteins Although this signaling pathway is often inhibitory, the Gβγ subunits activate isoforms of several signaling pathways including PLC-β, adenylyl cyclase, and phosphatidylinositol 3-kinase (PI3K)[3]. Further work must be done to determine which G protein subunits function as effectors downstream of GLR-3/GluK2 and the corresponding signaling cascades that enable neuronal excitation. We reported that extracellular calcium is required for cooling-evoked responses in CHO cells transfected with GLR-3 or GluK, indicating that the transduction cascade includes the activation of membrane-bound ion channels to allow for calcium influx and neuronal depolarization. ASER neuron is known to express GCYs and the CNG-gated ion channel TAX-4. One hypothetical model would be that Gi/o proteins activate GCYs to

increase intracellular cGMP, leading to the opening of TAX-4 channels and calcium influx. This could be easily confirmed by testing whether loss of TAX-4 abrogates ASER cold responses.

While our findings reveal that the *C. elegans* GLR-3 has lost sensitivity to glutamate, mouse GluK2 is activated by both cold and glutamate and elicits cellular responses via metabotropic and ionotropic mechanisms, respectively. These functions appear to be independent, as prior activation by cold did not alter GluK2 calcium responses to glutamate. This suggests that these responses are not additive and that cold does not modify glutamate sensitivity. Furthermore, disrupting channel pore function of GluK2 disrupted glutamate responses but not cold responses *in vitro*, supporting separate mechanisms of activation. It would be interesting to examine whether simultaneous application of glutamate and cold elicits an additive calcium response. This would suggest that independent functions of GluK2 receptor can function simultaneously.

How does cold activate GLR-3/GluK2? We show that the extracellular amino-terminal domain (ATD) is essential. Interestingly, the ATD domain of both AMPA and NMDA glutamate receptors is essential for dimerization of receptor subunits[4]. GluK2 subunits have likewise been reported to depend on extensive interactions between ATD domains to form dimers[4]. This suggests a model where disruption of the GLR-3/GluK2 ATD domain prevents proper assembly of individual subunits to form a functional GPCR that can be activated by cold. We find that GLR-3/GluK2 cold sensing is disrupted by P to L (proline to leucine) point mutations. Further work must be done to investigate the

importance of this mutation in mediating GLR-3/GluK2 cold sensing. One possibility is that the P to L mutation disrupts the subunit structure and prevents subunits from either binding or forming a functional GPCR. Of note, the ATD domain of glutamate receptors is not essential for activation by glutamate but is thought to instead modulate channel activity (i.e. open probability, channel deactivation or desensitization)[4]. This also supports our findings that the ATD domain is not essential for the core function of GluK2 as a glutamate-gated ionotropic receptor.

Findings in our *C. elegans* studies hint at additional physiological roles of GLR-3 in cold sensing. For instance, GLR-3 was identified using an unbiased screen for temperature sensing mutants using the cold-sensitive worm intestine. The rational for this screen was based on prior studies that found cold temperatures extend *C. elegans* lifespan via TRPA-1 expression in the intestine[5]. We now know that GLR-3 functions as a cold sensor and is expressed in the intestine as well. Follow up studies should examine whether GLR-3 has a role in cold-mediated lifespan extension. Notably, TRPA-1 is not confirmed to be a cold sensor and may instead function as a signal amplifier downstream[6]. It would be interesting to explore whether TRPA-1 functions downstream of GLR-3 to mediate this lifespan extension. Another potential future direction to explore in *C. elegans* is whether GLR-3 plays a role in thermotaxis behavior. In addition to ASER, we also found GLR-3 expression in the interneuron RIA, which some studies show plays a role in thermotaxis behavior[1,6].

Our findings also reveal that mouse, fish, and fly homologs of GLR-3 also function as cold sensors *in vitro.* Future work examining cold sensation roles of GLR-3

homologs *in vivo* will provide further insight into evolutionarily conserved functions. We report that 13.6% of mouse DRGs (isolated from T10-L6 vertebra) express GluK2, with ~2/3rds expressed in small diameter neurons, and the remaining third expressed in intermediate diameter neurons. It will be interesting to see if mammalian *in vivo* studies recapitulate our findings that GluK2 is essential for cold-induced DRG responses *in vitro*. Innocuous cool sensing is thought to depend on a subset (~5-10%) of small diameter DRG neurons that express TRPM8[7–9]. Do GluK2 cold sensing DRGs respond to innocuous cooling via TRPM8, or are these receptors expressed in distinct populations of DRGs?

Thermosensation and nociception are closely related, with many thermosensitive channels also implicated in sensing noxious stimuli and pain. The findings of this dissertation furthers our understanding of thermosensation at the molecular, cellular, circuit, and behavioral levels, with the potential to provide novel therapeutic targets and strategies for pain treatment.

In Chapter 3, we discover that the nematode *C. elegans* can sense airborne sound (See Figure 4.2)[10]. The sense of hearing is defined as the ability to detect and transduce airborne vibrations into electrical signals that enable the organism to sense and respond to sound. Based on this definition, we describe *C. elegans* responses to airborne vibrations as the "auditory response". We found that worms can sense and respond to airborne vibrations in the range of 20Hz to 6kHz despite lacking specialized auditory structures. Specifically, we report that airborne sound physically vibrates the exterior surface of the worm, activating the specialized multidendritic neurons FLP and

PVD which tile the head and body wall and trigger avoidance responses. By using forward genetic screens we uncover that the nicotinic acetylcholine receptor DES-2;DEG-3 is required for auditory sensation in FLP neurons. Importantly, our work for the first time reveals that airborne sound can be sensed in lower phyla.
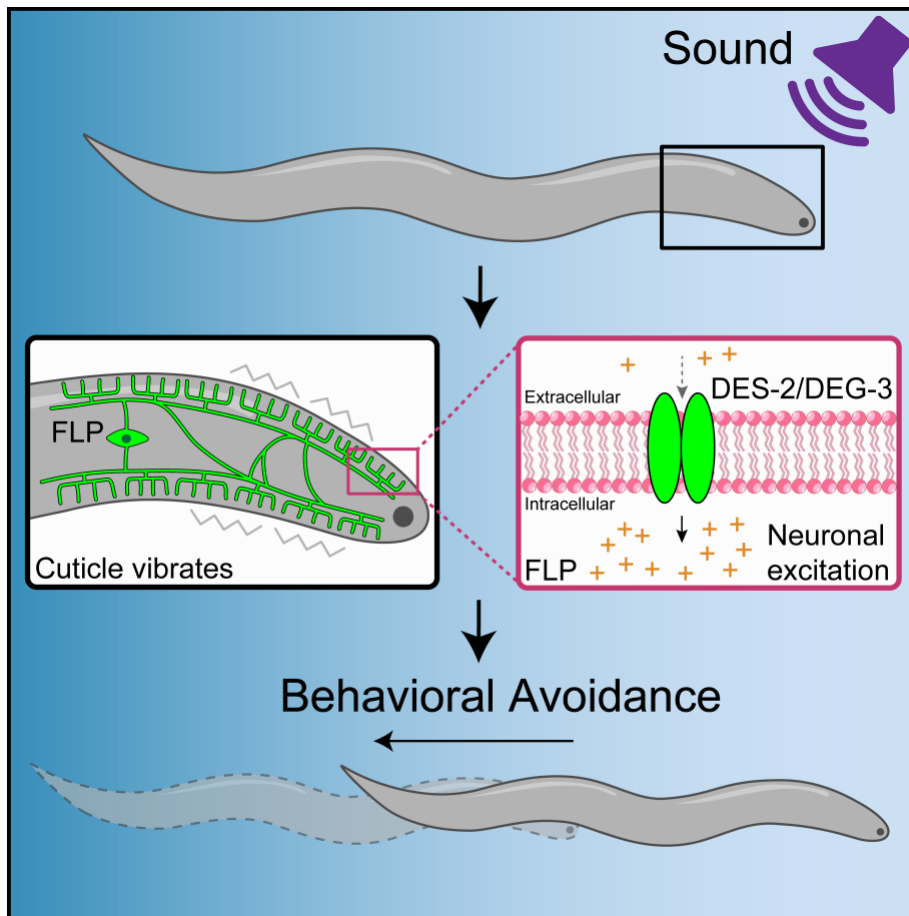
Figure 4.2. Graphical abstract of findings in Chapter 3.

Hearing is a fundamental sensory modality that has evolved independently several times in the Chordata and Arthropoda phyla[11]. In higher organisms, specialized sensory organs attuned to detect airborne vibrations are considered necessary for an animal to hear. The presence of sensory hair cells capable of transducing sound waves is a unifying theme among vertebrate ears and invertebrate chordotonal organs[11].

Auditory sensory organs also tend to be polymodal, most commonly playing a role in the sense of proprioception. Our work suggests that the worm body itself acts as an auditory sense organ that is capable of transducing sound waves. Several open questions remain. For instance, how does skin vibration lead to neuronal activation of FLP/PVD? Based on our results that the channel pore of DES-2;DEG-3 is required for FLP/PVD excitation, we suspect that it functions in the channel pore of a larger transduction complex similar to that observed in TRNs. If DES-2;DEG-3 does function as part of a larger complex, we expect additional proteins to be required to gate channel opening. Further investigation examining whether the FLP/PVD cytoskeleton or surrounding hypodermis/ECM are required for phonotaxis responses will provide insight.

Although research using the roundworm *C. elegans* began over 50 years ago, it continues to surprise us with its complex sensory capabilities despite its seeming simplicity. We anticipate that *C. elegans* will continue to provide exciting and unexpected insight into the evolution of sensory biology. In summary, the findings of this dissertation work shed novel insight into sensation at the molecular, cellular, circuit, and behavioral levels in all organisms, transforming the current understanding of how organisms detect, perceive, and respond to sensory cues.

References

1. Goodman, M. B. & Sengupta, P. How *Caenorhabditis elegans* Senses Mechanical Stress, Temperature, and Other Physical Stimuli. *Genetics* 212, 25–51 (2019).

2. Gong, J. *et al.* A Cold-Sensing Receptor Encoded by a Glutamate Receptor Gene. *Cell* 178, 1375-1386.e11 (2019).

3. Neves, S. R., Ram, P. T. & Iyengar, R. G protein pathways. *Science* 296, 1636–1639 (2002).

4. Traynelis, S. F. *et al.* Glutamate Receptor Ion Channels: Structure, Regulation, and Function. *Pharmacol. Rev.* 62, 405–496 (2010).

5. Xiao, R. *et al.* A Genetic Program Promotes C. elegans Longevity at Cold Temperatures via a Thermosensitive TRP Channel. *Cell* 152, 806–817 (2013).

6. Xiao, R. & Xu, X. Z. S. Temperature Sensation: From Molecular Thermosensors to Neural Circuits and Coding Principles. *Annu. Rev. Physiol.* 83, 205–230 (2021).

7. Peier, A. M. *et al.* A TRP channel that senses cold stimuli and menthol. *Cell* 108, 705–715 (2002).

8. Dhaka, A., Earley, T. J., Watson, J. & Patapoutian, A. Visualizing Cold Spots: TRPM8-Expressing Sensory Neurons and Their Projections. *J. Neurosci.* 28, 566–575 (2008).

9. McKemy, D. D., Neuhausser, W. M. & Julius, D. Identification of a cold receptor reveals a general role for TRP channels in thermosensation. *Nature* 416, 52–58 (2002).

10. Iliff, A. J. *et al.* The nematode C. elegans senses airborne sound. *Neuron* 109, 3633-3646.e7 (2021).

11. Fay, R. R. & Popper, A. N. Evolution of hearing in vertebrates: the inner ears and processing. *Hear. Res.* 149, 1–10 (2000).